



SYNTHESIS OF CHROMIUM, IRON, AND NICKEL COMPLEXES USING ARYL-BASED CHELATES AS ANCILLARY LIGANDS AND A SERIES OF BIS-(\pm -IMINOPYRIDYL) IRON COMPOUNDS WITH VARYING DONOR LIGANDS

by Emily C Volpe

This thesis/dissertation document has been electronically approved by the following individuals:

Wolczanski, Peter Thomas (Chairperson)

Chirik, Paul (Minor Member)

Coates, Geoffrey (Minor Member)

SYNTHESIS OF CHROMIUM, IRON, AND NICKEL COMPLEXES USING
ARYL-BASED CHELATES AS ANCILLARY LIGANDS AND A SERIES OF BIS-
(α -IMINOPYRIDYL) IRON COMPOUNDS WITH VARYING DONOR LIGANDS

A Dissertation

Presented to the Faculty of the Graduate School

of Cornell University

In Partial Fulfillment of the Requirements for the Degree of

Doctor of Philosophy

by

Emily C. Volpe

August 2010

© 2010 Emily C. Volpe

SYNTHESIS OF CHROMIUM, IRON, AND NICKEL COMPLEXES USING
ARYL-BASED CHELATES AS ANCILLARY LIGANDS AND A SERIES OF BIS-
(α -IMINOPYRIDYL) IRON COMPOUNDS WITH VARYING DONOR LIGANDS

Emily C. Volpe, Ph. D.

Cornell University 2010

Several classes of aryl-based chelates containing pyridine, oxazoline, or imine donors and their reactivity with 1st-row transition metals were investigated in light of the potential of carbon-based ligands to impart strong ligand fields. Heterolytic C-H bond activation of 2-phenylpyridine was achieved with Ni(OTf)₂. The cyclometalated product and its derivatives undergo substitution, insertion, and additional cyclometalation reactions. Aryl-oxazolines display a range of reactivity patterns which are dependent on the reaction conditions, the metal, and the particular ligand employed. Aryl-aryl coupling, oxazoline ring-opening, and methylene deprotonation were examined, but were tangential to the goal of making metal-aryl bonds. Successful arylation of nickel, iron and chromium was accomplished using a methylated benzyl-oxazoline aryl anion, and the spectroscopic, structural, and magnetic properties of these complexes are described. Tridentate arylpyridylimines or diarylimines undergo facile arylation with *cis*-(Me₃P)₄Fe(Me)₂ to give low-spin, six-coordinate iron compounds. Their thermal and oxidation behavior are studied, and the spectroscopic properties of their azaallyl derivatives are compared to previously-reported, related species. A highly-fluorinated congener of the diarylimine iron complexes was sought, and preliminary evidence of its divergent reactivity is noted. Finally, a series of iminopyridine complexes of the formula (N,N'- α -

iminopyridyl)₂Fe(L/X)_n have been examined by X-ray and Mössbauer spectroscopy. The redox-active nature of the iminopyridine ligands and the donating ability of the additional L/X ligands have been assessed.

BIOGRAPHICAL SKETCH

Emily Volpe was born in Wheeling, West Virginia to Louis, an English teacher at Wheeling Central Catholic High School, and Catherine, a part-time pharmacist and part-time stay-at-home mom. Emily grew up the third of five children, including Genevieve, Gretchen, Kate and Paul, all of whom shared her love of reading, watching old movies, playing the piano, and just being together. Eager to experience city life, and keeping in the family tradition of Jesuit education, she began her undergraduate studies at Georgetown University. As a chemistry major at Georgetown, she performed research under the guidance Professor Christian Wolf, where she realized that (a) she enjoyed working in a lab and (b) four years would be insufficient to learn all she wanted to know about chemistry. During her senior year she applied to graduate schools while completing the requirements for her English minor, a circumstance which happily permitted her to read novels in addition to textbooks. Emily deferred her acceptance to the Cornell University Department of Chemistry to do a very worthwhile year of service in the Jesuit Volunteer Corps, where she lived in Oakland, CA in a community of six volunteers and worked as a case manager at the Friendship House Association of American Indians. After a year in “rehab,” Emily started at Cornell and joined the real group of miscreants in the lab of Peter T. Wolczanski, where she realized that (a) she enjoyed working in a lab of miscreants, (b) five years of graduate school would be insufficient to learn all she wanted to know about chemistry, and (c) teaching – with the proper mix of care, confidence, and humility – is the best way to learn. At Cornell, Emily also met her friend, fellow organometallic chemist, and future husband, Kevin Sylvester, who celebrated and commiserated with her throughout the highs and lows of graduate research. After graduation, Emily will begin a one-year Visiting Assistant Professorship teaching general chemistry lectures and organic labs at Lafayette College in Easton, PA.

To my brother,
Paul Francis
Who would have been an apt chemistry student
And
To the rest of my loving family
Catherine, Louis, Genevieve, Gretchen and Kate

ACKNOWLEDGMENTS

I am indebted to my advisor, Prof. Peter Wolczanski, for being a teacher, mentor, and friend during the past five years. His knowledge and understanding of chemistry have certainly inspired my admiration; however, I am most amazed by his persistent faith in my ability to mature as a student and as a scientist. My goal as a future teacher and professional scientist is to be worthy of that confidence.

Many thanks are given to my committee members, Prof. Paul Chirik and Prof. Geoffrey Coates, for their support throughout my graduate career. To Paul: for providing constructive feedback after many literature and research talks, and for writing numerous letters of recommendation. To Geoff: for contributing to my thesis, and for being available when I sought committee-related advice.

To the Wolczanski Group: I am grateful to Andrew Chadeayne, Kurt Hirsekorn, Dave Manke, Dave Kuiper, Mike Marshak and Matt Chambers for fostering the unique sense of community that makes being a Wolczanski member an exciting and educational experience. My friends and classmates, Elliott and Brenda, have taught me much during these five years. Elliott: your kindness first convinced me to join the group, and your willingness and ability to think about anything, chemistry or otherwise, made me turn to you first for insight and advice. Brenda: you have made me a better chemist by your diligence and attention to detail, and your reliability is something I hope I have not taken for granted. To Dave Manke: your intelligence, sense of fun, and good taste in music have left a lasting impression on me; I am lucky to have been your labmate. To Erika: you are a worthy successor to Manke as a friend and labmate; I am looking forward to reading that *Science* paper... Valerie and Wes: the lab is in capable hands with you and Erika; good luck over the next four years! Thank you to Jae Ho for being a pleasure to work with for two summers.

I am grateful to Prof. Tom Rutledge for taking an interest in my development as a student and as a professional (and for writing many recommendation letters). I hope that, as a teacher, I may follow your example of providing encouragement, dispensing advice, and reminding others to “smile.”

To my roommate, Doris Pun: you were a steady friend throughout graduate school; I remember our time together with fondness, and will always admire your ability to “create order wherever [you] go.”

With Doris, my friend Hannah Toomey brought fun and friendship to my first year of graduate school.

Dr. Emil Lobkovsky and his work solving crystal structures are most appreciated. I am grateful to Dr. Ivan Keresztes for his willingness to help set up NMR experiments and analyze spectra. Jon Darmon and Pasquale Iacono are appreciated for their experimental assistance in acquiring Mössbauer data and running polymerization screens, respectively.

I would like to thank my family for being my first teachers, for fostering in me a desire to learn, and for trusting me to make my own decisions. All of you constitute an integral part of who I am; hence, a fraction of my accomplishments belongs to me, and the rest belongs to you.

Finally, I extend my love and appreciation to Kevin Sylvester, for being a true companion throughout the last three years. Though eager to graduate and to take on the new role of professor, I find the most joy in the prospect of beginning our lives together as husband and wife.

TABLE OF CONTENTS

Biographical Sketch.....	iii
Dedication.....	iv
Acknowledgements.....	v
List of Schemes.....	ix
List of Figures.....	xii
List of Tables.....	xiv
Preface.....	xvii
 Chapter 1: Heterolytic C-H bond activation in the synthesis of Ni{(2-aryl-κC²)pyridine-κN}₂ and derivatives.	
I. Introduction.....	1
II. Results and Discussion.....	2
III. Conclusions.....	13
IV. Experimental.....	14
V. References.....	18
 Chapter 2: Synthetic investigations of oxazoline-based aryl anions with 1st-row transition metals; Structures of (κ-C,N-{(<i>o</i>-C₆H₄)CMe₂(COCH₂CMe₂N)}FeCl(py) and [κ-C,N-{(<i>o</i>- C₆H₄)CMe₂(COCH₂CMe₂N)}Cr(μ-Cl)]₂.	
I. Introduction.....	21
II. Results and Discussion.....	22
III. Conclusions.....	38
IV. Experimental.....	38
V. References.....	46
 Chapter 3: Aryl-containing pyridine-imine and azaallyl chelates of iron toward strong field coordination compounds.	
I. Introduction.....	48

II. Results and Discussion.....	50
III. Conclusions.....	70
IV. Experimental.....	71
V. References.....	78

Chapter 4: Synthesis and electronic structure of bis-(α -iminopyridine) iron compounds, $(N,N'\text{-}\alpha\text{-iminopyridyl})_2\text{Fe}(\text{L/X})_n$ ($n = 1,2$).

I. Introduction.....	81
II. Results and Discussion.....	82
III. Conclusions.....	101
IV. Experimental.....	102
V. References.....	111

Chapter 5: A highly-fluorinated diarylimine: Towards a stable Fe(III) diaryl azaallyl.

I. Introduction.....	114
II. Results and Discussion.....	115
III. Conclusions.....	120
IV. Experimental.....	120
V. References.....	125

LIST OF SCHEMES

Scheme 1.1. Heterolytic C-H activation of 2-phenylpyridine using nickel(II)triflate.....	2
Scheme 1.2. Formation of neutral (2-arylpyridine)BrNi{(2-aryl- κC^2)-pyridine- κN } via halide substitution.....	5
Scheme 1.3. Methylation attempts with (2-arylpyridine)BrNi{(2-aryl- κC^2)-pyridine- κN } and presumed reductive elimination products.....	8
Scheme 1.4. Activation of second arylpyridine to form Ni{(2-aryl- κC^2)-pyridine- κN } ₂	9
Scheme 1.5. Possible pathway for reaction of (2-arylpyridine)BrNi{(2-aryl- κC^2)-pyridine- κN } with KO ^t Bu.....	10
Scheme 1.6. Reaction of Ni{(2-aryl- κC^2)-pyridine- κN } ₂ with diphenylacetylene.....	11
Scheme 1.7. DFT-calculated energy comparison of cis and trans isomers of 3a	13
Scheme 2.1. Syntheses of various oxazoline ligands.....	23
Scheme 2.2. Metalation of 4,4-dimethyl-2-phenyloxazoline on Zn, Fe, Co & Mn.....	24
Scheme 2.3. Acid/base reactivity of oxazolines PhCH₂Ox and PyCH₂Ox with Ti(NMe ₂) ₄ and Fe(N(TMS) ₂) ₂ (THF), respectively.....	26
Scheme 2.4. Oxidative addition to form [{ κ -C,N-(<i>o</i> -C ₆ H ₄)CMe ₂ (COCH ₂ CMe ₂ N)}Ni] ₂ (μ -Br) ₂ (4).....	27
Scheme 2.5. Temperature-dependent behavior of LiPhCMe₂Ox	28
Scheme 2.6. Aryloxazoline transfer from (PhCMe₂Ox) ₂ Zn.....	33
Scheme 2.7. Reactivity of low-temperature-generated LiPhCMe₂Ox	36
Scheme 3.1. General scheme of aryl-aryl coupling using directing-group ligands (DG = directing group).....	49
Scheme 3.2. Formation of 1,3-di-2-pyridyl-2-azaallyl (smif).....	49

Scheme 3.3. Synthesis of imine derivatives (ArH)CH ₂ Impy (Im1-Im3), (ArH)ImCH ₂ py (Im4-Im6) and (ArH)ImCH ₂ (ArH) (Im7-Im9).....	50
Scheme 3.4. Reaction of various pyridylimines with <i>cis</i> -(Me ₃ P) ₄ FeMe ₂	51
Scheme 3.5. Thermolysis of <i>trans</i> -{κ-C,N,N'-(<i>o</i> -Cl-Ar-2-yl)CH ₂ N=CH-2- py}(PMe ₃) ₂ FeCH ₃ (3) and <i>trans</i> -{κ-C,N,N'-(<i>p</i> - ^t Bu-Ar-2-yl)CH=NCH ₂ -2- py}(PMe ₃) ₂ FeCH ₃ (4), and formation of the zwitterionic <i>mer</i> -{κ-C,N,C'-(<i>p</i> - ^t Bu-Ar-2- yl)CHNCH(2-py-NCH ₃ -3-yl)}(PMe ₃) ₃ Fe (8).....	57
Scheme 3.6. Formation of iron(III) azaallyl <i>trans</i> -{κ-C,N,N'-(<i>p</i> - ^t Bu-Ar-2-yl)CHNCH- 2-py}(PMe ₃) ₂ FeCH ₃ (10).....	63
Scheme 3.7. Reactivity of diarylimines and related complexes.....	66
Scheme 3.8. Deprotonation attempts of [<i>mer</i> -{κ-C,N,C'-(Ph-2-yl)CH ₂ N=CH(Ph-2- yl)}(PMe ₃) ₃ Fe]OTf (14).....	69
Scheme 4.1. Redox states of the α-iminopyridine ligand, with characteristic bond lengths (Å).....	82
Scheme 4.2. Reactivity of <i>cis</i> -(Me ₃ P) ₄ FeMe ₂ with alkyl pyridine imines.....	83
Scheme 4.3. Reduction attempts with ethylene and an array of substituted olefins....	85
Scheme 4.4. Reductions with terminal or internal alkynes.....	86
Scheme 4.5. Proposed mechanism for the formation of [^{neo} HexNH(py)CH] ₂	87
Scheme 4.6. Synthesis and reactivity of <i>cis</i> -{κ-N,N'-(N-(2- pyridinylmethylene)alkylamine)} ₂ Fe(PMe ₃) (3-^{neo}Hex).....	88
Scheme 4.7. Synthesis of [{κ-N,N'-(N-(2-pyridinylmethylene)alkylamine)} ₃ Fe][OTf] ₂ (alkyl = CH ₂ C(CH ₃) ₃ , 6-^{neo}Pe ; (CH ₂) ₂ C(CH ₃) ₃ , 6-^{neo}Hex).....	92
Scheme 5.1. Synthesis of <i>trans</i> -{κ-C,N,C'-(2,4,5-trifluorophen-2-yl)CH=N- CH ₂ (3,4,5-trifluorophen-2-yl)}Fe(PMe ₃) ₂ (N ₂) (1-(N₂)).....	115
Scheme 5.2. Equilibrium between 1-(N₂) and 1-(H₂)	118

Scheme 5.3. Oxidation attempts with <i>trans</i> -{ κ -C,N,C'-(2,4,5-trifluorophen-2-yl)CH=N-CH ₂ (3,4,5-trifluorophen-2-yl)}Fe(PMe ₃) ₂ (N ₂) (1 -(N ₂)).....	119
---	-----

LIST OF FIGURES

Figure 1.1. Molecular view of (2-phenylpyridine)BrNi{(2-aryl- κC^2)-pyridine- κN } (2a) with hydrogens omitted.....	6
Figure 1.2. Molecular view of [(2-phenyl- κC^2)pyridine- κN]Ni[2-(2-(1,2-diphenylethenyl- κC^2)phenyl)pyridine- κN] (4a) with hydrogens omitted.....	11
Figure 1.3. DFT-calculated molecular orbital picture of 3a	13
Figure 2.1. Molecular view of one of the two independent molecules of [κ -N,N-{4,4-Me ₂ -(2- <i>o</i> -C ₆ H ₄)-2-oxazoline} ₂]CoCl ₂ (1-Co).....	25
Figure 2.2. Molecular view of [{ κ -N,O-C ₆ H ₄ -CMe ₂ C=NCMe ₂ CH ₂ -(μ -O)-}BrFe{ κ -N,O-C ₆ H ₄ -CMe ₂ C=NCMe ₂ CH ₂ -(μ -O)-}FeBr]Li{ κ -N,O-C ₆ H ₄ -CMe ₂ C=NCMe ₂ CH ₂ -(μ -O)-}(DME) (5) with solvent molecules removed.....	29
Figure 2.3. Molecular view of [{ κ -C,N-(<i>o</i> -C ₆ H ₄)CMe ₂ (COCH ₂ CMe ₂ N)}Cr] ₂ (μ -Cl) ₂ (6₂).	34
Figure 2.4. Molecular view of { κ -C,N-(<i>o</i> -C ₆ H ₄)CMe ₂ (COCH ₂ CMe ₂ N)}Fe(py)Cl (7-Cl).....	35
Figure 3.1. Molecular view of the cation of [<i>mer</i> -{ κ -C,N,C'-(<i>p</i> - ^t Bu-Ar-2-yl)CH=NCH ₂ (2-py-NCH ₃ -3-yl)}(PMe ₃) ₃ Fe]OTf (7).....	58
Figure 3.2. Molecular view of <i>mer</i> -{ κ -C,N,C'-(<i>p</i> - ^t Bu-Ar-2-yl)CHNCH(2-py-NCH ₃ -3-yl)}(PMe ₃) ₃ Fe (8).....	62
Figure 3.3. Uv-vis spectra of the two azaallyl complexes, Fe(II) 8 and Fe(III) 10 , relative to precursor imines, Fe(II) 7 and Fe(III) 9	65
Figure 3.4. Molecular view of the cation of [<i>mer</i> -{ κ -C,N,C'-(Ph-2-yl)CH ₂ N=CH(Ph-2-yl)}(PMe ₃) ₃ Fe]OTf (14).....	67
Figure 3.5. Proposed molecular orbital picture demonstrating the formation of a stable and unstable Fe(III) azaallyl.....	70

Figure 4.1. Molecular view of <i>cis,cis</i> -{ κ -N,N'-(N-(2-pyridinylmethylene)neopentylamine)} ₂ -Fe(CH ₃) ₂ (1 - ^{neo} Pe).....	83
Figure 4.2. Molecular view of <i>cis</i> -{ κ -N,N'-(N-(2-pyridinylmethylene)neohexylamine)} ₂ Fe(PhCCPh) (2 - ^{neo} Hex).....	88
Figure 4.3. Molecular view of <i>cis</i> -{ κ -N,N'-(N-(2-pyridinylmethylene)alkylamine)} ₂ -Fe(PMe ₃) (3 - ^{neo} Hex). Disordered methyl groups of the PMe ₃ ligand are removed for clarity.....	89
Figure 4.4. Molecular view of [<i>cis</i> -{ κ -N,N'-(N-(2-pyridinylmethylene)neohexylamine)} ₂ Fe(PMe ₃)(CH ₃)]OTf (5 - ^{neo} Hex).....	91
Figure 4.5. Wieghardt's five-coordinate bis-iminopyridine iron phosphine complex (7).....	97
Figure 4.6. Mössbauer spectra (overlaid) of 1 - ^{neo} Pe , 2 - ^{neo} Hex , 3 - ^{neo} Hex , 5 - ^{neo} Hex , and 6 - ^{neo} Pe	98
Figure 4.7. Mössbauer comparison including related complexes from the literature.....	99
Figure 4.8. Labeling scheme for ¹ H and ¹³ C NMR assignments.....	103
Figure 5.1. Proposed molecular orbital description for the formation of both stable and unstable Fe(III) azaallyl species.....	114
Figure 5.2. Molecular view of <i>trans</i> -{ κ -C,N,C'-(2,4,5-trifluorophen-2-yl)CH=N-CH ₂ (3,4,5-trifluorophen-2-yl)}Fe(PMe ₃) ₂ (N ₂) (1 -(N ₂)).....	116
Figure 5.3. Plot of lnT ₁ (ms) versus 1/T (K ⁻¹) for 1 -(H ₂).....	123

LIST OF TABLES

Table 1.1. ^1H NMR data (d, J (Hz); benzene- d_6) for [bis(2-arylpyridine)Ni{(2-aryl- κC^2)pyridine- $\kappa\text{N}}$]}OTf (aryl = phenyl, 1a ; tolyl, 1b), [(2-arylpyridine)BrNi{(2-aryl- κC^2)pyridine- $\kappa\text{N}}$]} (aryl = phenyl, 2a ; tolyl, 2b), Ni{(2-aryl- κC^2)pyridine- $\kappa\text{N}}$ }_2 (aryl = phenyl, 3a ; tolyl, 3b), and [(2-aryl- κC^2)pyridine- $\kappa\text{N}}$]Ni[2-(2-(1,2-diphenylethenyl- κC^2)aryl)pyridine- $\kappa\text{N}}$] (aryl = phenyl, 4a ; tolyl, 4b). ^a	3
Table 1.2. $^{13}\text{C}\{^1\text{H}\}$ NMR data (benzene- d_6) for [bis(2-phenylpyridine)Ni{(2-phenyl- κC^2)pyridine- $\kappa\text{N}}$]}OTf (1a), [(2-arylpyridine)BrNi{(2-aryl- κC^2)pyridine- $\kappa\text{N}}$]} (aryl = phenyl, 2a ; tolyl, 2b), Ni{(2-aryl- κC^2)pyridine- $\kappa\text{N}}$ }_2 (aryl = phenyl, 3a ; tolyl, 3b), and [(2-aryl- κC^2)pyridine- $\kappa\text{N}}$]Ni[2-(2-(1,2-diphenylethenyl- κC^2)aryl)pyridine- $\kappa\text{N}}$] (aryl = phenyl, 4a ; tolyl, 4b). ^{a,b}	4
Table 1.3. Crystallographic data for (2-phenylpyridine)BrNi{(2-aryl- κC^2)-pyridine- $\kappa\text{N}}$ (2a) and [(2-phenyl- κC^2)pyridine- $\kappa\text{N}}$]Ni[2-(2-(1,2-diphenylethenyl- κC^2)phenyl)pyridine- $\kappa\text{N}}$] (4a).	6
Table 1.4. Core distances (Å) and angles (°) for [(2-phenylpyridine)BrNi{(2-phenyl- κC^2)pyridine- $\kappa\text{N}}$]} (2a), Ni{(2-phenyl- κC^2)pyridine- $\kappa\text{N}}$ }_2 (3a), and [(2-phenyl- κC^2)pyridine- $\kappa\text{N}}$]Ni[2-(2-(1,2-diphenylethenyl- κC^2)phenyl)pyridine- $\kappa\text{N}}$] (4a).	8
Table 2.1. Crystallographic data for { $\kappa\text{-N,N'-(2,2'-(4,4-dimethyl-2-phenyloxazoliny))biphenyl}}$ }CoCl ₂ (1-Co), [{ $\kappa\text{-N,O-C}_6\text{H}_4\text{-CMe}_2\text{C=NCMe}_2\text{CH}_2\text{-(}\mu\text{-O)}$ }]BrFe{ $\kappa\text{-N,O-C}_6\text{H}_4\text{-CMe}_2\text{C=NCMe}_2\text{CH}_2\text{-(}\mu\text{-O)}$ }FeBr]Li{ $\kappa\text{-N,O-C}_6\text{H}_4\text{-CMe}_2\text{C=NCMe}_2\text{CH}_2\text{-(}\mu\text{-O)}$ }(DME) (5), [{ $\kappa\text{-C,N-(4,4-dimethyl-2-(2-phenylpropan-2-yl)-oxazoline)}$ }]Cr ₂ ($\mu\text{-Cl}$) ₂ (6), and { $\kappa\text{-C,N-(4,4-dimethyl-2-(2-phenylpropan-2-yl)-oxazoline)}$ }Fe($\eta\text{-N-pyridyl}$)Cl (7)).	31
Table 2.2. Core distances (Å) and angles (°) for { $\kappa\text{-N,N'-(2,2'-(4,4-dimethyl-2-phenyloxazoliny))biphenyl}}$ }CoCl ₂ (1-Co), [{ $\kappa\text{-N,O-C}_6\text{H}_4\text{-CMe}_2\text{C=NCMe}_2\text{CH}_2\text{-(}\mu\text{-O)}$ }]BrFe{ $\kappa\text{-N,O-C}_6\text{H}_4\text{-CMe}_2\text{C=NCMe}_2\text{CH}_2\text{-(}\mu\text{-O)}$ }FeBr]Li{ $\kappa\text{-N,O-C}_6\text{H}_4\text{-CMe}_2\text{C=NCMe}_2\text{CH}_2\text{-(}\mu\text{-O)}$ }(DME) (5), [{ $\kappa\text{-C,N-(4,4-dimethyl-2-(2-phenylpropan-2-yl)-oxazoline)}$ }]Cr ₂ ($\mu\text{-Cl}$) ₂ (6), and { $\kappa\text{-C,N-(4,4-dimethyl-2-(2-phenylpropan-2-yl)-oxazoline)}$ }Fe($\eta\text{-N-pyridyl}$)Cl (7)).	31

CMe ₂ C=NCMe ₂ CH ₂ -(μ-O)}(DME) (5), [{κ-C,N-(4,4-dimethyl-2-(2-phenylpropan-2-yl)-oxazoline)}Cr] ₂ (μ-Cl) ₂ (6 ₂), and {κ-C,N-(4,4-dimethyl-2-(2-phenylpropan-2-yl)-oxazoline)}Fe(η-N-pyridyl)Cl (7).....	32
Table 3.1. ¹ H and ³¹ P{ ¹ H} NMR assignments (δ (J(Hz), assnmt) ^{a,b} for imine and imine-derived complexes.....	52
Table 3.2. ¹³ C NMR assignments (δ (J _{PC} (Hz), assnmt) ^{a,b,c} for imine and imine-derived complexes.....	54
Table 3.3. Selected crystallographic and refinement data for [<i>mer</i> -{κ-C,N,C'-(<i>p</i> - ^t Bu-Ar-2-yl)CH=NCH ₂ (2-py-NCH ₃ -3-yl)}(PMe ₃) ₃ Fe]OTf (7), <i>mer</i> -{κ-C,N,C'-(<i>p</i> - ^t Bu-Ar-2-yl)CHNCH(2-py-NCH ₃ -3-yl)}(PMe ₃) ₃ Fe (8), and [<i>mer</i> -κ-C,N,C'-(Ph-2-yl)CH ₂ N=CH(Ph-2-yl)}Fe(PMe ₃) ₃]OTf (14).....	59
Table 3.4. Selected distances (Å) and angles (°) for [<i>mer</i> -{κ-C,N,C'-(<i>p</i> - ^t Bu-Ar-2-yl)CH=NCH ₂ (2-py-NCH ₃ -3-yl)}(PMe ₃) ₃ Fe]OTf (7), <i>mer</i> -{κ-C,N,C'-(<i>p</i> - ^t Bu-Ar-2-yl)CHNCH(2-py-NCH ₃ -3-yl)}(PMe ₃) ₃ Fe (8), and [<i>mer</i> -κ-C,N,C'-(Ph-2-yl)CH ₂ N=CH(Ph-2-yl)}Fe(PMe ₃) ₃]OTf (14).....	60
Table 4.1. Selected crystallographic and refinement data for <i>cis,cis</i> -{κ-N,N'-(N-(2-pyridinylmethylene)neopentylamine)} ₂ -Fe(CH ₃) ₂ (1-neoPe), <i>cis</i> -{κ-N,N'-(N-(2-pyridinylmethylene)neohexylamine)} ₂ Fe(PhCCPh) (2-neoHex), <i>cis</i> -{κ-N,N'-(N-(2-pyridinylmethylene)alkylamine)} ₂ Fe(PMe ₃) (3-neoHex), and [<i>cis</i> -{κ-N,N'-(N-(2-pyridinylmethylene)neohexylamine)} ₂ Fe(PMe ₃)(CH ₃)]OTf (5-neoHex).....	93
Table 4.2. Selected distances (Å) and angles (°) for <i>cis,cis</i> -{κ-N,N'-(N-(2-pyridinylmethylene)neopentylamine)} ₂ -Fe(CH ₃) ₂ (1-neoPe), <i>cis</i> -{κ-N,N'-(N-(2-pyridinylmethylene)neohexylamine)} ₂ Fe(PhCCPh) (2-neoHex), <i>cis</i> -{κ-N,N'-(N-(2-pyridinylmethylene)alkylamine)} ₂ Fe(PMe ₃) (3-neoHex), and [<i>cis</i> -{κ-N,N'-(N-(2-pyridinylmethylene)neohexylamine)} ₂ Fe(PMe ₃)(CH ₃)]OTf (5-neoHex).....	94
Table 4.3. Reaction conditions for each attempted polymerization run.....	108

Table 5.1. Crystallographic data for <i>trans</i> -{ κ -C,N,C'-(2,4,5-trifluorophen-2-yl)CH=N-CH ₂ (3,4,5-trifluorophen-2-yl)}Fe(PMe ₃) ₂ (N ₂) (1 -(N ₂)).....	117
--	-----

PREFACE

The field of transition metal catalysis is dominated by second- and third-row metals. These metals readily undergo two-electron processes, such as oxidative addition and reductive elimination, which are integral in many catalytic schemes. Recent investigations have shown that increased 6s/5d mixing in third-row versus second-row species contributes to a greater density of states in the latter.^{1,2} This access to lower energy pathways for second-row metals to greater reactivity for the second-row, perhaps best demonstrated by the wealth of palladium chemistry versus that of its platinum neighbor.³

By analogy, first-row metals should show even greater reactivity because of a greater density of states.⁴ A major impetus for developing first-row metal catalysts is their greater availability, lower cost, and reduced toxicity. Unfortunately, the field strengths of the first row are smaller, and unproductive one-electron processes often dominate reaction behavior.⁵

One approach to this problem involves the use of ligands designed to increase the field strength of these metals. Simply thinking in an angular overlap context, carbon-based ligands should beget stronger fields than their nitrogen- or oxygen-containing counterparts, because of better orbital overlap and greater proximity

¹ Hirsekorn, K.F.; Hulley, E.B.; Wolczanski, P.T.; Cundari, T.R. *J. Am. Chem. Soc.* **2008**, *130*, 1183-1196.

² a) Kuiper, D.S.; Douthwaite, R.E.; Mayol, A.-R.; Wolczanski, P.T.; Lobkovsky, E.B.; Cundari, T.R.; Lam, O.P.; Meyer, K. *Inorg. Chem.* **2008**, *47*, 7139-7153. b) Kuiper, D.S.; Wolczanski, P.T.; Lobkovsky, E.B.; Cundari, T.R. *J. Am. Chem. Soc.* **2008**, *130*, 12931-12943. c) Kuiper, D.S.; Wolczanski, P.T.; Lobkovsky, E.B.; Cundari, T.R. *Inorg. Chem.* **2008**, *47*, 10542-10553.

³ a) Collman, J.P.; Hegedus, L.S.; Norton, J.R.; Finke, R.G. *Principles and Applications of Organotransition Metal Chemistry*; University Science Books: Mill Valley, CA, 1987. b) Crabtree, R.H. *The Organometallic Chemistry of the Transition Metals*, 4th Ed.; John Wiley & Sons: New York, 2005.

⁴ Figgis, B.N.; Hitchman, M.A. *Ligand Field Theory and Its Applications*; Wiley-VCH: New York, 2000.

⁵ a) Klinker, E.J.; Shaik, S.; Hirao, H.; Que, L. *Angew. Chem. Int. Ed.* **2009**, *48*, 1291-1295. b) Dhuri, S.N.; Seo, M.S.; Lee, Y.M.; Hirao, H.; Wang, Y.; Nam, W.; Shaik, S. *Angew. Chem. Int. Ed.* **2008**, *47*, 3356-3359. c) DeAngelis, F.; Jin, N.; Car, R.; Groves, J.T. *Inorg. Chem.* **2006**, *45*, 4268-4276.

between ligand and metal orbitals. The aim of this work is to design sp^2 -aryl-based chelates, with stabilizing pyridine, oxazoline, or imine functional groups, as strong-field ligands for first-row transition metals. Included in this goal is the observation of second- and third-row behavior, including ease of oxidation, in complexes of the first row.

CHAPTER 1

HETEROLYTIC C-H BOND ACTIVATION IN THE SYNTHESIS OF
NI{(2-ARYL-κC²)PYRIDINE-κN}₂ AND DERIVATIVES*

I. Introduction

A primary goal in this research is to generate strong fields and possibly high oxidation states of first-row metals by rational design or judicious choice of ligands. We have focused on aryl-, carbon-based ligands with chelating heteroatom donors, for reasons stated in the introduction, and commercially available 2-phenylpyridine fits neatly into this model.

As a chelating ligand, 2-phenylpyridine (2-ppy) is well-known in the organometallic literature. It has been widely explored in complexes of the form (2-ppy)₂M(L)(X) and (2-ppy)₃M (M = Co(III), Rh(III), Ir(III)).^{1,2,3,4} These group 9 metal species can be thought of as neutral analogues of cationic Ru(II) and Os(II) bipyridine derivatives; indeed, they exhibit similar photophysical behavior and have been applied to the development of electroluminescent devices.

Hafnium complexes with 2-phenylpyridylamido ligands have been present in the polymerization literature. They were first shown to polymerize isotactic propylene,⁵ and have since demonstrated living behavior for the polymerization of 1-hexene,⁶ and have been employed in the chain-shuttling synthesis of block copolymers.⁷

Sanford and coworkers have utilized the 2-phenylpyridine framework in a host of ligand-directed *ortho*-C-H functionalizations by palladium.⁸ Due to the relative ease with which Pd(II) undergoes cyclometalation reactions, and because of its tolerance for oxidizing agents, the Sanford group has realized useful catalysis in the formation

* Reproduced in part with permission from: Volpe, E. C.; Chadeayne, A. R.; Wolczanski, P. T.; Lobkovsky, E. B. *J. Organomet. Chem.* **2007**, 692, 4774-4783. Copyright 2007 Elsevier.

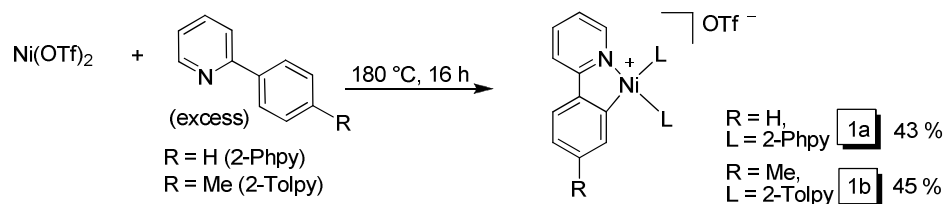
of new C-C, C-N, C-O, C-S, and C-X bonds. They have employed the 2-phenylpyridine ligand in mechanistic studies^{9,10,11} and in model compounds^{12,13} to investigate the details of these *ortho*-functionalization processes, and their success in doing so has helped to establish the paradigm of the (II/IV) catalytic couple in palladium chemistry.

Motivated by the atom-economical, cost-effective, simple virtues of cyclometalation by C-H activation, we sought a similar route to nickel complexes. Since first-row metals do not share the heavier metals' predilection for aryl C-H bonds, we foresaw the necessity of using an electrophilic metal center as our starting point. Acetates, trifluoroacetates, acetylacetonates, and triflates have been known to engender electrophilicity on metals, and hence a metal triflate became our readily available precursor in this study.

II. Results and Discussion

A. Synthesis of [bis(2-phenylpyridine)Ni{(2-phenyl- κ C²)pyridine- κ N}]OTf via heterolytic C-H bond activation.

Preliminary studies in our laboratory¹⁴ showed that heating a mixture of Ni(OTf)₂ in excess 2-phenylpyridine at 180 °C resulted in cyclometalation of one 2-phenylpyridine ligand to afford cationic [bis(2-phenylpyridine)Ni{(2-phenyl- κ C²)pyridine- κ N}]OTf (**1a**) (Scheme 1.1). A switch to 2-tolylpyridine introduced a convenient NMR handle, and led to increase solubility and a synthesis of **1b**. ¹H and ¹³C NMR data for all relevant diamagnetic compounds are listed in Tables 1.1 and 1.2.



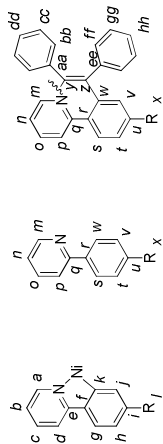
Scheme 1.1. Heterolytic C-H activation of 2-phenylpyridine using nickel(II)triflate.

Table 1.1. ^1H NMR data (d, J (Hz); benzene- d_6) for [bis(2-arylpyridine)Ni{(2-aryl- κC^2)pyridine- κN }]OTf (aryl = phenyl, **1a**; tolyl, **1b**), [(2-arylpyridine)BrNi{(2-aryl- κC^2)pyridine- κN }] (aryl = phenyl, **2a**; tolyl, **2b**), Ni{(2-aryl- κC^2)pyridine- κN }₂ (aryl = phenyl, **3a**; tolyl, **3b**), and [(2-aryl- κC^2)pyridine- κN][Ni[2-(2-(1,2-diphenylethenyl- κC^2)aryl)pyridine- κN] (aryl = phenyl, **4a**; tolyl, **4b**).^a

	<i>a</i> (i)	<i>b</i> (j)	<i>c</i> (k)	<i>d</i> (l)	<i>e</i> (m)	<i>f</i> (n)	<i>g</i> (o)	<i>h</i> (p)	<i>q</i> (r-aa)
1a	9.29(5.5)	6.08	6.46(8.5)	6.52	8.40(6.0)	7.12	7.12	5.49(8.0)	7.99(7.5)
1b	8.56(8.5)	6.76-6.87	6.58-6.64	6.76-6.87	7.99(7.5)	7.20-7.21	7.03	7.20-7.21	
	9.36(5.5)	6.06	6.47	6.66(8.0)	8.43(6.0)	6.73(8.0)	2.09	5.41	8.00
	8.50(8.5)	7.02	6.52-6.58	6.87	8.00	7.00	1.89, 1.91	7.08	
2a	9.94(7.0)	6.12(8.0)	6.56-6.63	6.83(5.0)	6.68-6.77	6.56-6.44	6.83	5.36(9.5)	8.90(9.0)
	9.45(6.5)	6.30(8.0)	6.97(9.5)	7.19	8.90(9.0)	6.68-6.77	7.19	6.68-6.77	
2b	9.54(5.5)	6.12(6.5)	6.60	6.67(8.0)	6.72-6.81	6.60	1.84	5.23	8.93(8.1)
	9.98(6.0)	6.33(6.5)	6.72-6.81	6.86(8.0)	8.93(8.0)	7.03(7.5)	1.98	7.03	
3a	7.72(5.0)	6.27(6.5)	6.92(7.8)	7.12(8.5)	7.31(7.5)	7.35(7.0)	7.15	8.39(7.5)	
3b	8.73(5.6)	6.26(8.0)	6.94(10.0)	7.01(8.4)	7.33(8.0)	7.36(8.0)	2.35	8.22	
4a	7.79(5.5)	6.28(7.0)	6.77(7.5)	7.22	7.43(7.5)	7.30	7.30	7.49(8.0)	
	7.06(7.5)	6.04(6.0)	6.85	7.22	7.30	7.11(7.5)	7.30	8.47(7.5)	6.86-7.01
4b	7.84(4.0)	6.28(5.0)	6.78	7.18	7.40(7.5)	7.34(7.5)	2.49	7.44	
	7.11(7.5)	6.04(5.0)	6.78	7.18	7.40(7.5)	7.34(7.5)	1.78	8.31	6.87-7.06

^a Shift assignments are based on correlations with free ligands, literature precedent and the accompanying compounds; the assignments are tentative. Coupling constants, where quoted, are phenomenological. First row corresponds to {(2-aryl- κC^2)pyridine- κN } ligand as shown in illustration; second row corresponds to remaining 2-arylpyridine or pyridine-derived fragment.

Table 2.1. $^{13}\text{C}\{^1\text{H}\}$ NMR data (benzene- d_6) for [bis(2-phenylpyridine)Ni{(2-phenyl- κC^2)pyridine- κN }]OTf (**1a**), [(2-arylpyridine)BrNi{(2-aryl- κC^2)pyridine- κN }] (aryl = phenyl, **2a**; tolyl, **2b**), Ni{(2-aryl- κC^2)pyridine- κN }}₂ (aryl = phenyl, **3a**; tolyl, **3b**), and [(2-aryl- κC^2)pyridine- κN]Ni[2-(2-(1,2-diphenylethenyl κC^2)aryl)pyridine- κN] (aryl = phenyl, **4a**; tolyl, **4b**).^{a,b}

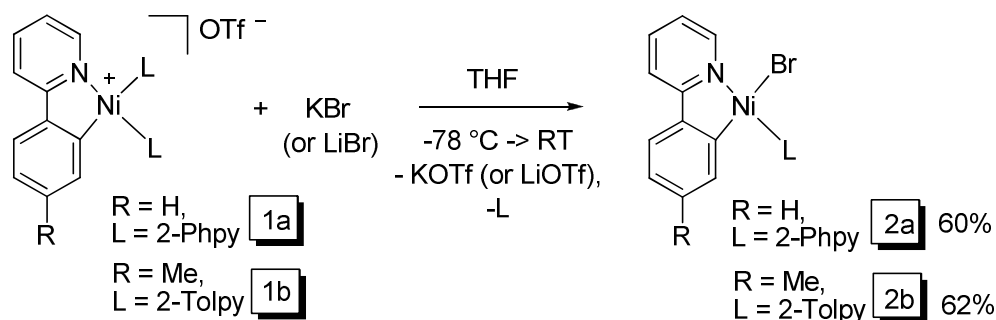


	a	b	c	d	e	f	g	h	i	j	k	l
m	n	o	p	q	r	s	t	u	v	w	x	
y	z	aa	bb	cc	dd	ee	ff	gg	hh	ii		
1a	153.4	117.5	125.6	138.4	163.3	147.2	130.2	123.2	127.7	122.5	162.8	
	139.0	122.3	122.8	130.4	143.6	138.3	129.4	128.7	c	128.7	129.4	
	150.7	121.1	125.8	136.0	148.9	140.6	129.8	129.3	129.2	129.3	129.8	
2a	153.8	117.2	125.6	138.0	164.6	147.1	134.5	c	124.9	122.2	162.1	
	156.2	121.7	c	130.0	151.1	141.3	136.9	128.9	122.4	128.9	136.9	
2b	153.7	117.0	125.5	137.9	164.7	144.6	135.4	c	138.5	122.1	162.2	21.5
	156.1	121.3	125.9	136.9	150.9	140.1	129.8	c	138.6	c	129.8	22.3
3a	148.9	118.4	121.7	142.7	165.4	147.7	124.2	137.1	130.4	122.3	165.1	
3b	148.8	118.1	121.3	143.6	165.5	145.3	125.2	137.0	139.8	122.1	165.2	22.5
4a	148.8	118.0	125.2	137.1	164.1	147.4	131.6	122.7	124.5	122.5	162.6	
	146.6	120.9	125.1	136.3	148.5	139.4	123.9	125.7	c	141.6	166.0	
	184.4	148.9	143.7	130.0	129.9	c	132.0	131.2	129.8	128.9		
4b	148.7	117.8	125.2	137.1	164.2	144.2	137.0	122.7	125.1	122.4	162.7	21.5
	146.6	120.5	125.1	136.2	145.0	139.8	124.3	124.9	c	142.6	166.1	23.0
	c	c	129.9	148.8	c	c	131.2	132.2	c			

^a Shift assignments are based on correlations with free ligands, literature precedent and the accompanying compounds; the assignments are tentative. First row corresponds to {(2-aryl- κC^2)pyridine- κN }} ligand as shown in illustration; second row corresponds to remaining 2-arylpyridine (**1a**, **2a**, **2b**) or pyridyl fragment (**4a**, **4b**); third row corresponds to other 2-phenylpyridine (**1a**) or diphenylacetylene fragment (**4a**, **4b**). ^b Limited solubility of **1b** prevented data acquisition. ^c Obscured by solvent or unobserved.

B. Synthesis of (2-arylpyridine)BrNi{(2-aryl- κC^2)-pyridine- κN }.

Substitution of triflate anion with a coordinating halide was explored as a means to a more soluble, neutral derivative. Removal of one pendant 2-arylpyridine ligand at this stage was also desirable, as the presence of the non-volatile liquid as a byproduct in subsequent substitution and alkylation attempts hampered isolation of clean material [*vide infra*]. Addition of excess KBr or LiBr to **1a** or **1b** afforded clean transformation to the corresponding bromides, (2-arylpyridine)BrNi{(2-aryl- κC^2)-pyridine- κN } (aryl = phenyl, **2a**; aryl = tolyl, **2b**) (Scheme 1.2). The 2-arylpyridine byproduct was easily washed away from the product with a THF/ether mixture.



Scheme 1.2. Formation of neutral (2-arylpyridine)BrNi{(2-aryl- κC^2)-pyridine- κN } via halide substitution.

X-ray diffraction quality crystals of **2a** were grown from THF/ether (Figure 1.1). Relevant crystallographic data are presented in Table 1.3. The crystal structure reveals square planar geometry about nickel and *trans* disposition of the bromide with respect to the aryl-carbon. This orientation is consistent with a greater *trans*-effect of the aryl carbon versus the 2-arylpyridine nitrogen. Isomerization was not observed in a variety of solvents, such as benzene, toluene, THF, or acetonitrile. We are unable to conclude whether **2a** and **2b** are the thermodynamic products, given the similar ranking of Br⁻ and pyridine in the *trans*-influence series.

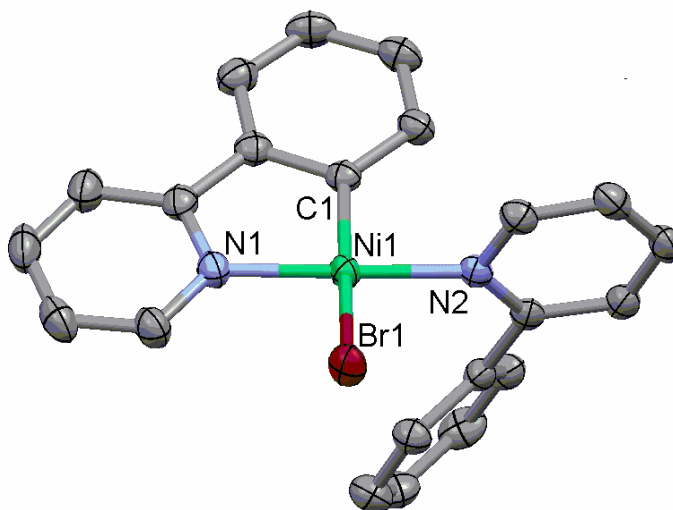


Figure 1.1. Molecular view of (2-phenylpyridine)BrNi{(2-aryl- κC^2)-pyridine- κN } (**2a**) with hydrogens omitted.

Table 1.3. Crystallographic data for (2-phenylpyridine)BrNi{(2-aryl- κC^2)-pyridine- κN } (**2a**) and [(2-phenyl- κC^2)pyridine- κN]Ni[2-(2-(1,2-diphenylethenyl- κC^2)phenyl)pyridine- κN] (**4a**).

Formula	C ₂₆ H ₂₅ BrN ₂ NiO	C ₃₆ H ₂₆ N ₂ Ni
Formula weight	520.10 ^a	545.30
Crystal system	Triclinic	Monoclinic
Space group	P-1	P2(1)/c
Z	2	4
a (Å)	10.001(3)	10.6170(5)
b (Å)	10.593(4)	16.0815(6)
c (Å)	11.718(4)	15.6065(6)
α (°)	81.212(18)	90
β (°)	71.227(18)	96.212(2)
γ (°)	84.383(18)	90
V (Å ³)	1160.0(7)	2648.97(19)
r_{calc} (g cm ⁻³)	1.489	1.367
μ (mm ⁻¹)	2.579	0.761
Temperature (K)	173(2)	173(2)
λ (Å)	0.71073	0.71073
Final R indices [I > 2 σ (I)] ^{b,c}	R ₁ = 0.0266, wR ₂ = 0.0679	R ₁ = 0.0333, wR ₂ = 0.0877
R indices (all data) ^{b,c}	R ₁ = 0.0384, wR ₂ = 0.0708	R ₁ = 0.0516, wR ₂ = 0.0952
Goodness-of-fit ^d	1.066	1.061

^a The asymmetric unit contains one formula unit and a molecule of THF, as does Z. ^b $R_1 = \sum ||F_o| - |F_c|| / \sum |F_o|$. ^c $wR_2 = [\sum w(|F_o| - |F_c|)^2 / \sum wF_o^2]^{1/2}$. ^d GOF (all data) = $[\sum w(|F_o| - |F_c|)^2 / (n - p)]^{1/2}$, n = number of independent reflections, p = number of parameters.

Table 1.4. Core distances (Å) and angles (°) for [(2-phenyl-pyridine)BrNi{(2-phenyl- κC^2)pyridine- κN }] (**2a**), Ni{(2-phenyl- κC^2)pyridine- κN }₂ (**3a**), and [(2-phenyl- κC^2)pyridine- κN]Ni[2-(2-(1,2-diphenylethenyl- κC^2)phenyl)pyridine- κN] (**4a**).

	2a	3a	4a
Ni- κC	1.9044(18)	1.887(2)	1.8911(10)
		1.892(2)	
Ni- κN	1.9169(16)	1.9794(16)	1.9556(9)
		1.9619(18)	
Ni-N($\kappa\text{N}'$)	1.9018(15)		1.9336(10) ^a
Ni-Br	2.4410(7)		
Ni- $\kappa\text{C}'$			1.8844(10) ^a
C'=C			1.3462(15) ^a
κN -Ni- κC	84.62(7)	84.66(8)	84.78(4)
		84.73(8)	
Ni- κC -C	112.60(13) ^b	113.26(15) ^b	113.07(8) ^b
	130.09(14) ^c	130.23(16) ^c	130.94(8) ^c
		112.73(16) ^b	
		130.48(17) ^c	
Ni- κN -C	115.25(12) ^b	112.46(13) ^b	113.69(7) ^b
	126.76(14) ^c	126.99(15) ^c	127.87(9) ^c
		113.95(14) ^b	
		126.32(15) ^c	
κN -Ni-N	173.29(6)		
κC -Ni-N	90.01(7)		
κN -Ni-Br	96.24(5)		
κC -Ni-Br	167.32(5)		
N-Ni-Br	89.89(5)		
$\kappa\text{N}'$ -Ni- $\kappa\text{C}'$			84.53(4) ^e
κN -Ni- $\kappa\text{C}'$		156.24(8) ^d	175.41(4) ^e
		161.08(8) ^d	171.61(4) ^e
κN -Ni- $\kappa\text{N}'$		101.27(7) ^d	97.42(4) ^e
κC -Ni- $\kappa\text{C}'$		97.07(9) ^d	93.87(5) ^e
Ni- $\kappa\text{C}'$ -C(Ph)			115.81(8) ^e
Ni- $\kappa\text{C}'$ =C			119.79(8) ^e
^a Prime refers to carbon of cyclometalate insertion ring. ^b Internal cyclometalate angle. ^c External cyclometalate angle. ^d Angles defined with primes are between two different cyclometalates. ^e Angles defined with primes are between the cyclometalate and the cyclometalate insertion ring (primed).			

The N1-Ni1-C1 angle of 84.62(7)° is moderately diminished from 90° due to the chelate bite angle. In addition, the difference in the internal Ni-C1-C angle

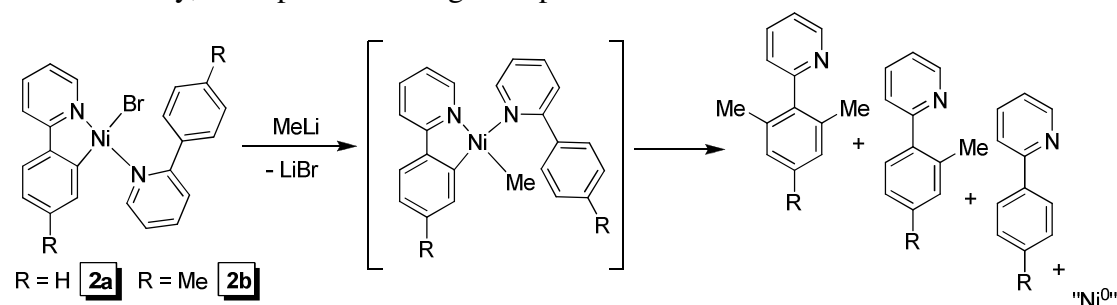
(112.60(13)°) versus the corresponding external Ni-C1-C angle (130.09(14)°) reflects constraint of the chelate. Additional pertinent distances and angles of **2a** are listed in Table 1.4.

C. Alkylation attempts on (2-arylpyridine)BrNi{(2-aryl-κC²)-pyridine-κN}.

With **2a** and **2b** in hand, we sought to prepare an alkyl derivative. Having an additional metal-carbon bond would presumably increase the field of the nickel compound. Also, a nickel-methyl complex could be seen as a neutral analogue to Brookhart's well-studied cationic α-diimine nickel-methyl catalysts for olefin polymerization.¹⁵ Anionic ligands for nickel catalysts of this kind are known,¹⁶ but very few are κ-C,N chelates.¹⁷

In previous attempts to alkylate **1a** using various aryl or alkyllithium reagents, a fleeting red intermediate was observed en route to eventual deleterious metal reduction. Low-temperature reactions of **2a** or **2b** with either MeLi or Me₂Zn also produced red solutions, along with black solid assumed to be Ni⁰. The NMR spectrum of the reaction mixture included new aromatic resonances and a three-proton singlet at 0.52 ppm, which could be reasonably assigned as a Ni-CH₃. Analysis of the reaction mixture by GC-MS revealed the presence of 2-(*o*-tolyl)pyridine and 2-(2,6-xylyl)pyridine in a 2:1 ratio. These products could result from reductive elimination from a putative {(2-aryl-κC²)-pyridine-κN}Ni(CH₃) fragment, as shown in Scheme 1.3.

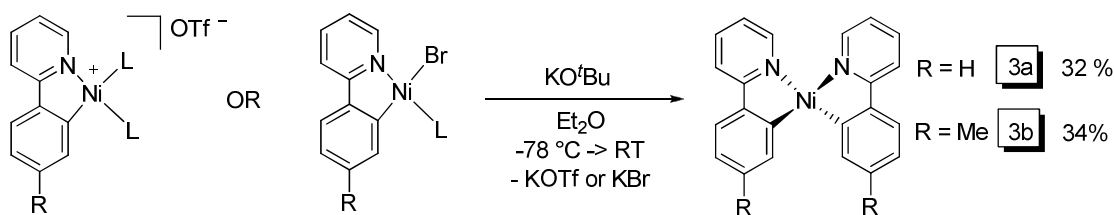
Unfortunately, attempts at isolating this species were unsuccessful.



Scheme 1.3. Methylation attempts with (2-arylpyridine)BrNi{(2-aryl-κC²)-pyridine-κN} and presumed reductive elimination products.

D. Synthesis of Ni{(2-phenyl- κ C²)pyridine- κ N}₂.

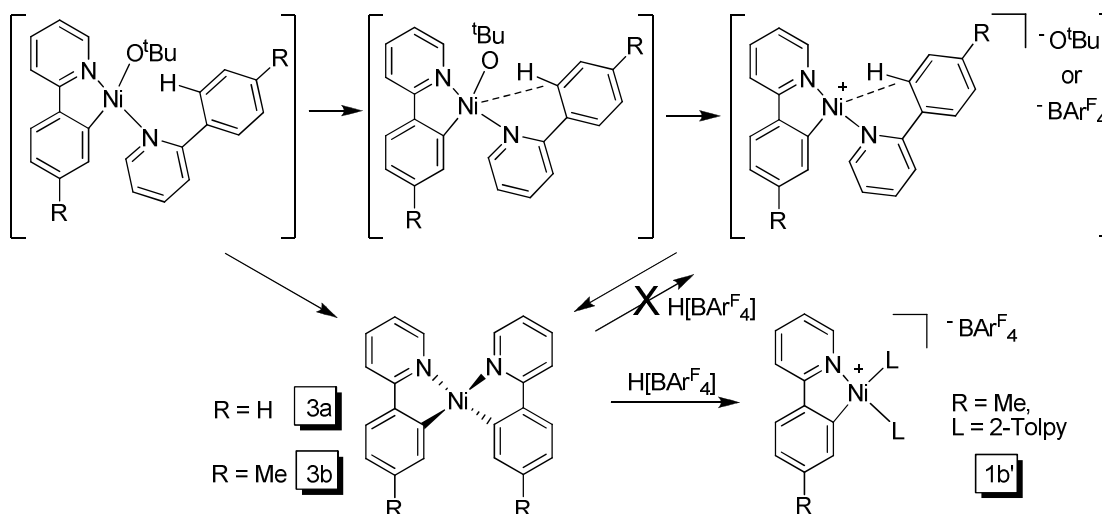
Attempts at alkoxide or aryloxide substitution on **1a** were also made. While treatment of **1a** with PhOLi resulted in no reaction after one week at room temperature, a new red material was isolated following treatment of **1a** with KO^tBu. This new product was identified, not as the nickel alkoxide, but as the doubly cyclometalated compound, Ni{(2-phenyl- κ C²)pyridine- κ N}₂ (**3a**).¹¹ This result could also be obtained by the reaction of **2a** or **2b** with KO^tBu, producing **3a** or **3b** more cleanly and in more reproducible yields (Scheme 1.4).



Scheme 1.4. Activation of second arylpyridine to form Ni{(2-aryl- κ C²)pyridine- κ N}₂.

It is interesting to note that **3a** and **3b** arise from the reaction with KO^tBu but not from an intermediate Ni-CH₃ complex. Two possible mechanisms for this transformation are presented in Scheme 1.5. If a Ni-O^tBu complex forms, an abstraction of one *ortho*-CH could lead directly to the formation of **3a** or **3b**. The increased electrophilicity of the Ni-O^tBu intermediate compared to the corresponding Ni-CH₃ intermediate could render this pathway feasible. Another possibility involves dissociation of Bu^tO⁻ to form a cationic complex with nickel bound to an *ortho*-CH-bond. Subsequent deprotonation at the activated CH-position by Bu^tO⁻ would lead to the observed product. An attempt was made to generate a similar cationic intermediate, by treating **3b** with one equivalent of H[BAr^F₄] (BAr^F₄ = B(3,5-(CF₃)₂C₆H₃)₄). Instead of the desired result, this reaction produced [bis(2-phenylpyridine)Ni{(2-phenyl- κ C²)pyridine- κ N}][BAr^F₄] (**1b'**), presumably by

disproportionation of the starting materials. As confirmation of this fact, the stoichiometric equivalent of the reaction was performed: $3/2 \mathbf{3b} + 2 \text{H}[\text{BAr}^{\text{F}}_4] \rightarrow \mathbf{1b}' + 1/2[\text{Ni(II)}][\text{BAr}^{\text{F}}_4]_2$, which produced expected amounts of $\mathbf{1b}'$. Additional minor BAr^{F}_4 resonances were observed, which could be attributed to a “[Ni(II)][BAr^F₄]₂” byproduct.

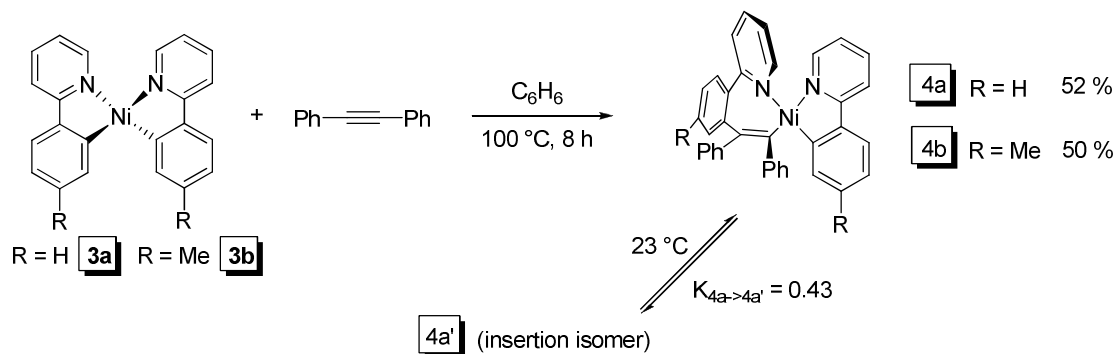


Scheme 1.5. Possible pathway for reaction of (2-arylpyridine)BrNi{(2-aryl-κC²)-pyridine-κN} with KO^tBu.

E. Synthesis of [(2-aryl-κC²)pyridine-κN]Ni[2-(2-(1,2-diphenylethenyl)-κC²)aryl]pyridine-κN].

In line with our assertion that carbon-based ligands should stabilize stronger fields, we sought to produce a five-coordinate derivative of Ni{(2-aryl-κC²)pyridine-κN}₂ (**3a**, **3b**). We reasoned that diphenylacetylene in the additional coordination site would satisfy the constraint of having two chelates with a restrictive bite angle (~85 °). When Ni{(2-aryl-κC²)pyridine-κN}₂ (aryl = phenyl, **3a**; tolyl, **3b**) was treated with diphenylacetylene, we observed the insertion of the PhCCPh moiety into one of Ni-C bonds to afford [(2-aryl-κC²)pyridine-κN]Ni[2-(2-(1,2-diphenylethenyl-

κC^2 aryl)pyridine- κN] (aryl = phenyl, **4a**; tolyl, **4b**) (Scheme 1.6). A view of **4a** as determined by X-ray crystallography is shown in Figure 1.2. In solution, **4a** converts to an equilibrium mixture with another compound (**4a'**) that exhibits a similar NMR spectrum. Presumably there is appreciable flexibility in the seven-membered ring of the metallacycle, which allows for the possibility of a conformational isomer.



Scheme 1.6. Reaction of $Ni\{(2\text{-aryl-}\kappa C^2)\text{pyridine-}\kappa N\}_2$ with diphenylacetylene.

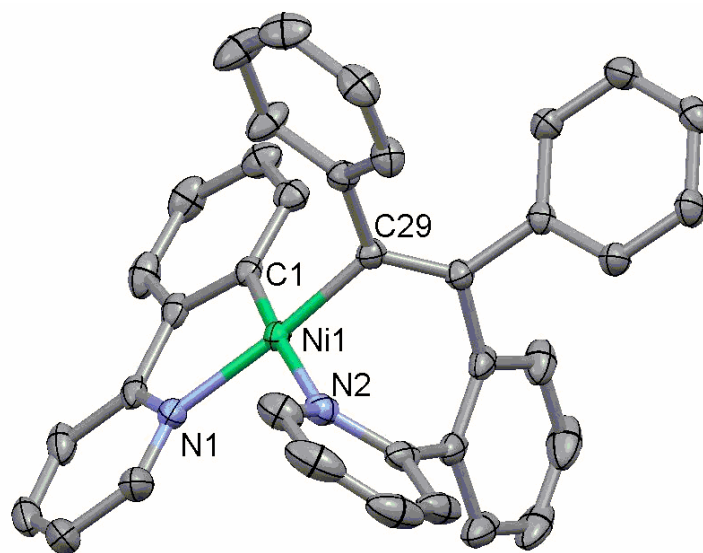


Figure 1.2. Molecular view of $[(2\text{-phenyl-}\kappa C^2)\text{pyridine-}\kappa N]Ni[2\text{-(2-(1,2-diphenylethenyl-}\kappa C^2)\text{phenyl)pyridine-}\kappa N]$ (**4a**) with hydrogens omitted.

Relevant crystallographic data regarding the structure of **4a** are provided in Table 1.1, and pertinent bond distances and angles are listed in comparison with those

for **2a** and **3a** in Table 1.2. The 2-phenylpyridine chelate angle, $\kappa\text{N-Ni-}\kappa\text{C}$ ($84.78(4)^\circ$), and Ni- κC and Ni- κN distances ($1.8911(10)$ and $1.9556(9)$ Å, respectively) effectively match those of **3a**. In fact, the molecule retains a nearly undistorted square planar geometry overall, due to the ability of the seven-membered chelate to undergo distortion itself.

F. Molecular orbital description of Ni{(2-phenyl- κC^2)pyridine- κN }₂.

In light of our goal that carbon-based ligands should impart strong fields, a rudimentary DFT calculation was performed on Ni{(2-phenyl- κC^2)pyridine- κN }₂ (**3a**) (see section IV.C. for computational details). The resulting molecular orbital picture reflects the standard description for a square-planar Ni(II) species, with a high-energy anti-bonding $d_{x^2-y^2}$ orbital and effectively non-bonding d_{z^2} , d_{yz} , d_{xy} , and d_{xz} orbitals (Figure 1.3). However, the calculated HOMO-LUMO gap of roughly 5 eV ($10Dq \sim >40,000\text{ cm}^{-1}$) is fairly enormous. While these calculated energies should not be read in an absolute sense,^{18,19} even a conservative interpretation may conclude that this energy gap is greater than one would predict for N-, O-, or X-type donors. Furthermore, the position of d_{z^2} contradicts our prediction based on the distortion of the two chelates with respect to one another. We had thought that this “twist” might decrease the antibonding character of d_{z^2} , yet it remains the HOMO.

Additional computational insight was gained by performing a geometry optimization on the unobserved *trans*- $\kappa\text{N-}\kappa\text{N}$ configuration of Ni{(2-aryl- κC^2)pyridine- κN }₂. The optimized structure maintained bond distances and angles in keeping with those of the *cis* conformation. An energy minimum calculation of the *trans*-isomer revealed it to be ~ 3 kcal/mol higher in energy than the *cis* (Scheme 1.7), a finding that supports the stronger *trans*-influence of aryl ligands compared to pyridine.

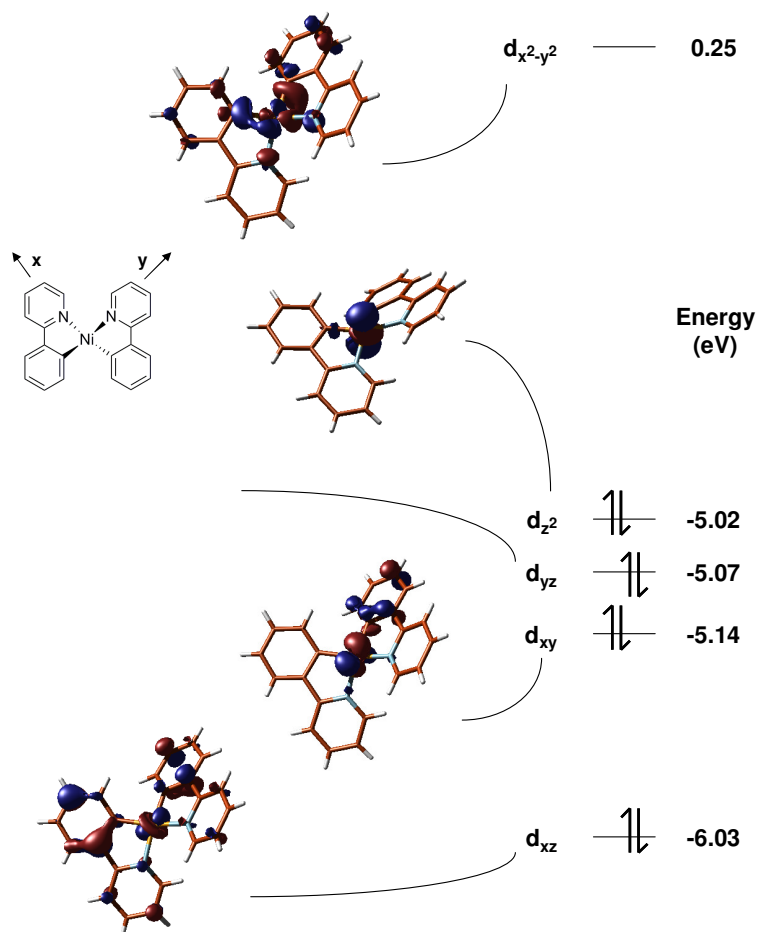
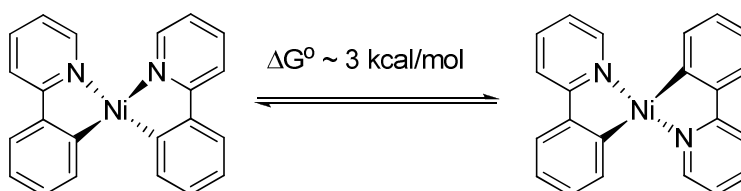


Figure 1.3. DFT-calculated molecular orbital picture of **3a**.



Scheme 1.7. DFT-calculated energy comparison of cis and trans isomers of **3a**.

III. Conclusions

We have synthesized a small series of cyclometalated, (2-aryl- κC^2)pyridine- κN -based nickel(II) complexes via heterolytic CH-bond-activation. This result

suggests that certain catalytic processes involving *ortho*-metalation with palladium or platinum may be possible with their first-row counterpart, provided the nickel center is sufficiently electrophilic. Each pseudo-square planar complex is low-spin and diamagnetic, lending support to the claim that carbon-based ligands should impart strong fields. The strong-field carbon ligand hypothesis is also borne out in the calculation of Ni{(2-aryl- κ C²)pyridine- κ N}₂ (**3a**), which contains two such metal-carbon bonds. We were not able to isolate a neutral nickel-methyl complex, though observed reductive elimination products from methylation attempts suggest that target as a possible intermediate. Finally, reaction of Ni{(2-aryl- κ C²)pyridine- κ N}₂ (**3a**) with diphenylacetylene resulted not in adduct formation, but insertion into one metal-carbon bond. Such an outcome indicates possible limitations of the 2-arylpyridine ligand due to its unyielding bite angle.

IV. Experimental

A. General Considerations

All manipulations were performed using either glovebox or high-vacuum techniques. Hydrocarbon and ethereal solvents were dried over and vacuum transferred from sodium benzophenone ketyl (3–4 mL tetraglyme/L were added to hydrocarbons). Benzene-*d*₆ was sequentially dried over sodium and stored over sodium or 4 Å molecular sieves. All glassware was base-washed and oven dried. Nickel(II)triflate was prepared according to literature procedures.²⁰

Diphenylacetylene (Aldrich) was used as received; 2-phenylpyridine and 2-*p*-tolylpyridine (Aldrich) were degassed and stored under nitrogen; KBr (Mallinckrodt) and LiBr (Aldrich) were dried for 4 days in a 150 °C oven and stored under nitrogen. KO^tBu (Alfa Aesar) was sublimed and stored under nitrogen. ¹H- and ¹³C{¹H}-NMR spectra were obtained using Mercury-300, Inova-400, and Inova-500 spectrometers.

Combustion analyses were performed by Robertson Microlit Laboratories, Madison, NJ.

B1. [bis(2-aryl-pyridine)Ni{(2-aryl- κ C²)pyridine- κ N}]OTf (aryl = phenyl, **1a; tolyl, **1b**; OTf = trifluoromethanesulfonate).**

A neat mixture of nickel(II)triflate (10.0 g, 28.0 mmol) and 2-phenylpyridine (20.0 g, 118 mmol) was heated at 180 °C in a bomb reaction vessel for 18 h. The resulting dark brown oil was triturated with THF (60 mL), giving a brown solution with yellow solid. This mixture was filtered and washed with THF (3 x 20 mL) to yield 8.5 g of yellow solid (43 %). Recrystallization of **1a** from hot toluene resulted in formation of bright yellow crystals suitable for X-ray diffraction. The same procedure was followed for **1b**, yielding a yellow-green solid (45 %).

B2. (2-aryl-pyridine)BrNi{(2-aryl- κ C²)pyridine- κ N} (aryl = phenyl, **2a; tolyl, **2b**)**

To a mixture of **1a** (1.49 mmol) and KBr (2.00 g, 16.8 mmol) was distilled 20 mL THF at -78 °C. A dark orange color developed as the solution was warmed to 23 °C and stirred for 10 min. After stirring for 6 h, the amber solution was filtered, the salt cake washed several times with THF, and the filtrate reduced in volume to 5 mL. Ether (15 mL) was added and the mixture was stirred for 10 min at 23 °C, yielding 400 mg (60 %) of bright orange solid (**2a**) which was collected by filtration. The same procedure was followed for **2b** except that LiBr was used in place of KBr. A red-orange solid was isolated in 62 % yield. Anal. Calcd. for H₂₁C₂₄BrN₂Ni (**4b**): C, 60.55; H, 4.45; N, 5.88. Found: C, 60.33; H, 4.73; N, 5.59.

B3. Ni{(2-aryl- κ C²)pyridine- κ N}₂ (aryl = phenyl, **3a; tolyl, **3b**)**

To a 250 mL flask charged was added **2a** (2.00 g, 5.45 mmol) and KO^tBu (612 mg, 5.45 mmol) and attached to a swivel frit was distilled 100 mL ether at -78 °C. The solution was allowed to warm to 23 °C and stirred for 3 h. Upon warming, the solution attained a dark red color. The resulting solution was filtered through the frit, the solid

washed five times with ether, and the red solution concentrated to 10 mL and cooled to -78 °C. This was filtered cold to leave a red solid (536 mg, 32 %). X-ray diffraction quality crystals were obtained by cooling a concentrated solution of the solid in ether to -35 °C. The same procedure was followed for **3b** with **2b** as the starting material (34 %). Anal. Calcd. for H₂₀C₂₄N₂Ni (**2b**): C, 72.95; H, 5.10; N, 7.09. Found: C, 70.55; H, 4.84; N, 6.80.

B4. [(2-aryl-κC²)pyridine-κN]Ni[2-(2-(1,2-diphenylethenyl-κC²)aryl)pyridine-κN] (aryl = phenyl, **4a; tolyl, **4b**).**

To a bomb reaction vessel of **3a** (70.0 mg, 0.191 mmol) and diphenylacetylene (34.0 mg, 0.191 mmol) were distilled 10 mL benzene at -78 °C. The vessel was allowed to warm to 23 °C and then placed in a 35 °C oil bath. This was slowly heated to 100 °C and remained at this temperature for 8 h. The resulting dark solution was stripped of solvent, triturated with ether, and filtered to give 54 mg of orange-brown solid (52 % yield). Layering a solution of **4a** in toluene with hexanes yielded orange-red, X-ray diffraction quality crystals. Leaving **4a** in benzene solution led to the appearance of a new product by ¹H NMR, proposed to be a conformational isomer (**4a'**). K_{eq} (**4a** → **4a'**) = 0.43. ¹H NMR (benzene-*d*₆): δ 9.05 (d, 1H, J = 6.0), 8.51 (d, 1H, J = 5.0), 8.06 (d, 1H, J = 5.5), 7.58 (d, 1H, J = 7.5), 7.51 (m, 1H), 7.28-6.75 (m, 17H), 6.52 (d, 2H, J = 5.5), 6.34 (“t,” 1H, J = 6.0), 6.19 (“t,” 1H, J = 6.0). The same procedure was followed for **4b**, which was isolated as an orange-brown solid (50 %).

C. Calculation Details

All calculations were done using the Gaussian 03 program.²¹ Computations were performed at the B3PW91 level of theory, employing Becke's three-parameter hybrid DFT/HF exchange functional²² and Perdew and Wang's nonlocal exchange parameter.²³ The CEP-31G effective core potential basis set was used.^{24,25,26} Atomic

coordinates from the X-ray structure of **3a** were used, and in all cases geometry optimizations were carried out without symmetry constraints.

REFERENCES

- 1) Dedelan, K.; Djurovich, P. I.; Garces, F. O.; Carlson, G.; Watts, R. J. *Inorg. Chem.* **1991**, *30*, 1685-1687.
- 2) Grushin, V.; Herron, N.; LeCloux, D. D.; Marshall, W. J.; Petrov, V. A.; Wang, Y. *J. Chem. Soc. Chem. Comm.* **2001**, 1494.
- 3) Lamansky, S.; Djurovich, P. I.; Murphy, D.; Razzaq-Abdel, F.; Lee, H.-E.; Adachi, C.; Burrows, P. E.; Forrest, S. R.; Thompson, M. E. *J. Am. Chem. Soc.* **2001**, *123*, 4304-4312.
- 4) Tamayo, A.; Alleyne, B.; Djurovich, P.I.; Lamansky, I.T.; Ho, N.; Bau, R.; Thompson, M.E. *J. Am. Chem. Soc.* **2003**, *125*, 7377-7387.
- 5) Boussie, T. R.; Diamond, G. M.; Goh, C.; Hall, K. A.; LaPointe, A. M.; Leclerc, M. K.; Murphy, V.; Shoemaker, J. A.W.; Turner, H.; Rosen, R. K.; Stevens, J. C.; Alfano, F.; Busico, V.; Cipullo, R.; Talarico, G. *Angew. Chem. Int. Ed.* **2006**, *45*, 3278-3283.
- 6) Domski, G. J.; Lobkovsky, E. B.; Coates, G. C. *Macromolecules* **2007**, *40*, 3510-3513.
- 7) Arriola, D. J.; Carnahan, E. M.; Hustad, P. D.; Kuhlman, R. L.; Wenzel, T. T. *Science* **2006**, *312*, 714-719.
- 8) Lyons, T. W.; Sanford, M. S. *Chem. Rev.* **2010**, *110*, 1147-1169.
- 9) Hull, K. L.; Lanni, E. L.; Sanford, M. S. *J. Am. Chem. Soc.* **2006**, *128*, 14047-14049.
- 10) Stowers, K. J.; Sanford, M. S. *Org. Lett.* **2009**, *131*, 4584-4587.
- 11) Deprez, N. R.; Sanford, M. S. *J. Am. Chem. Soc.* **2009**, *131*, 11234-11241.
- 12) Whitfield, S. R.; Sanford, M. S. *J. Am. Chem. Soc.* **2007**, *129*, 15142-15143.
- 13) Racowski, J. M.; Dick, A. R.; Sanford, M. S. *J. Am. Chem. Soc.* **2009**, *131*, 10974-10983.
- 14) Chadeayne, A. R. Thesis/Dissertation. Cornell University. 2006.

- 15) Johnson, L. K.; Killian, C. M.; Brookhart, M. *J. Am. Chem. Soc.* **1995**, *117*, 6414-6415.
- 16) Ittel, S. D.; Johnson, L. K.; Brookhart, M. *Chem. Rev.* **2000**, *100*, 1169-1203.
- 17) Gibson, V. C.; Spitzmesser, S. K. *Chem. Rev.* **2003**, *103*, 283-315.
- 18) a) Poli, R.; Cacelli, I. *Eur. J. Inorg. Chem.* **2005**, *12*, 2324-2331. b) Petit, A.; Cacelli, I.; Poli, R. *Chem.-Eur. J.* **2006**, *12*, 813-823.
- 19) Zhang, G.; Musgrave, C. B. *J. Phys. Chem. A* **2007**, *111*, 1554-1561.
- 20) Inada, Y.; Nakano, Y.; Inamo, M.; Nomura, M.; Funahashi, S. *Inorg. Chem.* **2000**, *39*, 4793.
- 21) Frisch, M. J.; Trucks, G. W.; Schlegel, H. B.; Scuseria, G. E.; Robb, M. A.; Cheeseman, J. R.; Montgomery, Jr., J. A.; Vreven, T.; Kudin, K. N.; Burant, J. C.; Millam, J. M.; Iyengar, S. S.; Tomasi, J.; Barone, V.; Mennucci, B.; Cossi, M.; Scalmani, G.; Rega, N.; Petersson, G. A.; Nakatsuji, H.; Hada, M.; Ehara, M.; Toyota, K.; Fukuda, R.; Hasegawa, J.; Ishida, M.; Nakajima, T.; Honda, Y.; Kitao, O.; Nakai, H.; Klene, M.; Li, X.; Knox, J. E.; Hratchian, H. P.; Cross, J. B.; Adamo, C.; Jaramillo, J.; Gomperts, R.; Stratmann, R. E.; Yazyev, O.; Austin, A. J.; Cammi, R.; Pomelli, C.; Ochterski, J. W.; Ayala, P. Y.; Morokuma, K.; Voth, G. A.; Salvador, P.; Dannenberg, J. J.; Zakrzewski, V. G.; Dapprich, S.; Daniels, A. D.; Strain, M. C.; Farkas, O.; Malick, D. K.; Rabuck, A. D.; Raghavachari, K.; Foresman, J. B.; Ortiz, J. V.; Cui, Q.; Baboul, A. G.; Clifford, S.; Cioslowski, J.; Stefanov, B. B.; Liu, G.; Liashenko, A.; Piskorz, P.; Komaromi, I.; Martin, R. L.; Fox, D. J.; Keith, T.; Al-Laham, M. A.; Peng, C. Y.; Nanayakkara, A.; Challacombe, M.; Gill, P. M. W.; Johnson, B.; Chen, W.; Wong, M. W.; Gonzalez, C.; Pople, J. A. Gaussian 03, revision C.02, Gaussian, Inc., Wallingford CT, 2004.
- 22) Becke, J. M. *J. Chem. Phys.* **1993**, *98*, 5648-5652.
- 23) Perdew, J. P., et. al. *Phys. Rev. B* **1992**, *46*, 6671-6687.

- 24) Stevens, W. J.; Basch, H.; Krauss, M. *J. Chem. Phys.* **1984**, *81*, 6026-6033.
- 25) Stevens, W. J.; Krauss, M.; Basch, H.; Jaisn, P. G. *Can. J. Chem.* **1992**, *70*, 612-630.
- 26) Cundari, T. R.; Stevens, W. J. *J. Chem. Phys.* **1993**, *98*, 5555.

CHAPTER 2

SYNTHETIC INVESTIGATIONS OF OXAZOLINE-BASED ARYL ANIONS WITH 1ST-ROW TRANSITION METALS; STRUCTURES OF (κ -C,N-{(*o*- C₆H₄)CMe₂(COCH₂CMe₂N)}FeCl(py) AND [κ -C,N-{(*o*- C₆H₄)CMe₂(COCH₂CMe₂N)}Cr(μ -Cl)]₂

I. Introduction

Initial forays into the development of strong-field, metal aryl complexes suggest that the design of a tunable ligand is key. C-H activation efforts with the 2-phenylpyridine ligand demonstrated the importance of solubility and bite angle with regard to their role in metalation, isolation, and reactivity. It is clear that additional factors such as steric bulk, chirality, and coordination number can influence future catalytic endeavors, and a ligand which can be easily modified is desirable.

Our next efforts with aryl-based ligands sought to incorporate oxazolines, a class of ligands which have been known in the literature for their versatility. Their facile synthesis from carboxylic acids or nitriles with potentially chiral, amino acid-derived amino alcohols enables the modular design of a wide range of ligands. Aryl oxazolines have already been employed in catalysis using 2nd- and 3rd-row transition metals,¹ with the workhorse ligand being the 2,6-bis(2-oxazolinyl)phenyl (Phebox) entity.² Some manganese,³ nickel,⁴ and copper^{5,6} oxazoline complexes have also been synthesized, and the isolation of new low-spin, 1st-row complexes containing this convenient functional group seemed quite plausible.

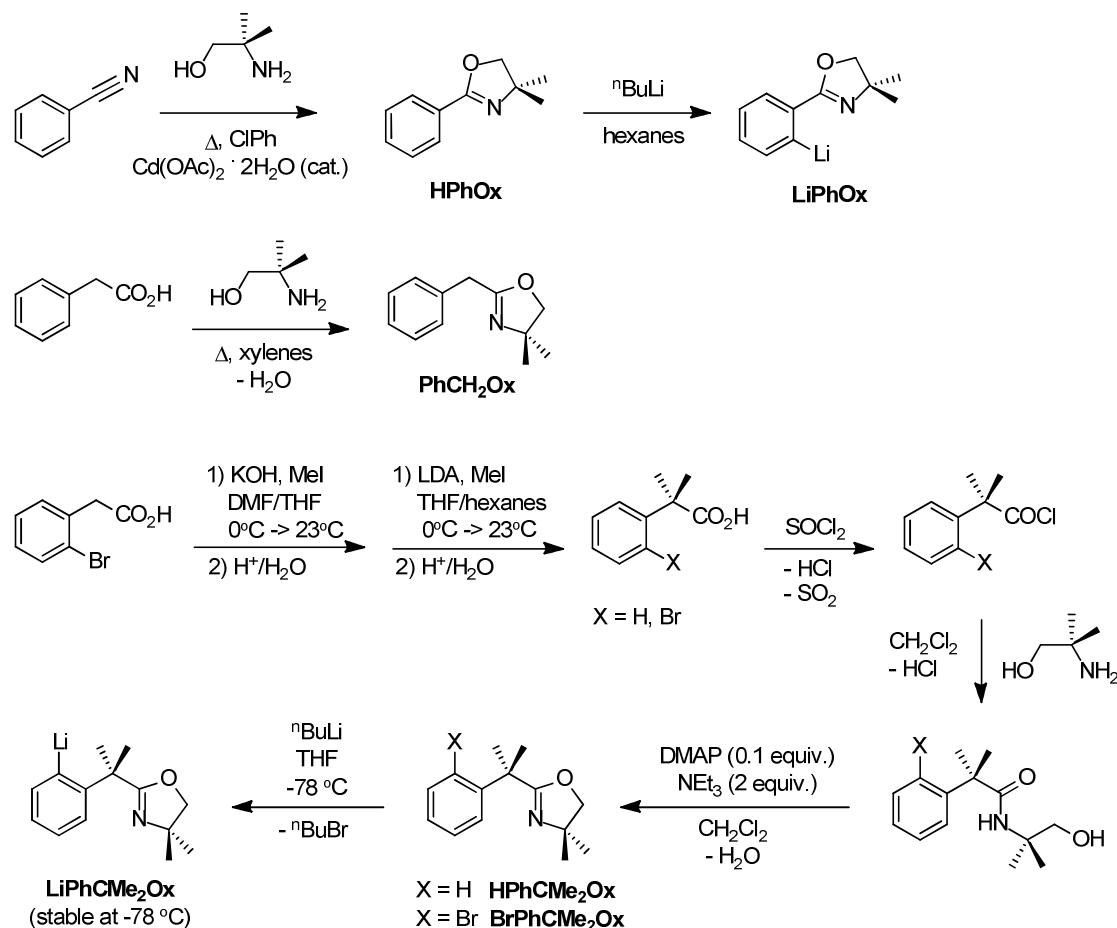
II. Results and Discussion

A. Ligand Syntheses.

Oxazoline ligands were prepared according to literature procedures or by adaptation of procedures for related compounds (Scheme 2.1). 2-phenyloxazolines are readily derived from benzonitrile by refluxing with the appropriate aminoalcohol and catalytic $\text{Cd}(\text{OAc})_2 \cdot 2\text{H}_2\text{O}$ in chlorobenzene. Using 2-amino-2-methyl-1-propanol, 4,4-dimethyl-2-phenyloxazoline (**HPhOx**) was prepared in 80% yield. The two methyl groups were incorporated with future solubility in mind and as an additional NMR handle. In a similar manner, 2-pyridylacetonitrile was converted to 4,4-dimethyl-2-(2-pyridylmethyl)oxazoline (**PyCH₂Ox**). Successful ortho-lithiation of **HPhOx** was achieved with $^n\text{BuLi}$ in hexanes to form **LiPhOx**, which was used on an *in situ* basis due to its moderate instability. Simple condensation of phenylacetic acid with 2-amino-2-methyl-1-propanol in xylenes, using a Dean-Stark trap, yielded 4,4-dimethyl-2-benzyloxazoline (**PhCH₂Ox**).

Dimethyl substitution on the methylene bridge necessitated modification of the oxazoline syntheses, as the increased steric congestion impeded the progress of simple condensation routes. The *ortho*-brominated derivative of 2-phenyl-2-methylpropionic acid (*o*-XArCMe₂COOH, X = Br) was unavailable for purchase, so double methylation of *o*-bromophenylacetic acid was achieved in two steps by a modified literature procedure. The first methyl group could be installed by mild deprotonation with KOH, followed by methyl iodide; the more basic $\text{LiN}(\text{iPr})_2$ was necessary for removal of the second proton and subsequent methylation. Carboxylic acids *o*-XArCMe₂COOH (X = H, Br) were converted to the more activated acid chlorides by refluxing in neat SOCl_2 . Treatment of crude products with 2-amino-2-methyl-1-propanol and base afforded the corresponding amides, which underwent cyclization using triethylamine and catalytic 4-DMAP to the oxazoline derivatives **HPhCMe₂Ox**

and **BrPhCMe₂Ox**, respectively. Lithium-halogen exchange of **BrPhCMe₂Ox** with ⁿBuLi generated aryllithium, **LiPhCMe₂Ox**, which was stable at -78 °C.



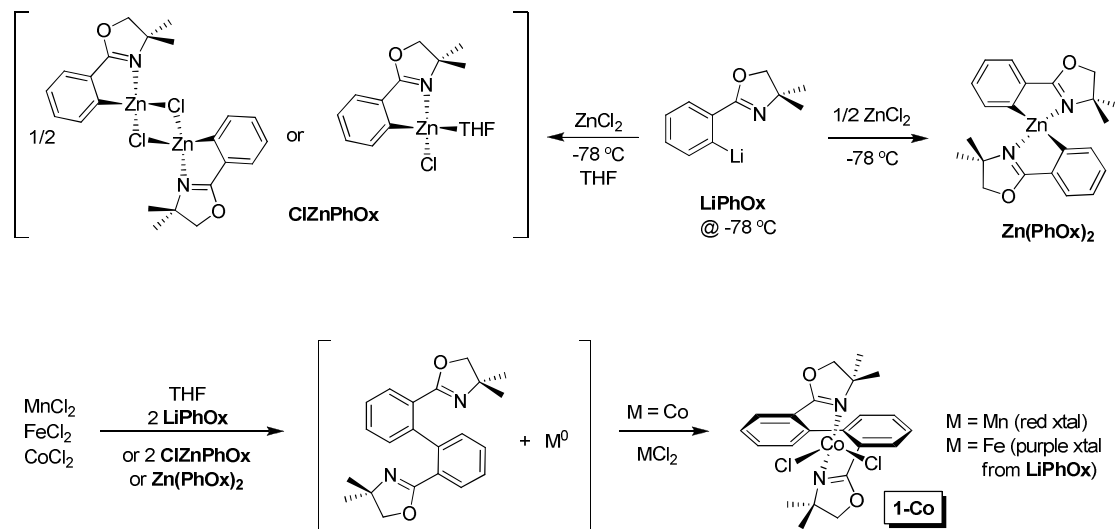
Scheme 2.1. Syntheses of various oxazoline ligands.

B. First-row metal reactivity with 4,4-dimethyl-2-phenyloxazoline.

1. Synthesis of Zn(PhOx)₂.

Due to the moderate degradation of ortho-lithiated **LiPhOx** in the solid state, a stable, isolable source of OxPh[−] was sought. Low-temperature generation of **LiPhOx**, followed by addition of one equivalent of ZnCl₂, led to the formation of **ClZnPhOx** (Scheme 2.2), which can be reasonably formulated as either the dimer, [(PhOx)ZnCl]₂, or the monomeric THF adduct, (PhOx)ZnCl(THF). A more well-defined organozinc

reagent was made using $\frac{1}{2}$ equivalent of ZnCl_2 , to yield Zn(PhOx)_2 as a white solid (80 %).



Scheme 2.2. Metalation of 4,4-dimethyl-2-phenyloxazoline on Zn, Fe, Co & Mn.

2. Reactivity with MCl_2 ($\text{M} = \text{Mn, Fe, Co}$).

With several metalating reagents in hand, chloride salts of manganese(II), iron(II), and cobalt(II) were chosen as starting materials. Reaction of these with two equivalents of either the lithium or zinc reagents resulted in isolation of a red crystalline solid for Mn(II), purple crystals for Fe(II), and blue-green crystals for Co(II). ^1H NMR spectroscopy of these reaction mixtures revealed paramagnetic products and the presence of coupled phenyloxazoline dimer, 4,4-dimethyl-(2-*o*- C_6H_4)-2-oxazoline, which was identified via comparison to a literature spectrum.⁷ Based on this information, the paramagnetic product was formulated to be the adduct, $[\kappa\text{-N,N}\{4,4\text{-Me}_2\text{-(2-}o\text{-C}_6\text{H}_4\text{)-2-oxazoline}\}_2]\text{CoCl}_2$ (**1-Co**), which was confirmed by X-ray crystallography (Figure 2.1). Formation of **1-Co** is likely to have occurred by initial metalation and reductive coupling of the phenyloxazoline, followed by ligation to remaining CoCl_2 . Observation of the organic dimer in mixtures of the analogous Fe

and Mn reactions implied that the paramagnetic products were likely adducts as well, therefore further characterization of these compounds was not pursued.

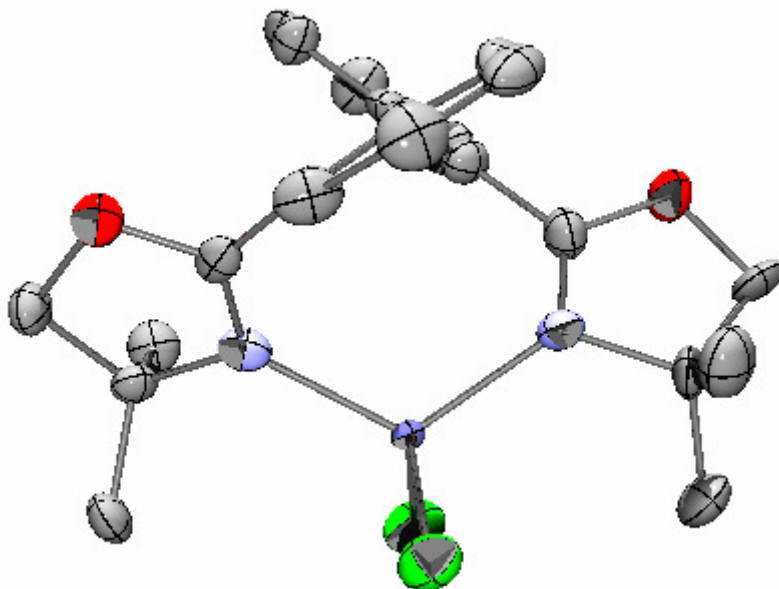


Figure 2.1. Molecular view of one of the two independent molecules of $[\kappa\text{-N,N}\{-4,4\text{-Me}_2\text{-(2-}o\text{-C}_6\text{H}_4\text{)-2-oxazoline}\}_2]\text{CoCl}_2$ (**1-Co**).

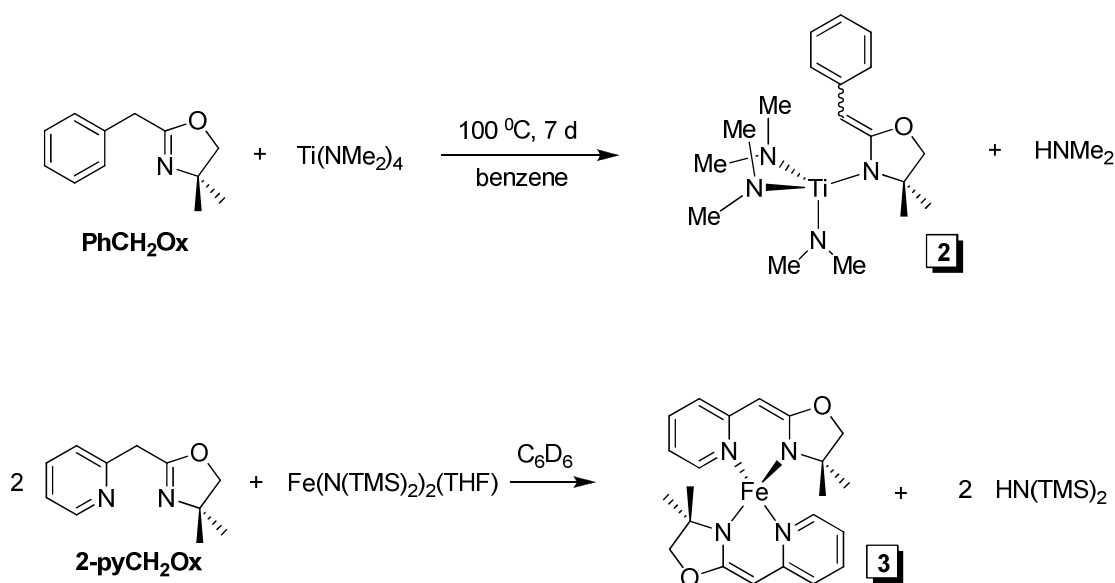
C. First-row metal reactivity with PhCH_2Ox and PyCH_2Ox .

1. Heterolytic C-H bond activation attempts.

It was suspected that the small bite angle of the phenyloxazoline may have prompted reductive coupling of the ligands. For this reason, a derivative with a methylene spacer, 4,4-dimethyl-2-benzyloxazoline (**PhCH₂Ox**), was employed. Efforts at heterolytic CH-bond activation of **PhCH₂Ox** with metal halides, or with metal amides $\text{Fe}(\text{N}(\text{TMS})_2)_2(\text{THF})$ and $\text{Fe}(\text{N}(\text{TMS})_2)_3$, were largely unsuccessful. Color changes to orange or yellow, and the presence of $\text{HN}(\text{TMS})_2$ in the metal amide reactions, indicated that a reaction had occurred, but quenching returned **PhCH₂Ox** unaltered. The relatively acidic methylene protons could not be ignored as potential participants in this chemistry, and a few test reactions were devised to determine their possible role in the reactivity of **PhCH₂Ox**.

2. PhCH₂Ox and titanium.

Ti(NMe₂)₄ was chosen as a metal amide source that should give diamagnetic products. Treatment of Ti(NMe₂)₄ with **PhCH₂Ox** led to no reaction at room temperature, but heating to 100 °C for seven days gave complete conversion to a new red product (Scheme 2.3). ¹H NMR reveals all five phenyl resonances, a single vinylic proton at δ 5.81, a methylene singlet, and methyl resonances in a 12:6:6 H ratio, consistent with the formulation (NMe₂)₃Ti{η-N-(4,4-Me₂-2-(CHPh)-oxazolidine)} (**2**). As expected, the internal amide base preferentially deprotonates at the methylene, not the aryl position.



Scheme 2.3. Acid/base reactivity of oxazolines **PhCH₂Ox** and **PyCH₂Ox** with Ti(NMe₂)₄ and Fe(N(TMS)₂)₂(THF), respectively.

3. PyCH₂Ox and iron.

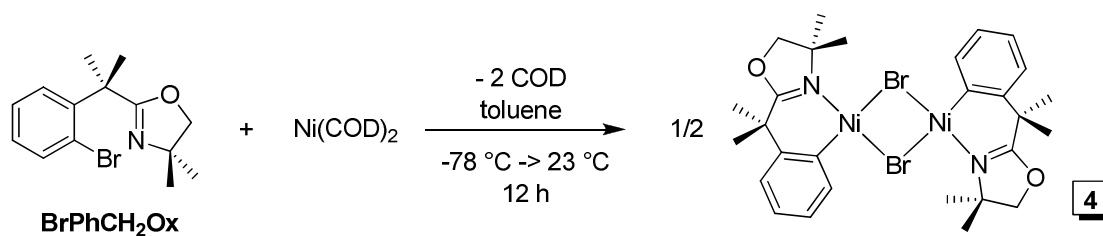
As another test of the involvement of the methylene protons, Fe(N(TMS)₂)₂(THF) was treated with a pyridyl analogue, 4,4-dimethyl-2-(2-pyridylmethyl)oxazoline, **2-PyCH₂Ox** in C₆D₆. Cherry red solutions containing

HN(TMS)₂ and a new paramagnetic product were observed with both one and two equivalents of **2-PyCH₂Ox**, but remaining iron starting material in the former suggested that two equivalents of the ligand were incorporated into the product, as shown in Scheme 2.3. The ¹H NMR spectrum was consistent of the bis-chelate, *bis*-{*bis*-{κ-N,N'-(4,4-dimethyl-(2-pyridylmethyl-yl)-oxazolidine}Fe (**3**), with diastereotopic methyl and methylene protons on the oxazoline moiety. With two convincing instances of methylene proton involvement in metalation reactions, attention was redirected to a protected derivative.

D. First-row metal reactivity with 4,4-dimethyl-2-(2-phenylpropan-2-yl)oxazoline.

1. Nickel oxidative addition.

Preliminary heterolytic C-H bond activation endeavors using dimethyl-protected **HPhCMe₂Ox** with metal halides or triflates failed to elicit the desired aryl-activation, so a switch to the halide-substituted **BrPhCMe₂Ox** was made. As Scheme 2.4 shows, oxidative addition was first attempted with Ni(COD)₂ in toluene to afford an insoluble fuchsia solid, postulated as dimeric [{κ-C,N-(*o*-C₆H₄)CMe₂(COCH₂CMe₂N)}Ni]₂(μ-Br)₂ (**4**) (80 %). Although not appreciably soluble in toluene, THF or CH₂Cl₂, **4** dissolved completely in CD₃CN to give a yellow-orange solution, most likely the monomeric acetonitrile adduct.

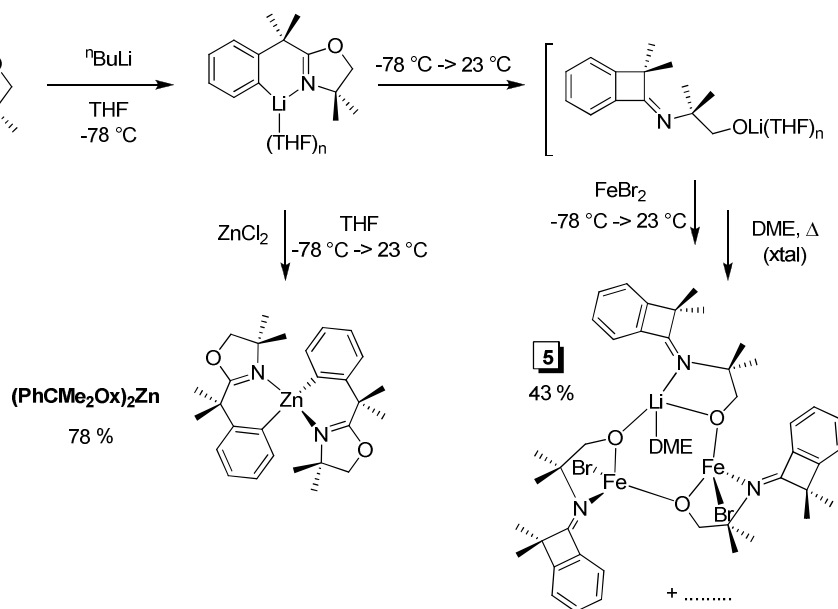


Scheme 2.4. Oxidative addition to form [{κ-C,N-(*o*-C₆H₄)CMe₂(COCH₂CMe₂N)}Ni]₂(μ-Br)₂ (**4**).

2. Lithiation behavior with zinc and iron.

Due to the dearth of suitable M^0 sources of iron and chromium, an anionic equivalent of **PhCMe₂Ox** was deemed necessary. Direct *ortho*-lithiation of **HPhCMe₂Ox** was impeded by the inclusion of the -CMe₂- linkage; however, lithium-halogen exchange of **BrPhCMe₂Ox** was effective to prepare **LiPhCMe₂Ox** as mentioned previously.

After low-temperature generation of **LiPhCMe₂Ox** (-78 °C), warming to room temperature allowed a rearrangement to the benzocyclobutanamine depicted in Scheme 2.5. Internal attack of the aryl anion on the oxazoline carbon causes ring-opening to the lithium alkoxide which, upon addition of half an equivalent of FeBr₂, forms the trinuclear lithium-iron alkoxide complex, **5**. Obtained as a yellow solid in 43 % from crystallization with DME, **5** contains two tetrahedral iron centers joined by bridging alkoxide ligands (Figure 2.2).



Scheme 2.5. Temperature-dependent behavior of **LiPhCMe₂Ox**.

If the lithiation reaction is held at $-78\text{ }^{\circ}\text{C}$, addition of one half equivalent of ZnCl_2 leads to the organozinc complex, $(\text{PhCMe}_2\text{Ox})_2\text{Zn}$ in 78 % yield (Scheme 2.5). Reaction of the aryllithium with ZnCl_2 apparently occurs more quickly than internal attack and ring-opening of the oxazoline. $(\text{PhCMe}_2\text{Ox})_2\text{Zn}$, a temperature-stable, white solid, was deemed a convenient surrogate for $\text{LiPhCMe}_2\text{Ox}$.

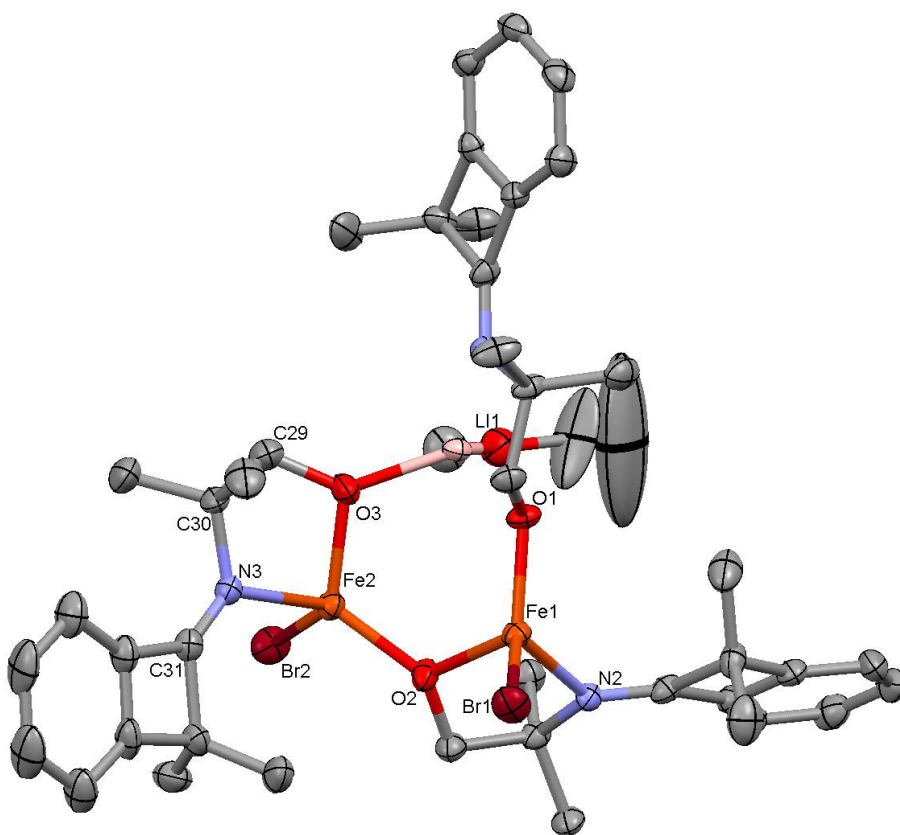


Figure 2.2. Molecular view of $[\{\kappa\text{-N,O-C}_6\text{H}_4\text{-CMe}_2\text{C=NCMe}_2\text{CH}_2\text{-(}\mu\text{-O)-}\}\text{BrFe}\{\kappa\text{-N,O-C}_6\text{H}_4\text{-CMe}_2\text{C=NCMe}_2\text{CH}_2\text{-(}\mu\text{-O)-}\}\text{FeBr}]\text{Li}\{\kappa\text{-N,O-C}_6\text{H}_4\text{-CMe}_2\text{C=NCMe}_2\text{CH}_2\text{-(}\mu\text{-O)-}\}(\text{DME})$ (**5**) with solvent molecules removed. Only those atoms of the bound DME that were not severely disordered are shown.

3. Structure of $[\{\kappa\text{-N,O-C}_6\text{H}_4\text{-CMe}_2\text{C=NCMe}_2\text{CH}_2\text{-(}\mu\text{-O)}\}\text{BrFe}\{\kappa\text{-N,O-C}_6\text{H}_4\text{-CMe}_2\text{C=NCMe}_2\text{CH}_2\text{-(}\mu\text{-O)}\}\text{FeBr}]\text{Li}\{\kappa\text{-N,O-C}_6\text{H}_4\text{-CMe}_2\text{C=NCMe}_2\text{CH}_2\text{-(}\mu\text{-O)}\}(\text{DME})$ (**5**).

Crystallographic data and pertinent bond distances and angles in **5** are contained in Tables 2.1 and 2.2, respectively. Figure 2.2 clearly shows the benzocyclobutanamine portion of the ligand. Each iron(II) center is ligated by a chelating alkoxyimine, a bridging alkoxide, and a bromide. The lithium ion is chelated by a third alkoxyimine, and is bound by an additional bridging alkoxide and disordered DME molecule. Distortion in the tetrahedral geometry about iron is mainly due to the constrained chelate angle ($\text{O2-Fe1-N2} = 80.74(11)^\circ$; $\text{O3-Fe2-N3} = 82.40(12)^\circ$); other core angles range from $\sim 109\text{--}125^\circ$ to compensate. The bond distances are typical for a high-spin, tetrahedral iron(II) center.

4. Synthesis of chromium oxazoline complexes.

In order to circumvent the potential ring-opening behavior of **LiPhCMe₂Ox**, metalation was next attempted using **(PhCMe₂Ox)₂Zn**. Treatment with $[\text{CrCl}_2(\text{THF})]_2$ (one half or fewer equivalents) in THF at -78°C led to the formation of the purple chromous dimer, $[\{\kappa\text{-C,N-(}o\text{-C}_6\text{H}_4\text{)CMe}_2(\text{COCH}_2\text{CMe}_2\text{N})\}\text{Cr}]_2(\mu\text{-Cl})_2$ (**6₂**), in 40 % yield (Scheme 2.6). Even with excess organozinc reagent and application of heat, only one oxazoline equivalent was transferred, with $[\text{ZnCl}(\text{ArOx})]_2$ as the proposed byproduct. **6₂** was only sparingly soluble in benzene or toluene, and in THF dissolved to a blue solution believed to contain the monomeric THF adduct, $\{\kappa\text{-C,N-(}o\text{-C}_6\text{H}_4\text{)CMe}_2(\text{COCH}_2\text{CMe}_2\text{N})\}\text{CrCl}(\text{THF})$ (**6-THF**). Evans' method measurement of **6-THF** gives the expected $\mu_{\text{eff}} = 4.9 \mu_{\text{B}}$ for a high-spin $S = 2$ chromous center. However, Gouy balance measurements of the dimeric **6₂** reveal a significantly attenuated moment of $2.5 \mu_{\text{B}}$, indicating a substantial chromium-chromium interaction, resulting

in antiferromagnetic coupling. X-ray diffraction quality crystals of **6₂** were grown from hot benzene solution (Figure 2.3), and structural details are described below.

Table 2.1. Crystallographic data for { κ -N,N'-(2,2'-(4,4-dimethyl-2-phenyloxazolinyl)biphenyl)}CoCl₂ (**1-Co**), [κ -N,O-C₆H₄-CMe₂C=NCMe₂CH₂-(μ -O)]BrFe{ κ -N,O-C₆H₄-CMe₂C=NCMe₂CH₂-(μ -O)}FeBr[Li{ κ -N,O-C₆H₄-CMe₂C=NCMe₂CH₂-(μ -O)}(DME) (**5**), [κ -C,N-(4,4-dimethyl-2-(2-phenylpropan-2-yl)-oxazoline)}Cr]₂(μ -Cl)₂ (**6₂**), and { κ -C,N-(4,4-dimethyl-2-(2-phenylpropan-2-yl)-oxazoline)}Fe(η -N-pyridyl)Cl (**7**).

	1-Co	5	6₂	7
Formula	C ₂₂ H ₂₄ N ₂ O ₂ Cl ₂ Co	C ₅₀ H ₇₂ N ₃ O ₇ Br ₂ Li ₂ Fe ₂ ^d	C ₂₈ H ₃₆ N ₂ O ₂ Cl ₂ Cr	C ₂₂ H ₂₆ N ₂ OClFe ^e
Formula weight	478.29	1105.57	607.49	425.75
Crystal system		Triclinic	Monoclinic	Monoclinic
Space group	P2 ₁ /n	P-1	P2 ₁ /c	P2 ₁ /c
Z	8	2	2	4
a (Å)	15.555(3)	13.7059(10)	6.9943(10)	15.8720(7)
b (Å)	10.169(2)	14.3972(10)	26.459(4)	9.0323(4)
c (Å)	28.108(6)	15.3609(11)	8.1697(11)	15.5493(8)
α (°)	90	68.213(3)	90	90
β (°)	90.88(3)	84.999(4)	104.974(5)	109.904(3)
γ (°)	90	75.078(4)	90	90
V (Å ³)	4445.8(15)	2719.6(3)	1460.6(4)	2096.00(17)
ρ_{calc} (gcm ⁻³)	1.429	1.350	1.381	1.349
μ (mm ⁻¹)	1.033	2.051	0.954	0.860
T (K)	173(2)	173(2)	173(2)	173(2)
λ (Å)	0.71073	0.71073	0.71073	0.71073
Final R indices [$>2\sigma(I)$] ^{a,b}	R ₁ = 0.0532 wR ₂ = 0.1027	R ₁ = 0.0639 wR ₂ = 0.1732	R ₁ = 0.0534 wR ₂ = 0.1344	R ₁ = 0.0530 wR ₂ = 0.1408
R indices (all data) ^{a,b}	R ₁ = 0.1215 wR ₂ = 0.1143	R ₁ = 0.1196 wR ₂ = 0.2031	R ₁ = 0.0798 wR ₂ = 0.1499	R ₁ = 0.0774 wR ₂ = 0.1561
Goodness-of-fit ^c	0.979	1.037	1.052	1.048

^a $R_1 = \Sigma ||F_o| - |F_c|| / \Sigma |F_o|$, ^b $wR_2 = [\Sigma w(|F_o| - |F_c|)^2 / \Sigma wF_o^2]^{1/2}$, ^c GOF (all data) = $[\Sigma w(|F_o| - |F_c|)^2 / (n - p)]^{1/2}$, n = number of independent reflections, p = number of parameters. ^d Two molecules of DME are included in the unit cell. ^e 1/2 benzene included in the unit cell.

Table 2.2. Core distances (Å) and angles (°) for { κ -N,N'-(2,2'-(4,4-dimethyl-2-phenyloxazoliny)biphenyl)}CoCl₂ (**1-Co**), [{ κ -N,O-C₆H₄-CMe₂C=NCMe₂CH₂-(μ -O)}BrFe{ κ -N,O-C₆H₄-CMe₂C=NCMe₂CH₂-(μ -O)}FeBr]Li{ κ -N,O-C₆H₄-CMe₂C=NCMe₂CH₂-(μ -O)}(DME) (**5**), [{ κ -C,N-(4,4-dimethyl-2-(2-phenylpropan-2-yl)-oxazoline)}Cr]₂(μ -Cl)₂ (**6₂**), and { κ -C,N-(4,4-dimethyl-2-(2-phenylpropan-2-yl)-oxazoline)}Fe(η -N-pyridyl)Cl (**7**).

	1-Co		5		6₂	7
	M = Co1	M = Co2	M = Fe1	M = Fe2	M = Cr	M = Fe
M-C _{Ar}					2.091(4)	1.984(4)
M-N _{Ox} (1)	2.042(4)	2.037(4)	2.125(3)	2.122(3)	2.071(3)	2.053(3)
M-N _{Ox} (2)	2.045(4)	2.052(4)				
M-X(1)	2.2380(16)	2.2189(15)	2.4085(7)	2.4469(7)	2.4362(13)	2.2797(8)
M-X(2)	2.2569(16)	2.2486(16)			2.3638(13)	
M-N _{py}						2.090(3)
N _{Ox} -C _{Ox}	1.272(6)	1.275(6)			1.264(5)	1.272(4)
	1.281(6)	1.296(6)				
M-M					3.537	
M-O _{chelate}			2.009(2)	1.929(3)		
M-O _{nonchelate}			1.909(3)	1.924(3)		
Li-N _{chelate}			2.112(7)			
Li-O _{chelate}			1.966(7)			
Li-O _{nonchelate}			1.915(7)			
Li-O _{DME}			1.992(9)			
N _{Ox} -M-C _{Ar}					87.20(14)	95.73(13)
N _{Ox} -M-X(1)	103.13(12)	106.07(12)	113.49(9)	105.05(8)	93.82(10)	107.74(8)
N _{Ox} -M-X(2)	109.98(11)	109.98(12)			173.58(11)	
N _{Ox} '-M-X(1)	108.25(12)	108.01(12)				
N _{Ox} '-M-X(2)	102.35(12)	100.72(12)				
C _{Ar} -M-X(1)					171.55(12)	134.14(10)
C _{Ar} -M-X(2)					94.82(11)	
M-C _{Ar} -C _{outer}					122.4(3)	121.7(3)
M-C _{Ar} -C _{inner}					121.9(3)	121.4(3)
Cl(1)-M-Cl(2)	115.05(6)	114.23(6)			85.08(4)	
M-Cl-M					94.92(4)	
N _{Ox} -M-N _{py} (Ox')	118.61(15)	118.12(16)				105.43(11)
N _{py} -M-Cl						101.26(7)
N _{py} -M-C _{Ar}						109.82(13)
O _{chelate} -M-N			80.74(11)	82.40(12)		
O _{nonchelate} -M-N			116.35(12)	124.91(12)		
O _{chelate} -M-O _{non}			111.89(11)	116.61(11)		
O _{chelate} -M-X			110.08(8)	117.20(9)		
O _{nonchelate} -M-X			118.13(8)	108.84(8)		
N-Li-O _{chelate}			85.6(2)			
N-Li-O _{nonchelate}			117.2(3)			
N-Li-O _{DME}			115.7(3)			
O _{chelate} -Li-O _{non}			109.0(3)			
O _{chelate} -Li-O _{DME}			115.3(4)			
O _{non} -Li-O _{DME}			111.6(3)			
Fe-O-Li			121.5(2)	116.1(2)		
Fe-O-Fe			119.75(13)			

Table 2.2. (Continued)

$N_{Ox}-C_{Ox}-C_{ipso}-C_o$	60.3(7)	63.9(7)
$N_{Ox'}-C_{Ox'}-C_{ipso'}-C_{o'}$	59.9(2)	59.3(7)
$C_{ipso}-C_o-C_{o'}$	119.2(7)	113.6(7)
$C_{ipso'}$		

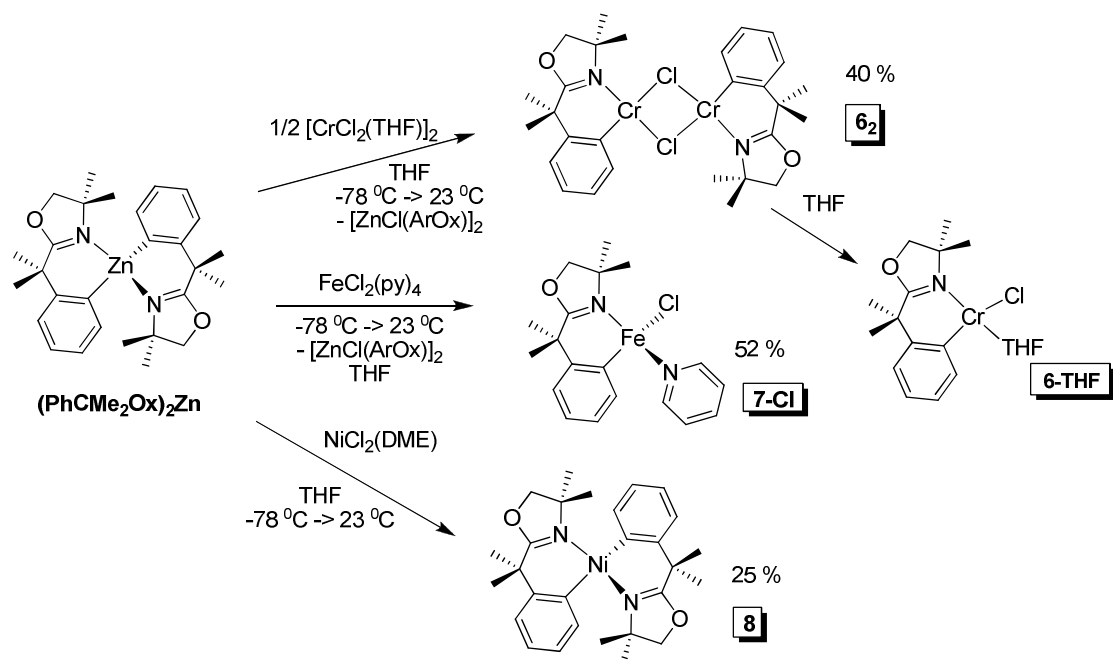
**Scheme 2.6.** Aryloxazoline transfer from $(PhCMe_2Ox)_2Zn$.**5. Structure of $\{[\kappa-C,N-(o-C_6H_4)CMe_2(COCH_2CMe_2N)]Cr\}_2(\mu-Cl)_2$ (**62**).**

Figure 2.3 reveals the structure of **62**, which contains two square-planar chromium centers joined by two bridging chlorides and each capped by two opposing oxazoline chelates in overall C_2 symmetry. Pertinent bond distances and angles are listed in Table 2.2. A new chromium-carbon bond is evident, with a distance of 2.091(4) Å. The chromium- nitrogen (2.071(3) Å) and chromium-chloride bond lengths (2.4362(13) and 2.3638(13) Å, respectively) are typical. A shorter C-N distance of 1.264(5) Å indicates the double bond in the oxazoline ring. Though not out

of the realm of metal-metal interaction, the chromium-chromium distance of 3.537 Å is fairly long and certainly not indicative of multiple bond character.

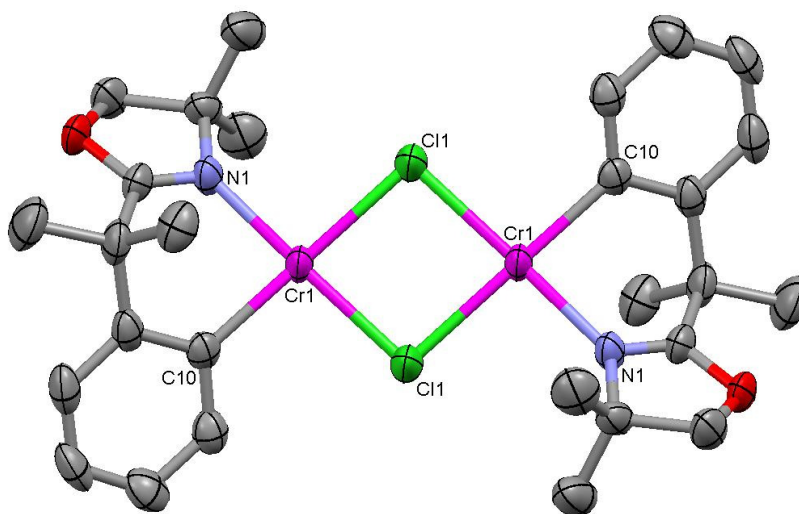


Figure 2.3. Molecular view of $[\{\kappa\text{-C,N-}(o\text{-C}_6\text{H}_4)\text{CMe}_2(\text{COCH}_2\text{CMe}_2\text{N})\}\text{Cr}]_2(\mu\text{-Cl})_2$ (**62**).

The bite angle of the chelate is 87.20(14) °, owing to the puckering in the CMe₂ unit; the remaining core angles experience only mild distortion as a consequence (N-Cr-Cl1 = 93.82(10) °; C-Cr-Cl2 = 94.82(11) °; Cl1-Cr-Cl2 = 85.08(4) °). Symmetry of the bound aryl group is reflected in the nearly identical Cr-C10-C9 and Cr-C10-C5 angles of 122.4(3) and 121.9(3) °, respectively.

6. Synthesis of iron oxazoline complexes.

Since (PhCMe₂Ox)₂Zn provided moderate phenyloxazoline transfer with chromium, it was next employed as a metathesis agent with iron. Treating FeCl₂(py)₄ with one or more equivalents of (PhCMe₂Ox)₂Zn led to isolation of a yellow paramagnetic compound, identified by X-ray crystallography as $\{\kappa\text{-C,N-}(o\text{-C}_6\text{H}_4)\text{CMe}_2(\text{COCH}_2\text{CMe}_2\text{N})\}\text{Fe}(\text{py})\text{Cl}$ (**7-Cl**) (52 %, Figure 2.4). As with chromium, only one phenyloxazoline was transferred, regardless of the amount of organozinc reagent employed.

Though a single crystal was obtained, purification of the bulk material was hampered by similar solubilities of **7-Cl** and the $[\text{ZnCl}(\text{ArOx})]_2$ byproduct. An alternate synthesis via low-temperature generation of **LiPhCMe₂Ox** and subsequent addition of $\text{FeCl}_2(\text{py})_4$ afforded **7-Cl** with increased purity and yield (Scheme 2.7, 85 %). Single crystals of this material were grown to obtain unit cell parameters, confirming the identity of **7-Cl**. Fortunately, reaction of **LiPhCMe₂Ox** with the iron precursor is faster than intermolecular attack and oxazoline ring-opening.

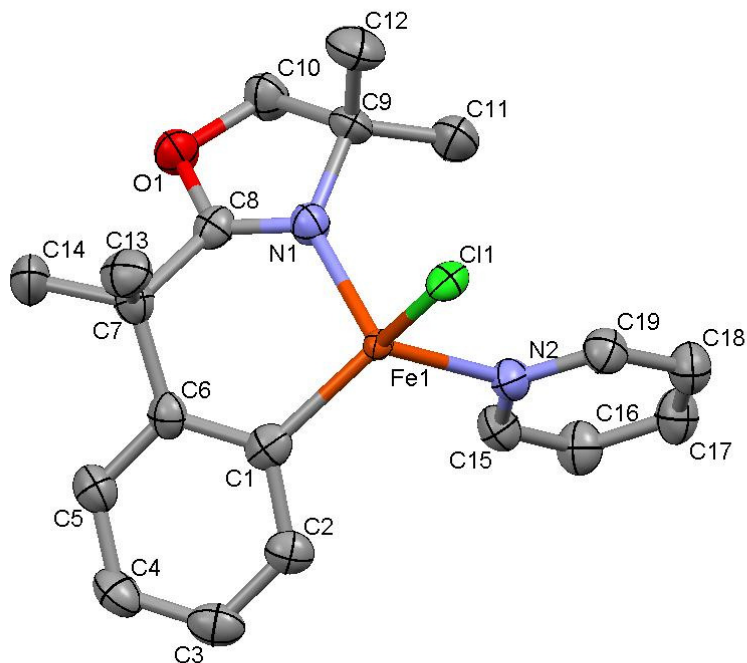
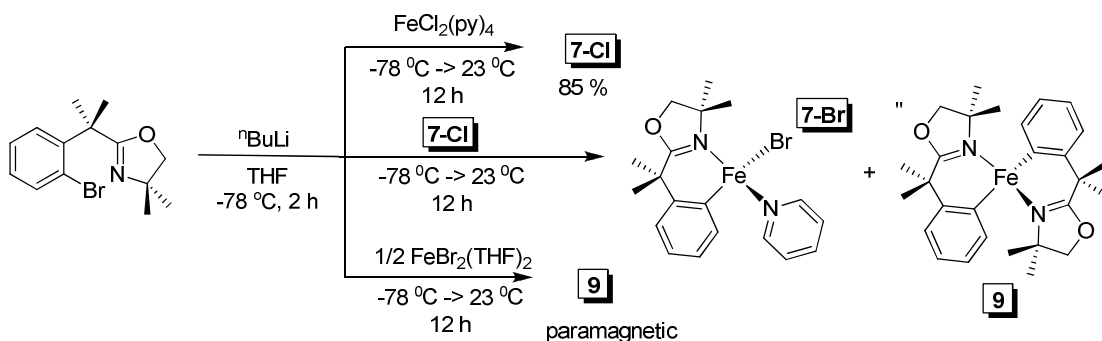


Figure 2.4. Molecular view of $\{\kappa\text{-C,N-(}o\text{-C}_6\text{H}_4\text{)CMe}_2\text{(COCH}_2\text{CMe}_2\text{N))Fe(py)Cl}$ (**7-Cl**).



Scheme 2.7. Reactivity of low-temperature-generated **LiPhCMe₂Ox**.

Given this successful result with **LiPhCMe₂Ox**, a second phenyloxazoline transfer was attempted. Low-temperature generation of **LiPhCMe₂Ox**, followed by addition of **7-Cl** (1 equiv) and slow warming to room temperature, gave a tan solution which contained one major paramagnetic species. Yellow crystals grown from benzene/Et₂O were identified as the bromide derivative, **7-Br**, which likely resulted from metathesis of the starting material with LiBr generated in the reaction. However, a quench of the mother liquor failed to generate free pyridine, suggesting that **7-Br** may have been a minor product of the reaction. A second crystal was grown which possessed a different unit cell from that of either **7-Cl** or **7-Br**; unfortunately, the crystal quality was not good enough to obtain a structure. To corroborate this result, lithiation of two equivalents of **BrPhCMe₂Ox**, followed by addition of FeBr₂, yielded the same paramagnetic product, as the major species above. The product is formulated at the bis-oxazoline compound, **9** (Scheme 2.7), but efforts to unambiguously assign the structure are ongoing.

7. Structure of {κ-C,N-(*o*-C₆H₄)CMe₂(COCH₂CMe₂N)}Fe(py)Cl (**7-Cl**).

Comparison of the bond distances in **7-Cl** and **6₂** shows marked similarities (Table 2.2). The Fe-C_{Ar}, Fe-N_{Ox}, and N_{Ox}-C_{Ox} distances (1.984(4), 2.053(3), and 1.272(4) Å) are nearly identical to their chromium analogues (2.091(4), 2.071(3), 1.264(5) Å). The bite angle of the chelate, however, is significantly larger at

95.73(13) ° (versus 87.20(14) °), and the related torsion angle is correspondingly diminished (51.3 versus 52.9 °). Gratifyingly, the ability of the CMe₂ spacer to accommodate these geometric demands validates its intentional incorporation into the ligand design. The remaining core angles reflect some distortion in the tetrahedral geometry (N_{Ox}-Fe-Cl = 107.74(8) °; C_{Ar}-Fe-Cl = 134.14(10) °; N_{Ox}-Fe-N_{py} = 105.43(11) °; N_{py}-Fe-Cl = 101.26(7) °; N_{py}-Fe-C_{Ar} = 109.82(13) °), but nothing unusual for high-spin iron(II).

8. Synthesis of {κ-C,N-(4,4-dimethyl-2-(2-phenylpropan-2-yl)-oxazoline)}₂Ni (**8**).

Only in one instance was transfer of two phenyloxazoline ligands observed with confidence. Treatment of NiCl₂(DME) with one equivalent of (PhCMe₂Ox)₂Zn resulted in the formation of the diamagnetic bis-chelate, {κ-C,N-(4,4-dimethyl-2-(2-phenylpropan-2-yl)-oxazoline)}₂Ni (**8**), after crystallization from THF/Et₂O, in a modest 25 % yield (Scheme 2.6). ¹H NMR spectroscopy of the yellow-orange crystals reveals diastereotopic methylene and methyl protons, the latter of which occur at 3.66, 1.81, 0.94, 0.69 ppm, respectively. The unusual downfield resonance may be due to shielding effects on a methyl group oriented over an aromatic ring. Variable-temperature studies were undertaken, but coalescence of the methyl peaks was not achieved before the onset of degradation at 80 °C. It is possible that heating causes reorientation of the two aryl groups, such that deleterious reductive elimination is competitive with coalescence. The explanation for a second phenyloxazoline transfer in this unique case is also speculative; it may be that transfer of one phenyloxazoline may produce a nickel dimer, [ArOxNiCl]₂, which is prone to disproportionation. This rationalization is unsatisfactory, however, as it ignores the fact that related complex **4** seems quite stable to disproportionation.

III. Conclusions

The synthesis of 1st-row metal oxazoline complexes required creative solutions to unforeseen challenges. CH-activation of aryl-oxazolines was unsuccessful; aryl lithiation led to undesired reactivity, namely oxidative coupling and ring-opening of the aryl-oxazoline ligand; unprotected methylene protons were susceptible to deprotonation. Oxidative addition to nickel was a successful route to an aryl-oxazoline complex, and the aryl anion transfer from an organozinc agent led to new Cr, Fe, and Ni derivatives. So far only high-spin cases have been observed for Cr and Fe, though these compounds are characterized by low coordination and therefore an intrinsically smaller ligand field. Also, only one aryl-oxazoline transfer to Cr or Fe was achieved with sufficient evidence, but efforts to isolate bis-aryl-oxazoline complexes of these metals are ongoing.

IV. Experimental

A. General Considerations

For metal complexes, manipulations were performed using either glovebox or high-vacuum techniques. Ligand syntheses were performed under argon using Schlenk techniques. Hydrocarbon and ethereal solvents were dried over and vacuum transferred from sodium benzophenone ketyl (with 3-4 ml tetraglyme/L added to hydrocarbons). Methylene chloride was distilled from and stored over CaH₂. Benzene-*d*₆ and toluene-*d*₈ were sequentially dried over sodium and stored over sodium. THF-*d*₈ was dried over sodium benzophenone ketyl. Acetonitrile-*d*₃ was dried over CaH₂ and stored over 4 Å molecular sieves. The compounds HPhox,⁸ LiPhOx,⁹ PhCH₂Ox,¹⁰ Fe{N(TMS)₂}₂(THF),¹¹ Ni(COD)₂,¹² FeBr₂(THF)₂,¹³ CrCl₂(THF),¹⁴ FeCl₂(py)₄,¹⁵ and NiCl₂(DME)¹⁶ were prepared according to literature procedures. SOCl₂ (Aldrich) was used immediately or distilled prior to use; NEt₃ (Aldrich) was dried and stored over 4

Å molecular sieves; ZnCl_2 ¹⁷ was dried according to literature procedure; all other reagents were purchased and used as received. All glassware was oven-dried.

^1H - and $^{13}\text{C}\{^1\text{H}\}$ -NMR spectra were obtained using Mercury-300, Inova-400, and Inova-500 spectrometers, and chemical shifts are reported relative to benzene- d_6 (^1H , δ 7.16; $^{13}\text{C}\{^1\text{H}\}$, δ 128.39), THF- d_8 (^1H , δ 3.58; $^{13}\text{C}\{^1\text{H}\}$, δ 67.57), acetonitrile- d_3 (^1H , δ 1.94; $^{13}\text{C}\{^1\text{H}\}$, δ 1.79), toluene- d_8 (^1H , δ 2.09; $^{13}\text{C}\{^1\text{H}\}$, δ 20.40). Solution magnetic measurements were conducted via Evans' method in benzene- d_6 or toluene- d_8 . Combustion analyses were performed by Robertson Microlit Laboratories, Madison, NJ, and by services at the University of Erlangen-Nuremberg, Germany.

B. Procedures.

1. Ligands and ligand precursors.

a. 4,4-dimethyl-(2-pyridylmethyl)-2-oxazoline (PyCH₂Ox).

To a solution of 2-pyridylacetonitrile (440 mg, 3.72 mmol) and 2-amino-2-methylpropanol (663 mg, 7.45 mmol) in 10 mL toluene were added 50 mg (0.186 mmol) $\text{Cd}(\text{OAc})_2 \cdot 2\text{H}_2\text{O}$. The mixture was allowed to reflux under argon overnight. After washing with water, the crude mixture was extracted with CH_2Cl_2 , dried over MgSO_4 , filtered and concentrated to a light brown oil. The crude oil was distilled under reduced pressure to yield a yellow oil (70 %). ^1H NMR (400 MHz, benzene- d_6) δ 8.43 (d, 1H, $J=4$), 7.12 (d, 1H, $J=8$), 7.02 (t, 1H, $J=8$), 6.56 (t, 1H, $J=6$), 3.84 (s, 2H), 3.53 (s, 2H), 1.09 (s, 6H).

b. 4,4-dimethyl-2-(2-arylpropan-2-yl)-2-oxazoline (aryl = Ph, HPhCMe₂Ox; 2-BrPh, BrPhCMe₂Ox).

A 50-mL three neck round bottom flask fitted with a reflux condenser and external oil bubbler was flushed with argon and charged with 15 mL SOCl_2 . 13 mmol α,α -dimethyl-arylacetic acid (aryl = phenyl, HPhCMe₂Ox; 2-bromophenyl, BrPhCMe₂Ox) were added and the solution heated to reflux for 3 h. The cooled

mixture was then concentrated and triturated with CH₂Cl₂ (2 x 5 mL). The oily product was redissolved in 15 mL CH₂Cl₂. A solution of 2-amino-2-methyl-1-propanol (1.39 g, 15.6 mmol) and NEt₃ (2.72 mL, 19.5 mmol) in 20 mL CH₂Cl₂ was cooled to 0 °C. The acid chloride solution was added dropwise under argon. The reaction was allowed to warm slowly to room temperature and stirred overnight. The mixture was washed first with H₂O (20 mL) then with brine (20 mL), and the organics dried over MgSO₄, filtered and concentrated. The crude product was recrystallized from 6:1 hexanes/ethyl acetate to yield a white, crystalline solid (90 % after 3 crops).

10 mmol of the above amide, 4-(dimethylamino)pyridine (110 mg, 0.9 mmol), and NEt₃ (3.1 mL, 22 mmol) were dissolved in 30 mL CH₂Cl₂. A solution of *p*-toluenesulfonyl chloride in 20 mL CH₂Cl₂ was added via syringe under argon. After stirring at room temperature for two days, the reaction mixture was diluted with CH₂Cl₂ and extracted with saturated NH₄Cl followed by aqueous NaHCO₃. The organic layer was dried over MgSO₄, treated with decolorizing carbon, filtered and concentrated. The crude product was purified by flash chromatography (6:1 hexanes/ethyl acetate) to give a clear oil (65 %).

2. Metal complexes.

a. Zn(κ -C,N-4,4-Me₂-(*o*-C₆H₄)-2-oxazoline)₂ (Zn(PhOx)₂).

LiPhox (1.99 g, 10.98 mmol) and ZnCl₂ (0.75 g, 5.50 mmol) were weighed into a 100 mL round bottom flask attached to a swivel frit. 50 mL toluene were vacuum transferred at -78 °C. The mixture was stirred at this temperature for several hours and allowed to warm slowly overnight. After subsequent filtration and washing of the salt cake with toluene, the solvent was removed. The product was triturated and filtered in pentane, leaving a white solid (1.82 g, 80 %). ¹H NMR (400 MHz, benzene-*d*₆) δ 8.07 (d, *J* = 7.2, 1H), 8.03 (d, *J* = 8.0, 1H), 7.44 (t, *J* = 7.2, 1H), 7.22 (t, *J* = 7.6, 1H), 3.73 (s, 2H), 0.86 (s, 6H). ¹³C NMR (500 MHz, benzene-*d*₆) δ 173.64, 168.30,

139.61, 135.29, 131.70, 128.68, 125.87, 125.45, 82.43, 65.13, 28.52. Anal. Calcd for $C_{22}H_{24}N_2O_2Zn$: C, 63.95; H, 5.85; N, 6.77. Found: C, 63.60; H, 5.59; N, 6.75.

b. $[\kappa\text{-N,N}\text{-}\{4,4\text{-Me}_2\text{-(2-}o\text{-C}_6\text{H}_4\text{)}\text{-2-oxazoline}\}_2]\text{CoCl}_2$ (1-Co).

500 mg **LiPhox** (2.74 mmol) and 178 mg CoCl_2 (1.37 mmol) were placed in a 50-mL round bottom flask. Ether (25 mL) was vacuum transferred at -78°C . The reaction mixture was allowed to stir at -78°C for 2 h, then warmed slowly to room temperature overnight. The mixture was filtered in ether, stripped, and triturated with hexanes and filtered to yield a blue-green solid (395 mg, 60 %). X-ray diffraction quality crystals were grown from THF/hexanes.

c. $(\text{NMe}_2)_3\text{Ti}\{\eta\text{-N}\text{-(4,4-Me}_2\text{-2-(CHPh)-oxazolidine)}\}$ (2).

A mixture of $\text{Ti}(\text{NMe}_2)_4$ (500 mg, 2.23 mmol) and 4,4-dimethyl-2-(phenylmethyl)oxazoline (423 mg, 2.23 mmol) in 20 mL benzene was heated at 100°C in a bomb reaction vessel for 7 days. The solvent was removed to obtain a red-orange oil. Addition of diethyl ether (20 mL) led to precipitation of an orange solid, which was filtered and washed with ether (3 x 10 mL) (240 mg, 29 %). ^1H NMR (400 MHz, benzene- d_6) δ 7.32 (t, 2H, $J=7$), 7.21 (d, 2H, $J=7$), 7.05 (t, 1H, $J=7$), 5.81 (s, 1H), 4.13 (s, 2H), 3.14 (s, 12H), 2.55 (s, 6H), 1.30 (s, 6H). ^{13}C NMR (500 MHz, benzene- d_6) δ 158.85, 141.84, 128.92, 128.53, 123.66, 102.14, 85.82, 66.47, 46.35, 42.44, 26.84.

d. $\text{bis}\text{-}\{\kappa\text{-N,N'}\text{-(4,4-dimethyl-(2-pyridylmethyl-yl)-oxazolidine)}\}\text{Fe}$ (3).

A benzene- d_6 solution of $\text{Fe}\{\text{N}(\text{TMS})_2\}_2(\text{THF})$ (20 mg, 0.045 mmol) was added to 4,4-dimethyl-(2-pyridylmethyl)-2-oxazoline (17 mg, 0.089 mmol) in an NMR tube. Upon addition the solution turned cherry red. The proton NMR spectrum displayed a set of broad resonances in addition to hexamethyldisilazane. ^1H NMR (400 MHz, benzene- d_6) δ 189.64 (s, 1H), 53.89 (s, 1H), 51.07 (s, 1H), 23.75 (s, 1H), 10.29 (s, 1H), -12.09 (s, 1H), -21.72 (s, 1H), -37.67 (s, 3H), -47.90 (s, 3H).

e. $[\{\kappa\text{-C,N-}(o\text{-C}_6\text{H}_4)\text{CMe}_2(\text{COCH}_2\text{CMe}_2\text{N})\}\text{Ni}]_2(\mu\text{-Br})_2$ (4).

A solution of **BrPhCMe₂Ox** (108 mg, 0.365 mmol) in 5 mL toluene was added to Ni(COD)₂ (100 mg, 0.365 mmol) at -78 °C. Warming slowly to room temperature led to the formation of a pink precipitate. After stirring at room temperature for several hours, the resulting dark pink solid was isolated by filtration and washing several times with toluene (49 mg, 80 %). The compound is only sparingly soluble in toluene, THF, or dichloromethane, but dissolves in acetonitrile to give an orange-yellow solution. ¹H NMR (500 MHz, acetonitrile-*d*₃) δ 7.17 (br s, 1H), 6.89 (d, *J* = 5.5, 1H), 6.83 (t, *J* = 7.2, 1H), 6.72 (t, *J* = 6.3, 1H), 4.01 (s, 2H), 2.43 (s, 6H), 1.38 (s, 6H). ¹³C NMR (500 MHz, acetonitrile-*d*₃) δ 179.13, 149.04, 143.95, 138.62, 124.76, 124.45, 123.10, 82.60, 68.62, 44.59, 28.94, 27.70. Anal. Calcd for C₂₈H₃₆N₂O₂Ni: C, 47.38; H, 5.11; N, 3.95. Found: C, 45.14; H, 4.94, N, 3.59.

f. $[\{\kappa\text{-N,O-C}_6\text{H}_4\text{-CMe}_2\text{C=NCMe}_2\text{CH}_2\text{-}(\mu\text{-O})\}\text{BrFe}\{\kappa\text{-N,O-C}_6\text{H}_4\text{-CMe}_2\text{C=NCMe}_2\text{CH}_2\text{-}(\mu\text{-O})\}\text{FeBr}]\text{Li}\{\kappa\text{-N,O-C}_6\text{H}_4\text{-CMe}_2\text{C=NCMe}_2\text{CH}_2\text{-}(\mu\text{-O})\}(\text{DME})$ (5).

ⁿBuLi (0.21 mL, 1.6 M in hexanes) was added to a solution of **BrPhCMe₂Ox** (100 mg, 0.338 mmol) in 20 mL THF at -78 °C under argon. This was allowed to warm slowly and to stir at 25 °C for 1h. The solution was cooled to -78 °C and FeBr₂(THF)₂ (61 mg, 0.169 mmol) added via addition finger. The reaction was kept at -78 °C for 4 h and then allowed to warm slowly to room temperature. The reaction was filtered, stripped, triturated with pentane and filtered to give 67 mg of mustard-yellow solid (43 %). Red, X-ray diffraction quality crystals were grown from a cold solution of DME.

g. (PhCMe₂Ox)₂Zn.

ⁿBuLi (0.42 mL, 1.6 M in hexanes) was added to a solution of **BrPhCMe₂Ox** (200 mg, 0.676 mmol) in 40 mL THF at -78 °C under argon. After 3 h at -78 °C,

ZnCl₂ (46 g, 0.338 mmol) was added via addition finger. The reaction was kept at -78 °C for at least 4 h and then let slowly warm to room temperature. The reaction mixture was stripped, triturated with benzene, filtered, and the salt cake washed several times (4 x 30 mL). The mixture was stripped and triturated with pentane, yielding 131 mg (78 %) of white solid which was collected by filtration. ¹H NMR (500 MHz, benzene-*d*₆) δ 8.09 (dd, *J* = 6.5, 2.0, 1H), 7.49 (d, *J* = 7.0, 1H), 7.38 – 7.25 (m, 2H), 3.31 (s, 2H), 1.85 (s, 6H), 0.89 (s, 6H). ¹³C NMR (500 MHz, benzene-*d*₆) δ 177.88, 162.09, 151.94, 140.46, 125.79, 125.28, 123.59, 78.79, 68.34, 43.80, 31.00, 28.01. Anal. Calcd for C₂₈H₃₆N₂O₂Zn: C, 67.53; H, 7.29; N, 5.63. Found: C, 67.26; H, 7.50; N, 5.38.

h. [{κ-C,N-(*o*-C₆H₄)CMe₂(COCH₂CMe₂N)}Cr]₂(μ-Cl)₂ (6₂).

To a mixture of [CrCl₂(THF)]₂ (98 g, 0.251 mmol) and (PhCMe₂Ox)₂Zn (250 g, 0.502 mmol) were distilled 15 mL THF at -78 °C. The suspension was stirred at -78 °C for 5 h and then slowly warmed to room temperature. The resulting blue solution was filtered through Celite and stripped. Trituration with benzene resulted in formation of a purple solid (61 mg, 40 %). X-ray diffraction quality crystals were grown by hot filtration and recrystallization from benzene. Proton NMR showed broadened peaks, mostly outside the diamagnetic region. ¹H NMR (400 MHz, benzene-*d*₆) δ 17.17, 16.13, 14.00, 1.60, -2.86, -11.80, -77.80. Anal. Calcd for C₂₈H₃₆N₂O₂Cl₂Cr₂: C, 55.36; H, 5.97; N, 4.61. Found: C, 55.73; H, 5.79; N, 4.06.

i. {κ-C,N-(4,4-dimethyl-2-(2-phenylpropan-2-yl)-oxazoline)}CrCl(THF) (6-THF).

Purple **6-THF** dissolves in THF to give a blue solution. Evaporation of solvent gives a dark blue solid, presumably the monomeric THF adduct. If dissolved in THF-*d*₈, the NMR spectrum shows a set of broad, paramagnetic peaks.

¹H NMR (400 MHz, THF-*d*₈) δ 20.64, 17.86, 10.00, -2.00, -2.83, -16.55, -79.06.

j. $\{\kappa\text{-C,N-(}o\text{-C}_6\text{H}_4\text{)CMe}_2\text{(COCH}_2\text{CMe}_2\text{N)}\}\text{Fe(py)Cl (7-Cl)}$.

To a mixture of $\text{FeCl}_2(\text{py})_4$ (223 g, 0.502 mmol) and $(\text{PhCMe}_2\text{Ox})_2\text{Zn}$ (250 g, 0.502 mmol) were distilled 15 mL THF at $-78\text{ }^\circ\text{C}$. The suspension was stirred at $-78\text{ }^\circ\text{C}$ for 5 h and then slowly warmed and stirred at $25\text{ }^\circ\text{C}$ for 36 h. The golden brown solution was filtered and washed (2 x 10 mL). The filtrate was concentrated, cooled, and filtered cold to yield 100mg of yellow solid (52 %). X-ray diffraction quality crystals were grown by hot filtration and recrystallization from benzene.

Alternative preparation: $\text{BrPhCMe}_2\text{Ox}$ (250 mg, 0.844 mmol) in 5 mL THF was added to a solution of $n\text{-BuLi}$ (0.58 mL, 1.6 M in hexanes) in 10 mL THF at $-78\text{ }^\circ\text{C}$ under argon. After 2 h at $-78\text{ }^\circ\text{C}$, $\text{FeCl}_2(\text{py})_4$ (374 mg, 0.844 mmol) was added via addition finger. The reaction was kept at $-78\text{ }^\circ\text{C}$ for 5 h and then let slowly warm to room temperature overnight. The yellow-brown reaction mixture was stripped, triturated with benzene, filtered, and washed several times (2 x 15 mL). Concentration of the solvent yielded crystalline yellow material which was collected by filtration (190 mg, 58 %). $^1\text{H NMR}$ (400 MHz, benzene- d_6) δ 266.41 (1H), 246.08 (1H), 162.10 (2H), 137.15 (1H), 130.91 (1H), 80.85 (1H), 77.15 (1H), 42.38 (3H), 19.15 (2H), 15.36 (3H), -15.94 (2H), -32.35 (1H), -35.33 (3H). $\mu_{\text{eff}} = 4.7\text{ }\mu_{\text{B}}$ (Evans' Method). Anal. Calcd for $\text{C}_{19}\text{H}_{23}\text{N}_2\text{OClFe}$: C, 59.01; H, 6.00; N, 7.24. Found: C, 59.01; H, 5.91; N, 5.73.

k. $\{\kappa\text{-C,N-(}o\text{-C}_6\text{H}_4\text{)CMe}_2\text{(COCH}_2\text{CMe}_2\text{N)}\}_2\text{Ni (8)}$.

To a mixture of $\text{NiCl}_2(\text{DME})$ (88 mg, 0.282 mmol) and $(\text{PhCMe}_2\text{Ox})_2\text{Zn}$ (200 mg, 0.282 mmol) were distilled 25 mL THF at $-78\text{ }^\circ\text{C}$. The yellow suspension was stirred at $-78\text{ }^\circ\text{C}$ for 5 h and then slowly warmed to room temperature. The resulting orange solution was stripped, triturated with ether and filtered to give a peach-colored solid. The solid was recrystallized from an ether/THF mixture to give pale orange crystalline solid (34 mg, 25 %). The compound exhibits diastereotopic methyl groups

by NMR spectroscopy; however, coalescence of these peaks was not reached by heating up to 80 °C, beyond which temperature decomposition was observed. ^1H NMR (500 MHz, benzene- d_6) δ 7.23 (d, $J = 7.2$, 1H), 7.13 (d, $J = 7.7$, 1H), 6.98 (t, $J = 7.3$, 1H), 6.85 (t, $J = 7.1$, 1H), 3.66 (s, 3H), 3.36 (d, $J = 8.1$, 1H), 3.12 (d, $J = 8.1$, 1H), 1.81 (s, 3H), 0.94 (s, 3H), 0.69 (s, 3H). ^{13}C NMR (500 MHz, benzene- d_6) δ 177.82, 171.46, 148.36, 143.17, 124.28, 121.62, 121.20, 79.35, 68.97, 45.03, 35.51, 27.91, 25.47, 23.19. Anal. Calcd for $\text{C}_{28}\text{H}_{36}\text{N}_2\text{O}_2\text{Ni}$: C, 68.45; H, 7.39; N, 5.70. Found: C, 66.48; H, 6.88; N, 5.42.

REFERENCES

- 1) a) Davies, D.L.; Al-Duaij, O.; Fawcett, J.; Singh, K. *Organometallics* **2010**, *29*, 1413-1420. b) Chen, X.; Li, J.-J.; Hao, X.-S.; Goodhue, C.E.; Yu, J.-Q. *J. Am. Chem. Soc.* **2006**, *128*, 78-79. c) Giri, R.; Chen, X.; Yu, J.-Q. *Angew. Chem. Int. Ed.* **2005**, *44*, 2112-2115. d) Yuan, K.; Zhang, T.K.; Hou, X.L. *J. Org. Chem.* **2005**, *70*, 6085-6088. e) Davies, D.L.; Al-Duaij, O.; Fawcett, J.; Giardiello, M.; Hilton, S.T.; Russell, D.R. *Dalt. Trans.* **2003**, 4132-4138. f) Bonnardel, P.A.; Parish, R.V.; Pritchard, R.G. *J. Chem. Soc., Dalt. Trans.* **1996**, *15*, 3185-3193.
- 2) a) Nishiyama, H.; Ito, J. *Chem. Comm.* **2010**, *46*, 203-212. b) Nishiyama, H. *Chem. Soc. Rev.* **2007**, *36*, 1133-1141. c) Fossey, J.S.; Richards, C.J. *J. Organomet. Chem.* **2004**, *689*, 3056-3059. d) Fossey, J.S.; Richards, C.J. *Organometallics* **2004**, *23*, 367-373. e) Stark, M.A.; Jones, G.; Richards, C.J. *Organometallics* **2000**, *19*, 1282-1291. f) Motoyama, Y.; Mikami, Y.; Kawakami, H.; Aoki, K.; Nishiyama, J. *Chem. Lett.* **1997**, 951-952. g) Denmark, S.E.; Stavenger, R.A.; Faucher, A.-M.; Edwards, J.P. *J. Org. Chem.* **1997**, *62*, 3375-3389.
- 3) Djukic, J.-P.; Michon, C.; Heiser, D.; Kyritsakas-Gruber, N.; De Cian, A.; Doetz, K.H.; Pfeffer, M. *Eur. J. Inorg. Chem.* **2004**, *10*, 2107-2122.
- 4) Stol, M.; Snelders, D.J.M.; Godbole, M.D.; Havenith, R.W.A.; Haddleton, D.; Clarkson, G.; Lutz, M.; Spek, A.L.; van Klink, G.P.M.; van Koten, G. *Organometallics* **2007**, *26*, 3985-3994.
- 5) Berman, A.M.; Johnson, J.S. *J. Org. Chem.* **2006**, *71*, 219-224.
- 6) Wehman, E.; van Koten, G.; Jastrzebski, J.T.B.H.; Rotteveel, M.A.; Stam, C.H. *Organometallics* **1988**, *7*, 1477-1485.
- 7) Nagano, T.; Hayashi, T. *Org. Lett.* **2005**, *7*, 491-493.
- 8) Kumar, S.; Kandasamy, K.; Singh, H.B.; Butcher, R.J. *New J. Chem.* **2004**, *28*, 640-645.

- 9) Astley, S.T.; Stephenson, G.R. *Synlett*. **1992**, 6, 507-509.
- 10) Marshall, L.J.; Roydhouse, M.D.; Slawin, A.M.Z.; Walton, J.C. *J. Org. Chem.* **2007**, 72, 898-911.
- 11) Olmstead, M.M.; Power, P.P.; Shoner, S.C. *Inorg. Chem.* **1991**, 30, 2547-2551.
- 12) Krysan, D.J.; Mackenzie, P.B. *J. Org. Chem.* **1990**, 55, 4229-4230.
- 13) Ittel, S.D.; English, A.D.; Tolman, C.A.; Jesson, J.P. *Inorg. Chim. Acta* **1979**, 33, 101-106.
- 14) Kern, R. J. *J. Inorg. Nucl. Chem.* **1962**, 24, 1105-1109.
- 15) Golding, R.M.; Mok, K.F.; Duncan, J.F. *Inorg. Chem.* **1966**, 5, 774-778.
- 16) Ward, L.G.L. *Inorg. Syn.* **1971**, 13, 154-164.
- 17) Pray, A.R. *Inorg. Syn.* **1990**, 28, 321-322.

CHAPTER 3

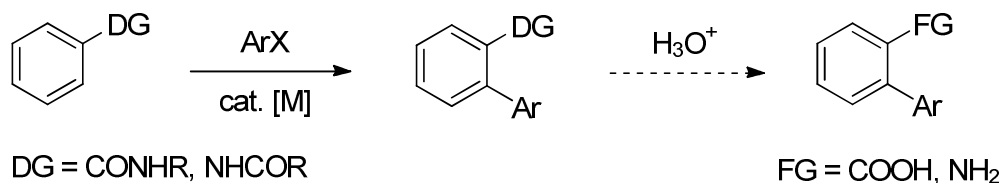
ARYL-CONTAINING PYRIDINE-IMINE AND AZAALLYL CHELATES OF IRON TOWARD STRONG FIELD COORDINATION COMPOUNDS*

I. Introduction

The ultimate purpose of creating strong fields in first row metals is to achieve catalysis with these less expensive and less toxic elements. Because the approach involves using sp^2 -aryl, carbon-based ligands, one can easily envision an aryl-aryl coupling scheme as a catalytic goal. Following previous efforts with 2-phenylpyridine and aryloxazolines, we chose to move to aryl-containing pyridine-imines as potential ligands for their ease of synthesis, an availability of substituted precursors, and the added kinetic stability afforded by the presence of two nitrogen donors.

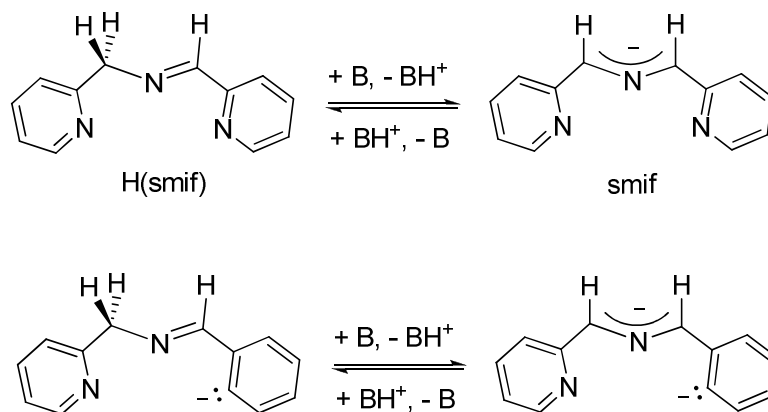
Our choice of aryl pyridine-imines was also inspired by the efforts of Yu, Daugulis, Fu, and others in the area of ligand-assisted, C-C bond-forming catalysis. In this approach, part of the ligand acts as a directing group for the aryl, vinyl, or alkyl portion to be functionalized (Scheme 3.1). In arguably the most synthetically useful cases, the directing group, or “ligand auxiliary” piece can be removed by hydrolysis to yield the functionalized coupled product. Ligand-assisted catalysis has been realized for sp^2 aryl^{1,2} and vinyl,³ activated sp^3 ,⁴⁻⁷ and more recently unactivated sp^3 substrates,⁸⁻¹¹ and with first- and second-row metals such as Ni,^{12,13} Cu,^{14,15} Pd,¹⁶ Ru,¹⁷ and Rh.^{18,19} To our knowledge, iron has not yet been employed in this type of catalysis, and its use would represent a valuable contribution to the field.

* Reproduced in part with permission from: Volpe, E. C.; Wolczanski, P. T.; Lobkovsky, E. B. *Organometallics* **2009**, 29, 364-377. Copyright 2009 American Chemical Society.



Scheme 3.1. General scheme of aryl-aryl coupling using directing-group ligands (DG = directing group).

Another motivation for investigating the aryl pyridine-imine ligand comes from a loosely related ligand, 1,3-di-2-pyridyl-2-azaallyl (smif, Scheme 3.2).^{20,21} The precursor of smif, a pyridyl pyridine-imine, undergoes facile deprotonation to give the delocalized anion, which has been shown to convey intense optical properties and relatively strong fields in its first-row metal complexes. We were interested in exploring the scope of the azaallyl unit; substitution of one pyridyl moiety of smif by an aryl group would lead to azaallyl complexes with similar properties. In a best-case scenario, the transformation of the aryl pyridine-imine to a stable azaallyl via simple deprotonation could be advantageous in a catalytic aryl-aryl coupling scheme.

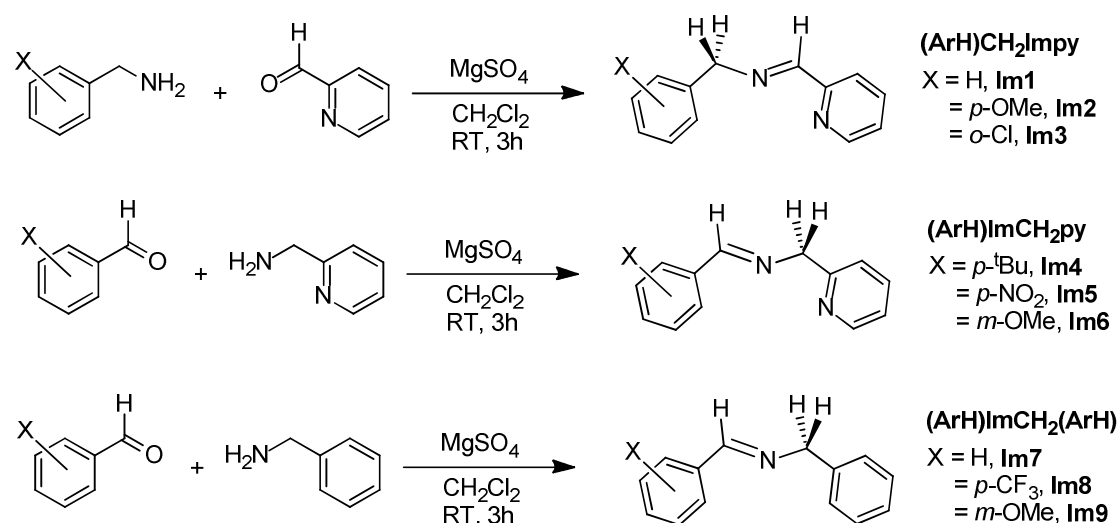


Scheme 3.2. Formation of 1,3-di-2-pyridyl-2-azaallyl (smif).

II. Results and Discussion

A. Imine synthesis.

A series of aryl- or pyridyl-imines were synthesized as potential ligands. Simple condensation of various benzylamines with 2-pyridine-carboxaldehyde, benzaldehydes with 2-(aminomethyl)-pyridine, and benzaldehydes with benzylamine led to the corresponding imine derivatives (Scheme 3.3). Variation of the aryl ring substitution afforded a range of electron-donating ability within each ligand set. The *ortho*-chlorinated imine (**Im3**) was first targeted as a possible means of metal arylation via Ar-Cl oxidative addition.

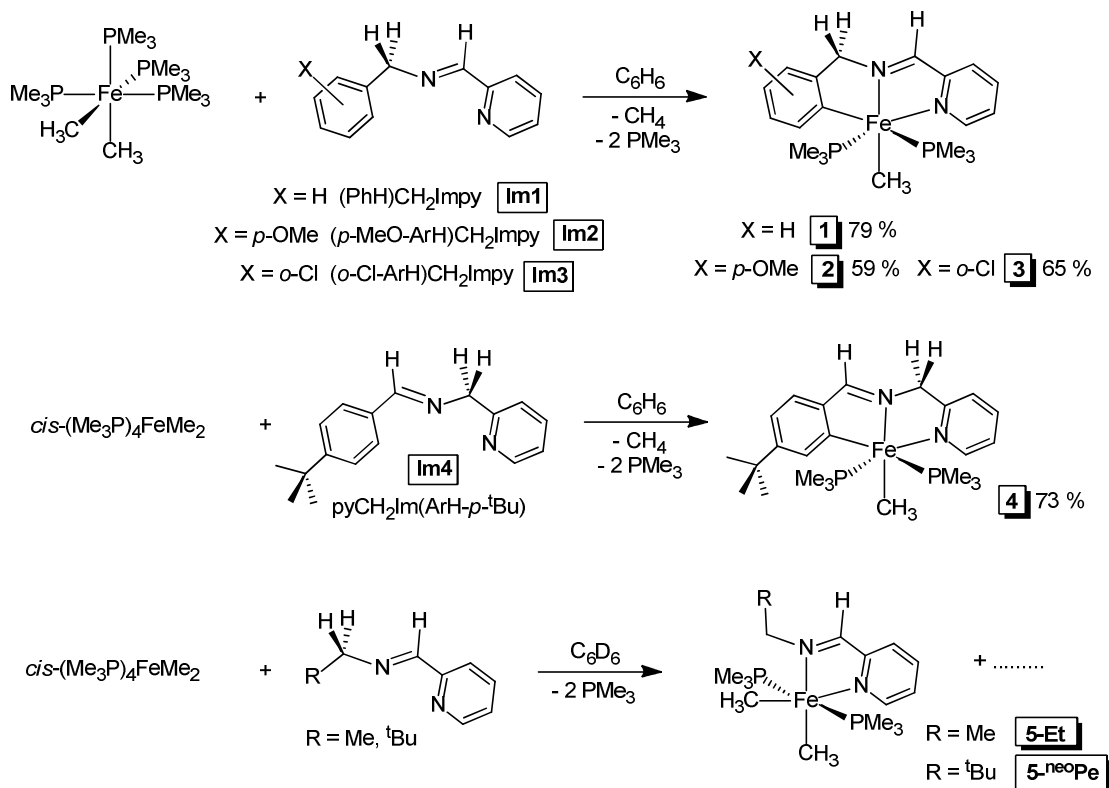


Scheme 3.3. Synthesis of imine derivatives (ArH)CH₂Impy (**Im1-Im3**), (ArH)ImCH₂py (**Im4-Im6**) and (ArH)ImCH₂(ArH) (**Im7-Im9**).

B. Synthesis of *trans*-{κ-C,N,N'-(Ar-2-yl)CH₂N=CH-2-py}(PMe₃)₂FeCH₃ (**1-3**) and *trans*-{κ-C,N,N'-(Ar-2-yl)CH=NCH₂-2-py}(PMe₃)₂FeCH₃ (**4**).

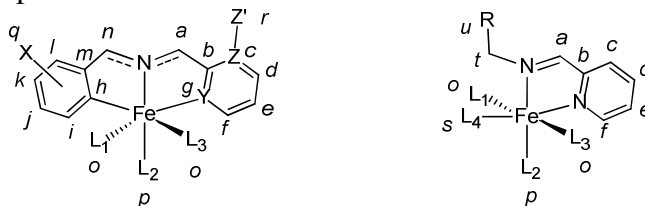
In search of a means to affect aryl activation of these imine derivatives, we were inspired by recent reports²²⁻²⁶ of aryl C-H bond activation by Karsch's *cis*-(Me₃P)₄FeMe₂ compound.²⁷ Gratifyingly, this complex was effective at activating the

aryl ring of both (ArH)CH₂Impy (**Im1-Im3**) and (ArH)ImCH₂py (**Im4**) ligand types (Scheme 3.4). The reaction proceeds with loss of one equivalent of methane and two equivalents of trimethylphosphine, to afford good yields (59-79 %) of *trans*-{κ-C,N,N'-(Ph-2-yl)CH₂N=CH-2-py}(PMe₃)₂FeCH₃ (**1**), *trans*-{κ-C,N,N'-(*p*-MeO-Ar-2-yl)CH₂N=CH-2-py}(PMe₃)₂FeCH₃ (**2**), and *trans*-{κ-C,N,N'-(*o*-Cl-Ar-2-yl)CH₂N=CH-2-py}(PMe₃)₂FeCH₃ (**3**), as dark green microcrystals, and *trans*-{κ-C,N,N'-(*p*-^tBu-Ar-2-yl)CH=NCH₂-2-py}(PMe₃)₂FeCH₃ (**4**), as dark blue crystals. A singlet in the ³¹P{¹H} NMR spectrum readily elucidated the *trans* arrangement of the phosphines in each of these complexes. ¹H, ¹³C{¹H} and ³¹P{¹H} NMR spectral data for all compounds are listed in Tables 3.1 and 3.2.



Scheme 3.4. Reaction of various pyridylimines with *cis*-(Me₃P)₄FeMe₂.

Table 3.1. ^1H and $^{31}\text{P}\{^1\text{H}\}$ NMR assignments (δ (J(Hz), assnmt)^{a,b} for imine and imine-derived complexes.



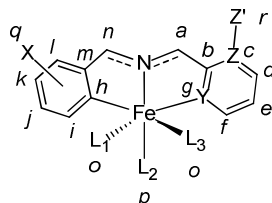
1	9.01 (s, <i>a</i>), 7.04 (m, <i>c</i>), 7.00 (t, 5, <i>d</i>), 6.87(m, <i>e</i>), 8.63 (d, 5, <i>f</i>), 7.21 (d, 5, <i>i</i>), 7.04 (m, <i>j</i>), 7.10 (t, 8, <i>k</i>), 6.92 (d, 5, <i>l</i>), 4.91 (s, <i>n</i>), 0.38 (s, <i>o</i>), 1.52 (t, 12, <i>p</i>); 6.37 (s, PMe_3 , <i>o</i>)
2	9.00 (s, <i>a</i>), 7.01 (m, <i>c</i>), 6.66 (d, 8, <i>d</i>), 6.58 (dd, 3, 6, <i>e</i>), 8.62 (d, 5, <i>f</i>), 7.01 (m, <i>i</i>), 7.13 (d, 8, <i>k</i>), 6.93 (d, 7, <i>l</i>), 4.94 (t, 4, <i>n</i>), 0.39 (t, 4, <i>o</i>), 1.47 (t, 14, <i>p</i>), 3.59 (s, OMe, <i>q</i>); 6.68 (s, PMe_3 , <i>o</i>)
3	8.93 (s, <i>a</i>), 7.04 (t, 5, <i>c</i>), 6.80 (t, 8, <i>d</i>), 6.72 (m, <i>e</i>), 8.46 (d, 5, <i>f</i>), 6.96 (m, <i>i</i>), 6.87 (m, <i>j</i>), 6.96 (m, <i>k</i>), 5.24 (t, 5, <i>n</i>), 0.33 (t, 5, <i>o</i>), 1.36 (t, 15, <i>p</i>); 8.44 (s, PMe_3 , <i>o</i>)
4	4.42 (s, <i>a</i>), 6.14 (m, <i>c</i>), 6.59 (t, 8, <i>d</i>), 6.14 (m, <i>e</i>), 8.05 (d, 5, <i>f</i>), 8.75 (s, <i>i</i>), 7.11 (d, 10, <i>k</i>), 7.57 (d, 10, <i>l</i>), 7.90 (s, <i>n</i>), 0.69 (s, <i>o</i>), -0.23 (t, 10, <i>p</i>), 1.52 (s, <i>q</i>); 22.84 (s, PMe_3 , <i>o</i>)
5-Et	9.18 (s, <i>a</i>), 7.05 (d, 8, <i>c</i>), 7.12 (t, 7, <i>d</i>), 7.20 (t, 6, <i>e</i>), 9.23 (d, 6, <i>f</i>), 0.49 (s, <i>o</i>), 1.29 (t, 13, <i>p</i>), -0.01 (t, 11, <i>s</i>), 3.96 (t, 7, <i>t</i>), 2.16 (“sx”, 8, <i>u</i> (CH ₂)), 1.11 (t, 7, <i>u</i> (CH ₃)), -0.59 (s, PMe_3 , <i>o</i>)
5^{-neo}Pe^c	9.31 (<i>a</i>), 7.03 (<i>c</i>), 7.13 (<i>d</i>), 7.20 (<i>e</i>), 9.46 (<i>f</i>), 0.51 (s, <i>o</i>), 1.12 (<i>p</i>), 0.13 (s), 3.80 (<i>t</i>), 1.28 (<i>u</i>); -1.43 (s, PMe_3 , <i>o</i>)
6	5.03 (br s, <i>a</i>), 8.40 (d, 2, <i>d</i>), 6.86 (dd, 8, 2, <i>e</i>), 7.91 (d, 8, <i>f</i>), 8.09 (s, <i>i</i>), 7.03 (d, 8, <i>k</i>), 7.34 (d, 8, <i>l</i>), 7.86 (br s, <i>n</i>), 0.55 (t, 4, <i>o</i>), 1.32 (d, 8, <i>p</i>), 1.43 (s, <i>q</i>); 24.77 (“t”, ^d 61, PMe_3 , <i>p</i>), 19.60 (d, 61, PMe_3 , <i>o</i>)
7^e	5.47 (s, <i>a</i>), 7.87 (d, 6, <i>d</i>), 7.01 (t, 7, <i>e</i>), 8.34 (d, 7, <i>f</i>), 8.02 (s, <i>i</i>), 6.92 (d, 8, <i>k</i>), 7.40 (d, 8, <i>l</i>), 8.68 (br s, <i>n</i>), 0.80 (t, 3, <i>o</i>), 1.58 (d, 5, <i>p</i>), 1.33 (s, <i>q</i>), 4.14 (s, <i>r</i>); 23.02 (“t”, ^d 61, PMe_3 , <i>p</i>), 18.82 (d, 61, PMe_3 , <i>o</i>)
8	5.84 (s, <i>a</i>), 6.73 (d, 6, <i>d</i>), 5.51 (t, 6, <i>e</i>), 5.80 (d, 6, <i>f</i>), 8.06 (s, <i>i</i>), 7.03 (d, 8, <i>k</i>), 7.18 (d, 8, <i>l</i>), 7.37 (s, <i>n</i>), 0.99 (s, <i>o</i>), 1.33 (d, 6, <i>p</i>), 1.50 (s, <i>q</i>), 2.38 (s, <i>r</i>); 27.33 (“t”, ^d 59, PMe_3 , <i>p</i>), 20.74 (d, 59, PMe_3 , <i>o</i>)
9^{e,f}	40.80 (1H), 28.75 (1H), 19.88 (1H), 16.92 (1H), 13.35 (2H, <i>a</i>), 1.29 (1H), 1.16 (9H, <i>q</i>), -0.46 (1H), -5.22 (3H), -15.30 (18H, <i>o</i>), -55.30 (1H)
10^{e,f}	30.12 (1H), 22.03 (1H), 13.76 (1H), 12.73 (1H), 1.91 (9H, <i>q</i>), 1.77 (3H), -1.71 (1H), -1.97 (1H), -12.36 (1H), -14.39 (18H, <i>o</i>), -27.00 (1H), -47.97 (1H)
11^g	4.79 (s, <i>a</i>), 7.03 (d, 8, <i>c</i>), 7.11 (t, 7, <i>d</i>), 7.12 (t, 7, <i>e</i>), 7.81 (d, 7, <i>f</i>), 8.13 (d, 8, <i>i</i>), 7.18 (m, <i>j</i>), 7.18 (m, <i>k</i>), 7.46 (d, 8, <i>l</i>), 8.02 (br s, <i>n</i>), 0.59 (s, <i>o</i>), 1.33 (d, 6, <i>p</i>); 23.73 (“t”, ^d 61, PMe_3 , <i>p</i>), 19.43 (d, 61, PMe_3 , <i>o</i>)
12	4.74 (br s, <i>a</i>), 7.00 (d, <i>c</i>), 7.11 (t, <i>d</i>), 7.14 (m, <i>e</i>), 7.73 (d, <i>f</i>), 8.51 (s, <i>i</i>), 7.28 (m, <i>k</i>), 7.28 (m, <i>l</i>), 7.94 (br s, <i>n</i>), 0.47 (t, <i>o</i>), 1.30 (d, <i>p</i>); 22.28 (“t”, ^d 63, PMe_3 , <i>p</i>), 18.01 (d, 63, PMe_3 , <i>o</i>)
13	4.84 (br s, <i>a</i>), 6.99 (d, 8, <i>c</i>), 7.09 (t, 7, <i>d</i>), 7.13 (m, <i>e</i>), 7.77 (d, 8, <i>f</i>), 7.93 (d, 8, <i>j</i>), 7.18 (m, <i>k</i>), 7.02 (d, 8, <i>l</i>), 8.03 (br s, <i>n</i>), 0.61 (t, 3, <i>o</i>), 1.36 (d, 6, <i>p</i>); 24.16 (“t”, ^d 62, PMe_3 , <i>p</i>), 19.51 (d, 62, PMe_3 , <i>o</i>)

Table 3.1. (Continued)

14^h 143.78 (2H, *n*), 37.27 (1H), 28.61 (1H), 17.42 (1H), 17.36 (1H), -14.21 (18H, *o*), -15.99 (9H, *p*), -22.59 (1H), -34.30 (1H), -36.32 (1H), -39.96 (1H), -56.33 (1H)

^aBenzene-*d*₆ unless otherwise noted. ^bAssignments for **7** were made based on HMBC and NOESY; assignments for the remaining compounds were made analogously, by literature comparison, or via COSY (**12**). ^cSignals broad; coupling not resolved. ^dActually appears as a non-first order dd in A₂B spin system; shifts and *J*_{pp} determined from simulation. ^eTHF-*d*₈. ^fParamagnetic spectra were assigned only on the basis of integrated intensity. ^gAssignments are for structure with N=C(*a*). ^hCD₂Cl₂.

Table 3.2. ^{13}C NMR assignments (δ (J_{PC} (Hz), assnmt)^{a,b,c} for imine and imine-derived complexes.



1	153.23 (<i>a</i>), 161.93 (<i>b</i>), 124.21 (t, 4, <i>c</i>), 126.93 (<i>d</i>), 120.61 (t, 1, <i>e</i>), 152.99 (<i>f</i>), 178.48 (t, 37, <i>h</i>), 140.31 (t, 4, <i>i</i>), 120.83 (t, 3, <i>j</i>), 121.49 (<i>k</i>), 117.94 (t, 3, <i>l</i>), 152.17 (<i>m</i>), 70.26 (<i>n</i>), 10.77 (t, 10, <i>o</i>), -4.61 (t, 33, <i>p</i>)
2	157.15 (<i>a</i>), 161.89 (<i>b</i>), 125.39 (t, 3, <i>c</i>), 126.98 (<i>d</i>), 120.52 (t, 3, <i>e</i>), 152.98 (<i>f</i>), 181.67 (t, 37, <i>h</i>), 145.58 (t, 1, <i>i</i>), 106.42 (<i>j</i>), 121.51 (<i>k</i>), 117.76 (t, 3, <i>l</i>), 152.12 (<i>m</i>), 69.67 (<i>n</i>), 10.84 (t, 11, <i>o</i>), -4.34 (t, 33, <i>p</i>), 54.83 (<i>q</i>)
3	149.43 (<i>a</i>), 161.70 (<i>b</i>), 125.54 (t, 4, <i>c</i>), 127.53 (<i>d</i>), 120.40 (t, 3, <i>e</i>), 152.61 (<i>f</i>), 185.33 (<i>h</i>), 138.52 (<i>i</i>), 120.77 (<i>j</i>), 121.65 (<i>k</i>), 125.22 (<i>l</i>), 152.60 (<i>m</i>), 70.25 (<i>n</i>), 10.68 (<i>o</i>), -4.38 (t, 33, <i>p</i>)
4	61.08 (<i>a</i>), 165.02 (<i>b</i>), 122.05 (<i>c</i>), 128.78 (<i>d</i>), 116.36 (<i>e</i>), 151.59 (<i>f</i>), 190.17 (<i>h</i>), 141.76 (<i>i</i>), 146.88 (<i>j</i>), 116.60 (<i>k</i>), 123.46 (<i>l</i>), 152.04 (<i>m</i>), 163.51 (<i>n</i>), 11.35 (<i>o</i>), -10.00 (<i>p</i>), 35.41 (CMe ₃ , <i>q</i>), 32.37 (C(CH ₃) ₃ , <i>q</i>)
6	66.23 (<i>a</i>), 172.55 (<i>b</i>), 141.97 (<i>d</i>), 120.57 (<i>e</i>), 150.09 (<i>f</i>), 178.00 (<i>g</i>), 201.77 (<i>h</i>), 142.78 (<i>i</i>), 148.34 (<i>j</i>), 117.12 (<i>k</i>), 126.22 (<i>l</i>), 151.51 (<i>m</i>), 170.09 (<i>n</i>), 17.59 (<i>o</i>), 23.84 (<i>p</i>), 35.12 (CMe ₃ , <i>q</i>), 32.42 (C(CH ₃) ₃ , <i>q</i>)
7^d	62.62 (<i>a</i>), 166.37 (<i>b</i>), 155.57 (<i>d</i>), 122.11 (<i>e</i>), 135.28 (<i>f</i>), 182.50 (<i>g</i>), 196.53 (<i>h</i>), 143.00 (<i>i</i>), 149.91 (<i>j</i>), 118.40 (<i>k</i>), 127.05 (<i>l</i>), 152.07 (<i>m</i>), 173.66 (<i>n</i>), 17.42 (t, 11, <i>o</i>), 23.26 (d, 16, <i>p</i>), 35.48 (CMe ₃ , <i>q</i>), 32.27 (C(CH ₃) ₃ , <i>q</i>), 46.60 (<i>r</i>)
8	108.95 (<i>a</i>), 160.77 (<i>b</i>), 145.20 (<i>d</i>), 121.20 (<i>e</i>), 135.80 (t, 3, <i>f</i>), 190.15 (td, 13, 19, <i>g</i>), 195.10 (td, 10, 25, <i>h</i>), 142.26 (<i>i</i>), 148.24 (d, 3, <i>j</i>), 117.56 (<i>k</i>), 127.31 (<i>l</i>), 154.22 (d, 5, <i>m</i>), 106.78 (<i>n</i>), 17.44 (td, 2, 10, <i>o</i>), 23.73 (d, 15, <i>p</i>), 34.88 (CMe ₃ , <i>q</i>), 32.59 (C(CH ₃) ₃ , <i>q</i>), 41.39 (<i>r</i>)
11^e	168.70 (t, 4, <i>a</i>), 151.86 (<i>b</i>), 125.87 (<i>c</i>), 116.13 (t, 4, <i>d</i>), 140.17 (<i>e</i>), 143.99 (<i>f</i>), 206.41 (m, <i>g</i>), 183.21 (m, <i>h</i>), 118.57 (<i>i</i>), 120.98 (t, 3, <i>j</i>), 141.44 (<i>k</i>), 124.71 (t, 3, <i>l</i>), 157.37 (<i>m</i>), 66.48 (<i>n</i>), 23.76 (d, 15, <i>o</i>), 17.63 (t, 10, <i>p</i>)
12^f	66.48 (<i>a</i>), 157.37 (<i>b</i>), 124.71 (t, 3, <i>c</i>), 141.44 (<i>d</i>), 120.98 (t, 3, <i>e</i>), 118.57 (t, 2, <i>f</i>), 183.21 (m, <i>g</i>), 206.41 (m, <i>h</i>), 143.99 (<i>i</i>), 140.17 (<i>j</i>), 116.13 (t, 4, <i>k</i>), 125.87 (<i>l</i>), 151.86 (<i>m</i>), 168.70 (t, 4, <i>n</i>), 23.34 (td, 3, 16, <i>o</i>), 17.30 (td, 3, 11, <i>p</i>)

^aBenzene-*d*₆ unless otherwise noted. ^bAssignments for **7** were made based on HMBC and NOESY; assignments for the remaining compounds were made analogously or by comparison to literature species. ^c J_{PC} are given when the resolution and signal-to-noise permitted an unambiguous assessment. ^dTHF-*d*₈. ^eAssignments are for structure with N=C(*a*). ^fSignal for CF₃ (*q*) not located.

In the case of alkyl-substituted pyridyl imines, reaction with *cis*-(Me₃P)₄FeMe₂ led to simple adducts, *trans,cis*-(Me₃P)₂(CH₃)₂Fe{κ-N,N'-RCH₂N=CH-2-py} (R = Me, **5**-Et; ^tBu, **5**-^{neo}Pe), from displacement of two trimethylphosphine ligands. When purple solutions of **5**-Et and **5**-^{neo}Pe were heated with the goal of inducing sp³ C-H activation, only degradation of the complexes was observed, hence no further data on these compounds was obtained.

C. Reactivity of Fe(II) iminopyridine and iminomethylpyridine complexes.

1. Ligand exchange attempts.

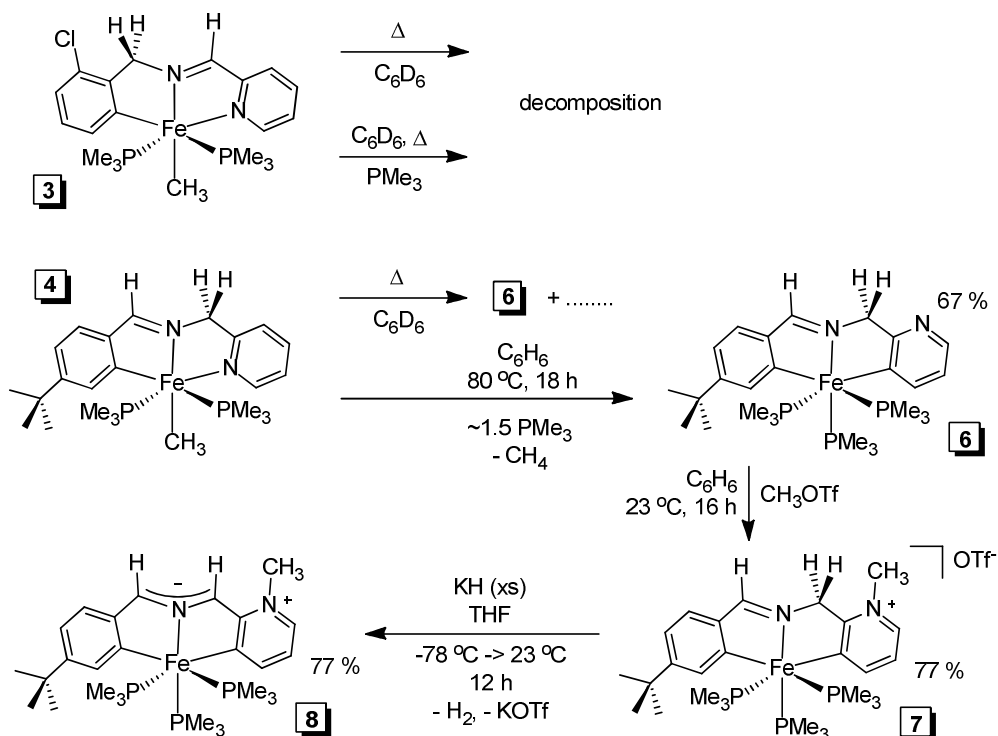
In catalytic processes which involve aryl C-C, C-N, C-O, or C-X bond formation, ligand exchange is a key step. With this goal in mind, we attempted to exchange imine ligands of complexes **1-3**. When *trans*-{κ-C,N,N'-(Ph-2-yl)CH₂N=CH-2-py}(PMe₃)₂FeCH₃ (**1**) and *trans*-{κ-C,N,N'-(*o*-Cl-Ar-2-yl)CH₂N=CH-2-py}(PMe₃)₂FeCH₃ (**3**) were treated with either one equivalent or an excess of **Im3** and **Im1**, respectively, no ligand exchange was observed. The same result was obtained with heating. The reactions lacked any evidence for the formation of bis-{κ-C,N,N'-(Ar-2-yl)CH₂N=CH-2-py}(PMe₃)₂Fe, a possible indication that the iron-methyl bond remained intact even at higher temperatures. Additional reactions of **1** and **3** with excess ArCH₂NH₂, showed no occurrence of transamination.

2. Thermal reactivity.

As previously mentioned, we had envisioned the chlorinated imine derivative (**Im3**) in a pathway involving reductive elimination and Ar-Cl oxidative addition to the Fe(0) center. With a remaining methyl ligand on the iron in complex **3**, this was still a possible event. As in our transamination attempts, thermolysis of **3** (with or without excess PMe₃) incurred no such behavior; both the iron-methyl and aryl-chloride bonds appear to be conserved until the starting material eventually decomposed with additional heating.

In contrast, thermolysis of **4** led to the formation of a new product, with minor side products (Scheme 3.5). The reaction with excess PMe_3 (~1.5 equiv) resulted in clean conversion to the product, which manifested a pseudo-triplet^{28,29} at 24.77 ppm (1P) and pseudo-doublet^{28,29} at 19.60 ppm (2P) ($J_{\text{PP}} = 61$ Hz) in the $^{31}\text{P}\{^1\text{H}\}$ NMR spectrum, indicative of a meridional configuration of three PMe_3 ligands. Upon scale-up the compound was isolated in 67 % yield as yellow-brown crystals. Further analysis by COSY and HMBC³⁰ NMR spectroscopy helped to confirm its identity as *mer*- $\{\kappa\text{-C,N,N'-(p-}^t\text{Bu-Ar-2-yl)CH=NCH}_2\text{(2-py-3-yl)}\}(\text{PMe}_3)_3\text{Fe}$ (**6**) and enabled assignment of each ^1H and ^{13}C resonance, listed in Tables 3.1 and 3.2.

The reaction likely proceeds by dissociation of pyridine, rotation about the $\text{C}_{\text{py}}\text{-CH}_2$ bond, loss of methane, and filling of the vacant site with PMe_3 . Methane was observed in the ^1H spectrum of a sealed NMR tube reaction, and by Toepler pump/IR analysis of reaction volatiles. Less certain is why the same process is not operative in the case of **3**. The $\text{Fe-N}_{\text{im}}\text{-C-C-N}_{\text{py}}$ metallacycle containing the sp^3 -hybridized carbon in **4** is more pinched than the sp^2 carbon-containing metallacycle of **3**, due to the smaller $\text{N}_{\text{im}}\text{-C-C}$ angle. Perhaps in the case of **4**, rotation of the pyridine ring brings the ortho C-H closer to the metal center/methyl group as a result of the smaller internal angle, whereas with **3**, the ortho C-H is held too far away for deprotonation to occur.



Scheme 3.5. Thermolysis of *trans*-{ κ -C,N,N'-(*o*-Cl-Ar-2-yl)CH₂N=CH-2-py}(PMe₃)₂FeCH₃ (**3**) and *trans*-{ κ -C,N,N'-(*p*-^tBu-Ar-2-yl)CH=NCH₂-2-py}(PMe₃)₂FeCH₃ (**4**), and formation of the zwitterionic *mer*-{ κ -C,N,C'-(*p*-^tBu-Ar-2-yl)CHNCH(2-py-NCH₃-3-yl)}(PMe₃)₃Fe (**8**).

3. Synthesis and structure of [*mer*-{ κ -C,N,C'-(*p*-^tBu-Ar-2-yl)CH=NCH₂(2-py-NCH₃-3-yl)}(PMe₃)₃Fe]OTf (**7**).

With *mer*-{ κ -C,N,N'-(*p*-^tBu-Ar-2-yl)CH=NCH₂(2-py-3-yl)}(PMe₃)₃Fe (**6**) in hand, we could explore the possibility of making a neutral, Fe(II) azaallyl, analogous to the ‘smif’ compounds previously reported. The first step involved methylation of the pyridine-nitrogen. Treatment of **6** with one equivalent of MeOTf in benzene at room temperature afforded insoluble brown crystals of the N-methyl derivative, [*mer*-{ κ -C,N,C'-(*p*-^tBu-Ar-2-yl)CH=NCH₂(2-py-NCH₃-3-yl)}(PMe₃)₃Fe]OTf (**7**) in 77 % (Scheme 3.5). Retention of the *mer*-configuration of the three phosphine ligands was manifested in the ³¹P{¹H} NMR spectrum, which exhibited the same A₂B pattern (δ 23.02 (1P), δ 18.82 (2P) (J_{PP} = 61 Hz))^{28,29} as in **6**.

X-ray crystal diffraction analysis was employed to verify methylation at nitrogen and to unambiguously confirm the presence of the second iron-carbon linkage in **6** and **7** (Figure 3.1). Relevant crystallographic data are presented in Table 3.3, and pertinent bond distances and angles are listed in Table 3.4. The structure shows pseudo-octahedral geometry about iron and validation of the *mer*-arrangement of phosphines. The average iron-phosphorus distances (2.243(3) Å), iron-carbon distances (2.0287(12) and 1.9940(13), respectively), and iron-N_{aza} distance (1.9347(11) Å) are standard. A distinction between the backbone N=CH bond (N1-C7 = 1.2885(15) Å) and N-CH₂ bond (N1-C8 = 1.4567(18) Å) is evident by the bond length discrepancy of ~0.17 Å.

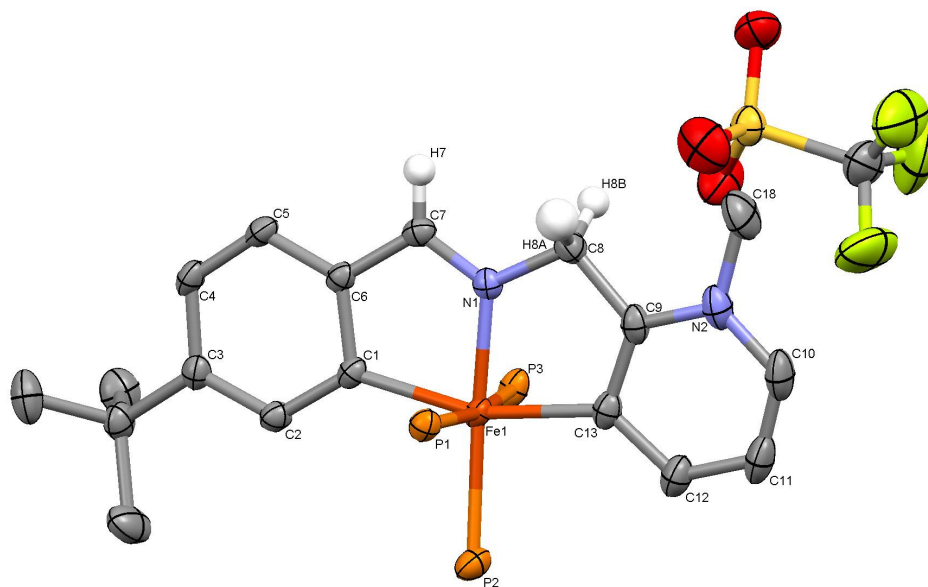


Figure 3.1. Molecular view of the cation of [*mer*-{ κ -C,N,C'-(*p*-^tBu-Ar-2-yl)CH=NCH₂(2-py-NCH₃-3-yl)}(PMe₃)₃Fe]OTf (**7**).

Table 3.3. Selected crystallographic and refinement data for [*mer*-{ κ -C,N,C'-(*p*-^tBu-Ar-2-yl)CH=NCH₂(2-py-NCH₃-3-yl)}(PMe₃)₃Fe]OTf (**7**), *mer*-{ κ -C,N,C'-(*p*-^tBu-Ar-2-yl)CHNCH(2-py-NCH₃-3-yl)}(PMe₃)₃Fe (**8**), and [*mer*- κ -C,N,C'-(Ph-2-yl)CH₂N=CH(Ph-2-yl)}Fe(PMe₃)₃]OTf (**14**).

	7	8	14
Formula	C ₂₈ H ₄₈ N ₂ O ₃ F ₃ P ₃ SFe	C ₂₇ H ₄₇ N ₂ P ₃ Fe	C ₂₄ H ₃₈ NO ₃ F ₃ P ₃ SFe
Formula weight	698.50	548.43	626.37
Crystal system	Triclinic	Monoclinic	Monoclinic
Space group	P-1	P2 ₁ /c	P2 ₁ /c
Z	2	4	8
<i>a</i> (Å)	9.1821(3)	16.9889(5)	24.1590(6)
<i>b</i> (Å)	13.7066(4)	9.3446(2)	12.6587(3)
<i>c</i> (Å)	14.5326(5)	19.4216(6)	18.8974(4)
α (°)	97.4860(10)	90	90
β (°)	105.8730(10)	105.4310(10)	93.2550(10)
γ (°)	102.5040(10)	90	90
<i>V</i> (Å ³)	1682.20(9)	2972.12(14)	5769.9(2)
<i>r</i> _{calc} (g cm ⁻³)	1.379	1.226	1.379
μ (mm ⁻¹)	0.701	0.686	0.807
Temperature (K)	173(2)	173(2)	173(2)
λ (Å)	0.71073	0.71073	0.71073
Final R indices [<i>I</i> > 2 σ (<i>I</i>)] ^{a,b}	R ₁ = 0.0419 wR ₂ = 0.0960	R ₁ = 0.0404 wR ₂ = 0.0920	R ₁ = 0.0418 wR ₂ = 0.0916
R indices (all data) ^{a,b}	R ₁ = 0.0623 wR ₂ = 0.1043	R ₁ = 0.0628 wR ₂ = 0.1012	R ₁ = 0.0730 wR ₂ = 0.1041
Goodness-of-fit ^c	1.059	1.038	1.037

^a $R_1 = \sum ||F_o| - |F_c|| / \sum |F_o|$. ^b $wR_2 = [\sum w(|F_o| - |F_c|)^2 / \sum wF_o^2]^{1/2}$. ^c GOF (all data) = $[\sum w(|F_o| - |F_c|)^2 / (n - p)]^{1/2}$, *n* = number of independent reflections, *p* = number of parameters.

The constraint of the ligand chelate renders bond angles N1-Fe-C1 (80.24(5) °) and N1-Fe-C13 (81.82(5) °) away from 90° and C1-Fe-C13 (161.95(6) °) less than 180 °, but apart from these and minor distortions about the phosphines, the core angles are close to ideal. A ~20 ° difference between the outer iron-aryl angle (Fe-C1-C2 = 134.83(9) °) and the inner angle (Fe-C1-C6 = 113.77(11) °) demonstrates asymmetric binding of the ring to the iron center. The same is true for the pyridyl ring, where the outer angle (Fe-C13-C9 = 113.23(9) °) exceeds the inner angle (Fe-C13-C12 = 134.15(12) °).

Table 3.4. Selected distances (Å) and angles (°) for [*mer*-{κ-C,N,C'-(*p*-^tBu-Ar-2-yl)CH=NCH₂(2-py-NCH₃-3-yl)}(PMe₃)₃Fe]OTf (**7**), *mer*-{κ-C,N,C'-(*p*-^tBu-Ar-2-yl)CHNCH(2-py-NCH₃-3-yl)}(PMe₃)₃Fe (**8**), and [*mer*-κ-C,N,C'-{(Ph-2-yl)CH₂N=CH(Ph-2-yl)}Fe(PMe₃)₃]OTf (**14**).

	7	8	14^a	
Fe-P1	2.2407(4)	2.2252(4)	2.2982(6)	2.3023(6)
Fe-P2	2.2470(4)	2.2122(4)	2.2959(6)	2.2728(6)
Fe-P3	2.2424(4)	2.2295(4)	2.3133(6)	2.3179(6)
Fe-N1	1.9347(11)	1.9622(12)	1.9372(16)	1.9406(15)
Fe-C1	2.0287(12)	2.0220(14)	2.033(2)	2.0521(18)
Fe-C13(C14)	1.9940(13)	2.0163(15)	2.036(2)	2.0444(18)
N1-C7	1.2885(15)	1.3028(19)	1.292(3)	1.294(2)
N1-C8	1.4567(18)	1.380(2)	1.464(3)	1.452(2)
C6-C7	1.4296(19)	1.432(2)	1.439(3)	1.436(3)
C8-C9	1.4958(19)	1.375(2)	1.494(3)	1.489(3)
P-C(av)	1.833(7)	1.838(6)	1.825(8)	
N1-Fe-C1	80.24(5)	80.66(5)	80.30(8)	80.25(7)
N1-Fe-C13(14)	81.82(5)	81.76(6)	81.82(8)	81.64(7)
N1-Fe-P1	86.52(4)	88.73(3)	89.26(5)	90.12(5)
N1-Fe-P2	175.30(4)	174.66(4)	175.66(5)	174.16(5)
N1-Fe-P3	89.95(4)	85.49(3)	86.48(5)	85.75(5)
C1-Fe-C13(14)	161.95(6)	162.04(6)	161.70(8)	160.04(8)
C1-Fe-P1	87.35(4)	85.24(4)	82.88(6)	82.35(5)
C1-Fe-P2	103.14(4)	103.74(4)	103.70(6)	105.09(6)
C1-Fe-P3	84.72(4)	87.38(4)	85.07(6)	84.31(5)
C13(14)-Fe-P1	93.52(4)	90.76(4)	93.06(6)	89.37(5)
C13(14)-Fe-P2	94.88(4)	94.02(4)	94.30(6)	93.41(6)
C13(14)-Fe-P3	93.33(4)	94.86(4)	97.70(6)	102.67(5)
P1-Fe-P2	90.354(16)	94.615(16)	92.90(2)	92.93(2)
P1-Fe-P3	171.773(14)	171.288(17)	167.73(2)	166.53(2)
P2-Fe-P3	93.603(16)	91.636(16)	92.14(2)	92.37(2)
Fe-N1-C7	119.55(10)	118.03(11)	119.55(14)	119.30(13)
Fe-N1-C8	120.10(8)	116.93(10)	119.51(14)	119.11(12)
Fe-C1-C2	134.83(9)	134.30(10)	134.26(16)	133.80(15)
Fe-C1-C6	113.77(11)	111.72(11)	111.36(14)	110.86(13)
Fe-C13(14)-C9	113.23(9)	110.08(10)	112.93(15)	111.93(13)
Fe-C13(14)-C12	134.15(12)	135.70(12)	132.55(17)	132.71(15)
Fe-P-C(av)	118.5(19)	118.9(22)	117.5(21)	

^aFirst values correspond to Figure 3.4; second values correspond to equivalent molecular distances and angles in second independent molecule.

4. Synthesis and structure of *mer*-{ κ -C,N,C'-(*p*-^tBu-Ar-2-yl)CHNCH(2-py-NCH₃-3-yl)}(PMe₃)₃Fe (**8**).

To make an azaallyl from [*mer*-{ κ -C,N,C'-(*p*-^tBu-Ar-2-yl)CH=NCH₂(2-py-NCH₃-3-yl)}(PMe₃)₃Fe]OTf (**7**), one can envision deprotonation of the relatively acidic methylene backbone as the final step. Indeed, addition of excess KH to **7** in THF at -78 °C led to a color change from brown to intense green with concomitant bubbling, presumably from loss of H₂ (Scheme 3.5). ¹H NMR integrations of the new product indicated replacement of the CH₂ singlet at 5.47 ppm (2H) with a new downfield singlet at 5.84 ppm (1H). Scale-up of the reaction yielded 61 % of the product as a green solid.

X-ray diffraction quality crystals of this more soluble compound were grown from THF/Et₂O solution, revealing the structure of the zwitterionic azaallyl complex, *mer*-{ κ -C,N,C'-(*p*-^tBu-Ar-2-yl)CHNCH(2-py-NCH₃-3-yl)}(PMe₃)₃Fe (**8**) (Figure 3.2). The structure affirms deprotonation to give an additional sp²-hybridized backbone carbon. Accordingly, the N1-C8 distance has significantly shortened from 1.4567(18) Å in **7** to 1.380(2) Å in **8**, and C8-C9 is also substantially shorter (1.375(2) Å in **8** versus 1.4958(19) Å in **7**). A difference in N1-C7 and N1-C8, 1.3028(19) and 1.380(2) Å, respectively, points to a slightly asymmetric azaallyl that is not completely delocalized. Furthermore, the short N1-C7 and C8-C9 distances indicate contribution from non-delocalized resonance structure resulting from dearomatization of the pyridine ring. Minor pinching of the Fe-N1-C8 and Fe-C13-C9 angles (120.10(8) ° to 116.93(10) ° and 113.23(9) ° to 110.08(10) °, respectively) has occurred to accommodate the larger internal N1-C8-C9 angle of the sp²-carbon-containing chelate. These comparisons are delineated in Table 3.4.

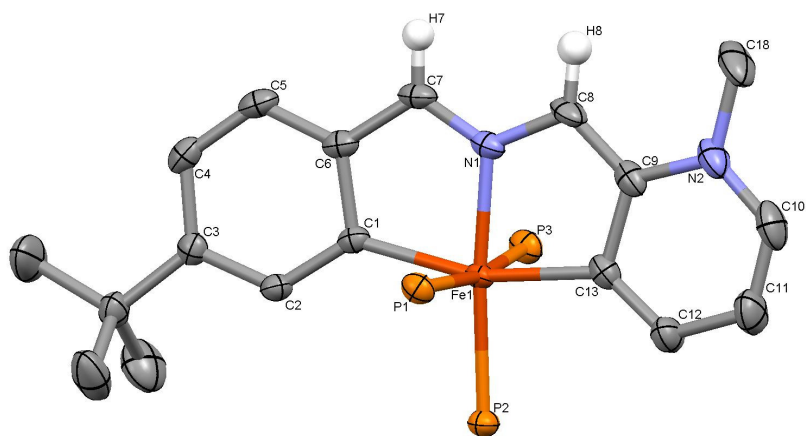


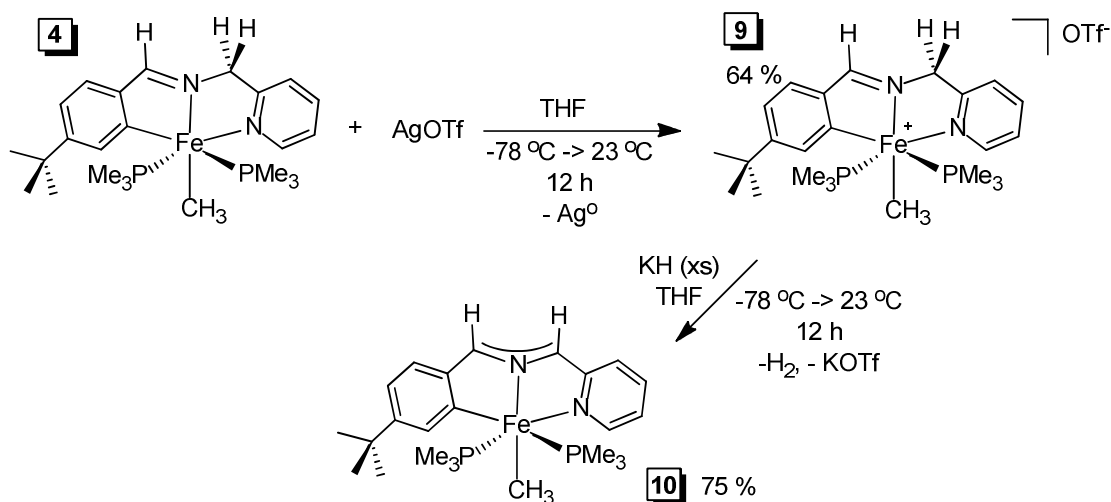
Figure 3.2. Molecular view of *mer*-{ κ -C,N,C'-(*p*-^tBu-Ar-2-yl)CHNCH(2-py-NCH₃-3-yl)}(PMe₃)₃Fe (**8**).

Remaining deviations in bond distances and angles of **8** relative to its precursor **7** are inconsequential; as the deprotonation reaction is solely ligand-based, structural changes are expected for the ligand rather than the core.

D. Iron (III) iminopyridine derivatives.

1. Synthesis of [*trans*-{ κ -C,N,N'-(*p*-^tBu-Ar-2-yl)CH=NCH₂-2-py}(PMe₃)₂FeCH₃]OTf (**9**).

The success of azaallyl formation with cation **7** prompted efforts to isolate an iron (III) azaallyl. Given the previous utility and solubility of the ^tBu-derivative, *trans*-{ κ -C,N,N'-(*p*-^tBu-Ar-2-yl)CH=NCH₂-2-py}(PMe₃)₂FeCH₃ (**4**), it was selected for the study. Treatment of **4** with one equivalent of AgOTf in THF resulted in isolation of a less-soluble, red-orange crystalline solid in 64 %, identified as [*trans*-{ κ -C,N,N'-(*p*-^tBu-Ar-2-yl)CH=NCH₂-2-py}(PMe₃)₂FeCH₃]OTf (**9**) (Scheme 3.6). The compound exhibited paramagnetic resonances in the ¹H NMR spectrum (Table 3.1). A Gouy balance measurement confirmed the paramagnetic nature of **9**, giving a μ_{eff} reading of 1.51 μ_{B} (23 °C), consistent with one unpaired electron on a low-spin d⁵, S = ½ iron center.



Scheme 3.6. Formation of iron(III) azaallyl *trans*-{ κ -C,N,N'-(*p*-^tBu-Ar-2-yl)CHNCH-2-py}(PMe₃)₂FeCH₃ (**10**).

2. Synthesis of *trans*-{ κ -C,N,N'-(*p*-^tBu-Ar-2-yl)CHNCH-2-py}(PMe₃)₂FeCH₃ (**10**).

Taking advantage of the acidic methylene proton, **9** was treated with excess KH in THF at -78 ° (Scheme 3.6). The resulting intense blue-green solution yielded blue-green microcrystals of *trans*-{ κ -C,N,N'-(*p*-^tBu-Ar-2-yl)CHNCH-2-py}(PMe₃)₂FeCH₃ (**10**, 75 %). A magnetic measurement by Evans' method (23 °C, C₆D₆) gave a μ_{eff} of 1.90 μ_{B} , also consistent with a low-spin d⁵, S = 1/2 center. While integration of the paramagnetic ¹H NMR spectrum intimated the replacement of a methylene with a CH, UV-visible spectroscopy also established azaallyl formation.

E. UV-visible spectra of azaallyls *mer*-{ κ -C,N,C'-(*p*-^tBu-Ar-2-yl)CHNCH(2-py-NCH₃-3-yl)}(PMe₃)₃Fe (**8**) and *trans*-{ κ -C,N,N'-(*p*-^tBu-Ar-2-yl)CHNCH-2-py}(PMe₃)₂FeCH₃ (**10**).

Previously synthesized azaallyl compounds of the “smif” ligand were characterized by intense intraligand (IL) bands ($\epsilon \sim 15,000 - 30,000 \text{ M}^{-1}\text{cm}^{-1}$),^{20,21} similar to those seen in metal porphyrin complexes.³⁰ Calculations show that the bands originate from transitions from the CNC^{nb} orbitals of the azaallyl unit to pyridine π^* orbitals.²¹ Compounds **8** and **10**, where one pyridine ring of smif has been replaced

with a ^tBuAr moiety, display UV-visible spectra with similar characteristics. Fe(II) complex **8** has IL bands at 417 nm ($\epsilon \sim 21,100 \text{ M}^{-1}\text{cm}^{-1}$) and 613 nm ($\epsilon \sim 7,900 \text{ M}^{-1}\text{cm}^{-1}$), while Fe (III) complex **10** manifests bands at 417 ($\epsilon \sim 29,200 \text{ M}^{-1}\text{cm}^{-1}$) and 646 ($\epsilon \sim 8,300 \text{ M}^{-1}\text{cm}^{-1}$). The source of the intense bands is best demonstrated by a direct spectral comparison of **8** and **10** with their immediate imine precursors **7** and **9**, as seen in Figure 3.3.

In addition to their relative intensities, the lower-energy bands in the azaallyl spectra present an interesting feature. A vibrational progression is visible for both **8** and **10**, with GS($v = 0$) \rightarrow ES($v = 0$) around 613 nm and 646 nm, respectively. The progression for **10** is approximately 1100 cm^{-1} , and its IR spectrum does show absorptions in this region. For **8**, the apparent progression is $\sim 1200 \text{ cm}^{-1}$, and absorptions in this area of the IR spectrum are plentiful. Though more obscured in the spectrum, a vibrational progression may also be deduced in the high-energy region, around $\lambda_{\text{max}} = 417 \text{ nm}$ for both **8** and **10**. It is reasonable that these absorptions arise from bending of the CNC azaallyl fragment, with an excited state of proper symmetry giving rise to the progression. Also, these CNC bending modes may be coupled to intraligand CNC^{nb} to π^* transitions, due to the inherent low symmetry of the complexes.

It is also possible that a MLCT absorption gives rise to the band at 646 nm for **10**. Reasoning suggests that one of the occupied t_{2g} d orbitals lies above the CNC^{nb} orbital (i.e., the oxidized d^5 configuration is stable, *vide infra*). Therefore, a MLCT may be operable. This assignment would shift the progression to a higher energy (606 nm), and a corresponding MLCT for complex **8** which should be of higher energy could be located under the band at 650 nm .

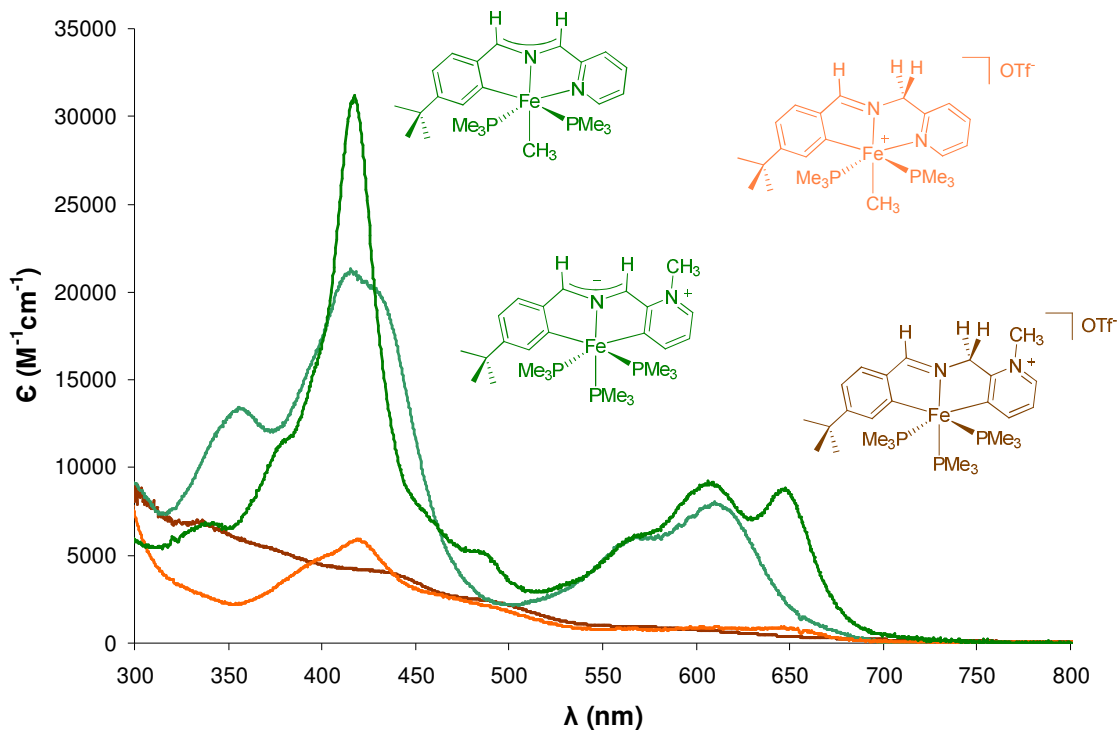
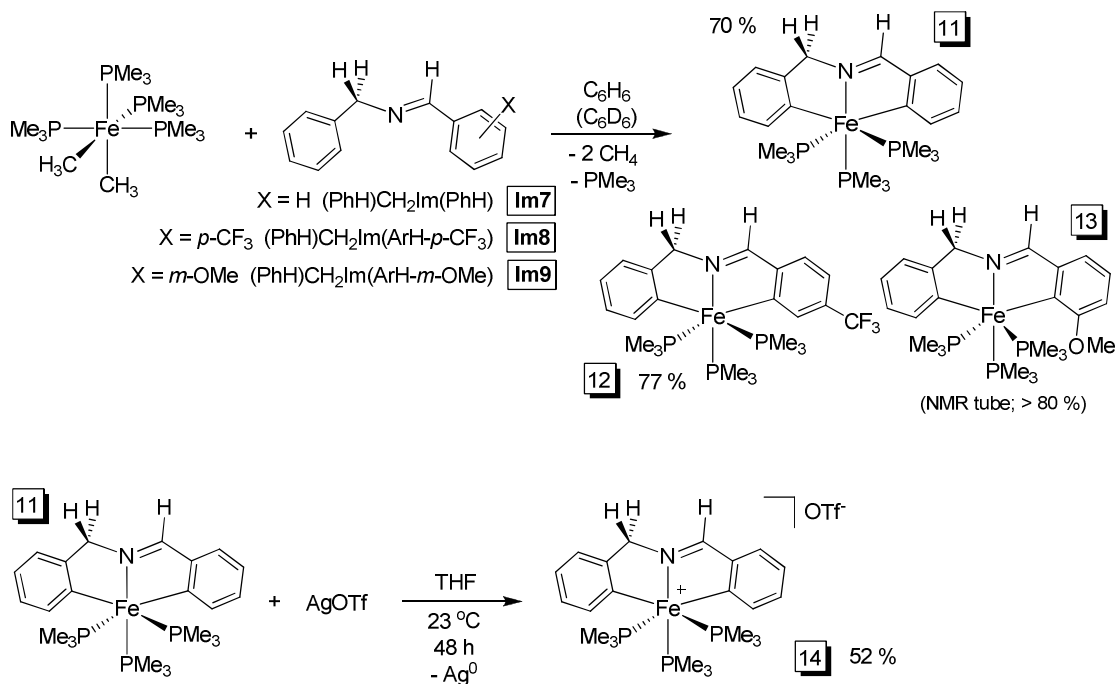


Figure 3.3. UV-vis spectra of the two azaallyl complexes, Fe(II) **8** (green) and Fe(III) **10** (dark green), relative to precursor imines, Fe(II) **7** (brown) and Fe(III) **9** (orange).

F. Synthesis of diarylimino Fe(II) derivatives.

The ease with which “diaryl” complexes **6-8** and iron(III) species **9** and **10** were synthesized led to a modified ligand type, diarylimines. It was hoped that the presence of an extra iron-aryl bond would facilitate oxidation, perhaps even to iron(IV). In a similar manner as the pyridylimine complexes, addition of diaryl imines **Im7**, **Im8**, and **Im9** to *cis*-(Me₃P)₄FeMe₂ afforded Ar-H activated products *mer*-{κ-C,N,C'-(Ph-2-yl)CH₂N=CH(Ar-2-yl-X)}(PMe₃)₃Fe (X = H, **11**; 4-CF₃, **12**; 3-OMe; **13**) (Scheme 3.7). The reaction proceeds with loss of one equivalent of PMe₃ and two equivalents of methane, in 70-80 % yield, to afford brown-red (**11**), dark pink (**12**), or cherry red (**13**) products.



Scheme 3.7. Reactivity of diarylimines and related complexes.

G. Reactivity of *mer*- $\{\kappa\text{-C,N,C}'\text{-(Ph-2-yl)CH}_2\text{N=CH(Ph-2-yl)}\}(\text{PMe}_3)_3\text{Fe}$.

1. Synthesis and structure of [*mer*- $\{\kappa\text{-C,N,C}'\text{-(Ph-2-yl)CH}_2\text{N=CH(Ph-2-yl)}\}(\text{PMe}_3)_3\text{Fe}]\text{OTf}$ (**14**).

The parent complex, **11**, was treated with one equivalent of AgOTf at -78°C in THF to give purple crystals of [*mer*- $\{\kappa\text{-C,N,C}'\text{-(Ph-2-yl)CH}_2\text{N=CH(Ph-2-yl)}\}(\text{PMe}_3)_3\text{Fe}]\text{OTf}$ (**14**) (Scheme 3.7). Gouy balance measurement of the compound gave $\mu_{\text{eff}} = 1.91 \mu_{\text{B}}$ (23°C), indicative of the low-spin, d^5 , $S = \frac{1}{2}$ iron center. Twelve broad, shifted resonances in the ^1H NMR spectrum corroborated the paramagnetic nature of the Fe(III) compound.

X-ray diffraction quality crystals of **14** were grown from THF/ Et_2O , revealing the structure shown in Figure 3.4. Crystallographic data are listed in Table 3.3, and relevant bond distances and angles for each of two molecules in the asymmetric unit are given in Table 3.4. The backbone N=CH bond ($\text{N1-C7} = 1.292(3) \text{ \AA}$) is clearly

distinguished from the N-CH₂ bond (N1-C8 = 1.464(3) Å). The two Fe-C distances are effectively the same (2.0333(2) and 2.036(2) Å). With the exception of slightly increased Fe-P distances (~2.3 Å), more irregular angles associated with the phosphines, and a mildly longer Fe-C14 distance, the core distances about the metal and within the imine ligand are very similar to those of **7**. A reasonable origin for the longer Fe-P bond lengths in **14** is the contraction of the 3d orbitals, and the resulting decreased orbital overlap in the ferric center versus the ferrous center of **7**.

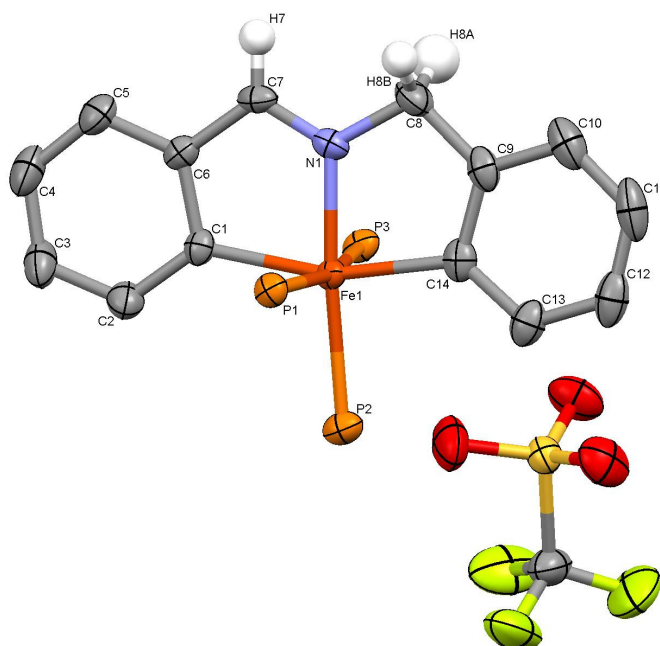


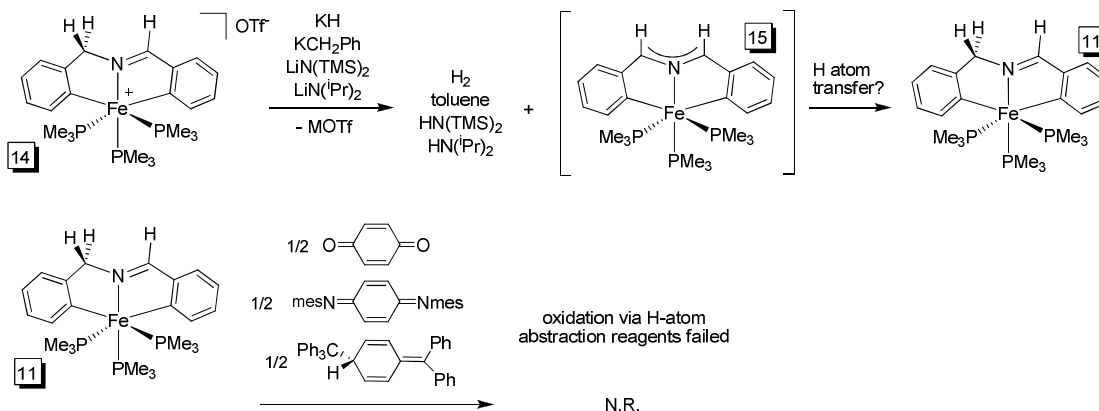
Figure 3.4. Molecular view of the cation of [*mer*-{ κ -C,N,C'-(Ph-2-yl)CH₂N=CH(Ph-2-yl)}(PMe₃)₃Fe]OTf (**14**).

Complex **14** represents one of the relatively few examples of crystallographically-characterized Fe(III) aryl species. Others include (Ar)Fe(III)(porphyrin) derivatives³¹⁻³⁵ and a tetraarylanion, [Fe(C₆Cl₅)₄][Li(THF)₄].³⁶ The strong-field nature of the porphyrin ligand in the former and the highly-chlorinated arenes on the latter presumably impart stability in these complexes. Other

Fe(III) aryls have been implicated in catalysis,³⁷⁻³⁹ polymerization,⁴⁰ and oxidation chemistry.⁴¹

2. Deprotonation attempts.

Deprotonation at the backbone CH₂ position of [*mer*-{κ-C,N,C'-(Ph-2-yl)CH₂N=CH(Ph-2-yl)}(PMe₃)₃Fe]OTf (**14**) was envisioned to be facile, as in the synthesis of *mer*-{κ-C,N,C'-(*p*-^tBu-Ar-2-yl)CHNCH(2-py-NCH₃-3-yl)}(PMe₃)₃Fe (**8**) and *trans*-{κ-C,N,N'-(*p*-^tBu-Ar-2-yl)CHNCH-2-py}(PMe₃)₂FeCH₃ (**10**). Removal of a proton from **14** would generate a neutral Fe(III) species with a novel, trianionic donor ligand, resulting from a negative charge on each aryl and on the azaallyl fragment. Efforts to affect this transformation, however, proved ineffective. Addition of a variety of bases, including KH, KCH₂Ph, LiN(TMS)₂ (TMS = trimethylsilyl), and LiN(ⁱPr)₂, induced a color change from purple to red, and the only observable organometallic product was the Fe(II) precursor, *mer*-{κ-C,N,C'-(Ph-2-yl)CH₂N=CH(Ph-2-yl)}(PMe₃)₃Fe (**11**) (Scheme 3.8). In each case, detection of the conjugate acid (H₂, toluene, HN(TMS)₂, and HN(ⁱPr)₂, respectively) indicated that deprotonation had indeed occurred; this event must be followed by a reductive scavenging of H[•] from an available source (e.g., solvent, glassware, etc.) to form the observed product. Direct reduction of **14** to **11** remains a possibility, though the milder amide bases should be less reducing.



Scheme 3.8. Deprotonation attempts of $[\text{mer}\{-\{\kappa\text{-C,N,C'}\text{-(Ph-2-yl)CH}_2\text{N=CH(Ph-2-yl)}\}(\text{PMe}_3)_3\text{Fe}\}\text{OTf}$ (**14**).

H. H-atom transfer attempts.

In recognition of the inherent difficulty of the deprotonation reaction, efforts were shifted towards synthesizing the neutral Fe(III) azaallyl via H-atom abstraction from $\text{mer}\{-\{\kappa\text{-C,N,C'}\text{-(Ph-2-yl)CH}_2\text{N=CH(Ph-2-yl)}\}(\text{PMe}_3)_3\text{Fe}$ (**11**). **11** was treated with several H-atom abstraction agents, as shown in Scheme 3.8. Unfortunately, no reaction occurred with these reagents at room temperature. Only in the case of the iminoquinone reagent did heating produce some of the corresponding dianiline; however, heating the iminoquinone without **11** led to the same result.

The possible origin of the instability of the suggested azaallyl intermediate in the deprotonation reactions of **14** may be explained by a simple orbital picture (Figure 3.5). If the filled CNC^{nb} orbital of the azaallyl lies above the $\text{t}_{2\text{g}}$ set in **14**, oxidation removes an electron from the CNC fragment, generating an unstable radical. On the other hand, if the CNC^{nb} orbital lies below an orbital of the $\text{t}_{2\text{g}}$ set, as in compounds **7** and **10**, oxidation occurs at the metal center, leading to a stable d^5 Fe(III) azaallyl. This description is supported by the fact that the related $(\text{smif})_2\text{Fe}$ complex, which computationally contains a CNC^{nb} orbital as its HOMO, cannot be oxidized to the related Fe(III) compound.

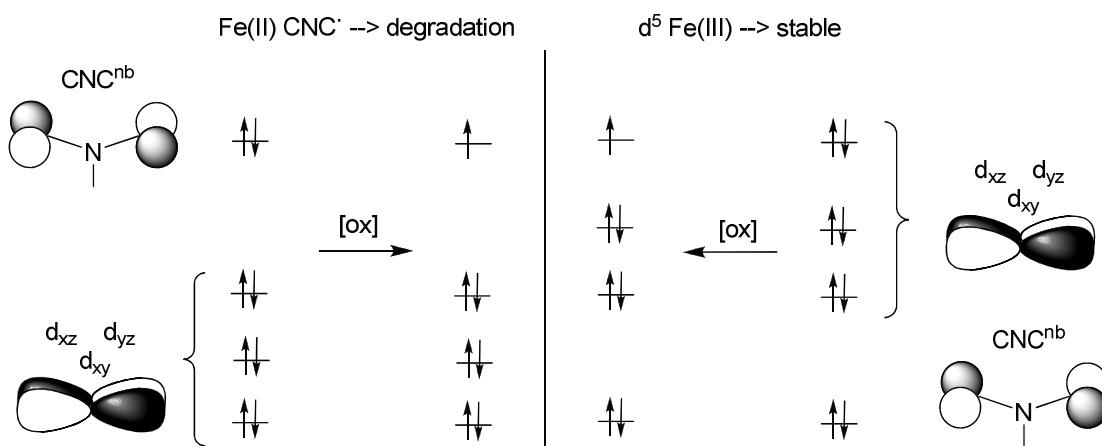


Figure 3.5. Proposed molecular orbital picture demonstrating the formation of a stable and unstable Fe(III) azaallyl.

III. Conclusions

A series of low-spin, d^5 and d^6 iron complexes with aryl-based, chelating arylpyridylimine or diarylimine ligands were synthesized. The organometallic d^5 Fe(III) complexes represent a class of compounds that are relatively rare in the literature. Two azaallyl derivatives of the arylpyridylimine ligand have been synthesized which retain the unusual optical properties of the previously reported smif system, expanding the scope of this class of ligands. A trianionic, diarylazaallyl ligand has been implicated as a transient but unstable species. Our results provide additional validity to the assertion that carbon-based ligands should support strong fields and moderately high oxidation states of first-row metals. Continued efforts will focus on stabilizing a trianionic azaallyl ligand, synthesizing strong field complexes without additional σ -donating phosphines, and realizing an as-yet elusive Fe(IV) species.

IV. Experimental

A. General considerations.

All manipulations were performed using either glovebox or high vacuum line techniques. Hydrocarbon solvents containing 1-2 mL of added tetraglyme, and ethereal solvents were distilled under nitrogen from purple sodium benzophenone ketyl and vacuum transferred from same prior to use. Benzene- d_6 and toluene- d_8 were dried over sodium, vacuum transferred and stored under N_2 . THF- d_8 was dried over sodium benzophenone ketyl. Methylene chloride- d_2 was dried over CaH_2 , vacuum transferred and stored over activated 4 Å molecular sieves. *cis*-(Me_3P) $_4$ FeMe $_2$ was prepared according to literature procedures.²⁷ Imines were also prepared via literature procedures or as described.⁴² All other chemicals were commercially available and used as received. All glassware was oven dried.

NMR spectra were obtained using Varian XL-400, INOVA 400, and Unity-500 spectrometers. Chemical shifts are reported relative to benzene- d_6 (1H δ 7.16; $^{13}C\{^1H\}$ δ 128.39), THF- d_8 (1H δ 3.58; $^{13}C\{^1H\}$ δ 67.57), and CD_2Cl_2 (1H δ 5.32; $^{13}C\{^1H\}$ δ 54.00). Infrared spectra were recorded on a Nicolet Avatar 370 DTGX spectrophotometer interfaced to an IBM PC (OMNIC software). UV-Vis spectra were obtained on a Shimadzu UV-2102 interfaced to an IBM PC (UV Probe software). Solution magnetic measurements were conducted via Evans' method in benzene- d_6 .⁴³ Solid state magnetic measurements were performed using a Johnson Matthey magnetic susceptibility balance calibrated with $HgCo(SCN)_4$.⁴⁴ Elemental analyses were performed by Robertson Microlit Laboratories, Madison, New Jersey.

B. Procedures.

1. General procedure for synthesis of imines Im1-Im9.

To a suspension of $MgSO_4$ (5-8 equiv.) in CH_2Cl_2 were added 1.5 mmol of aldehyde and 1.5 mmol of amine. After stirring for 2 h, the mixture was filtered and

concentrated to yield a clear to pale yellow oil in >98% purity (by ^1H NMR). Spectra and syntheses for Im1, Im2, Im5, and Im7 are in their respective literature references.⁴² Im3: ^1H NMR (C_6D_6 , 300 MHz): 8.53 (s, a), 8.10 (d, 8, c), 7.02 (t, 8, d), 6.62 (dd, 5, 8, e), 8.47 (d, 5, f), 7.18 (d, 8, h), 6.91 (t, 8, i), 6.79 (t, 8, j), 7.29 (d, 8, k), 4.71 (s, n). ^{13}C NMR (C_6D_6 , 300 MHz): 164.65 (a), 155.82 (b), 124.96 (c), 136.35 (d), 127.32 (e), 149.96 (f), 130.46 (h), 129.86 (j), 121.34 (k), 134.16 (l), 137.84 (m), 62.21 (n). *One signal obscured by solvent peak. Im4: ^1H NMR (C_6D_6 , 300 MHz): 5.00 (s, a), 7.39 (d, 8, c), 7.12 (d, 6, d), 6.65 (t, 6, e), 8.53 (d, 5, f), 7.78 (d, 8, h,l), 7.28 (d, 8, i,k), 8.10 (s, n), 1.17 (s, r). ^{13}C NMR (C_6D_6 , 300 MHz): 67.55 (a), 160.97 (b), 122.50 (c), 134.90 (d), 122.13 (e), 149.86 (f), 126.09 (i), 154.30 (j), 126.09 (k), 136.45 (m), 162.86 (n), 35.15 (q), 31.58 (r). *Two signals obscured by solvent peak. Im6: ^1H NMR(C_6D_6 , 300 MHz): 5.00 (s, a), 7.34 (d, 8, c), 7.08 (t, 8, d), 6.64 (dd, 6, 8, e), 8.52 (d, 5, f), 7.55 (s, h), 6.86 (dd, 3, 8, j), 7.12 (t, 8, k), 7.26 (d, 8, l), 8.03 (s, n), 3.28 (s, q). ^{13}C NMR (C_6D_6 , 300 MHz): 67.42 (a), 160.77 (b), 122.59 (c), 136.51 (d), 122.22 (e), 149.87 (f), 112.59 (h), 160.59 (i), 118.08 (j), 130.08 (k), 122.29 (l), 138.75 (m), 163.02 (n), 55.14 (q). Im8: ^1H NMR (C_6D_6 , 300 MHz): 4.57 (s, a), 7.28-7.21 (m, c,d,f,g), 7.14 (m, e), 7.32 (d, 8, h,l), 7.52 (d, 8, i,k), 7.80 (s, n). ^{13}C NMR (C_6D_6 , 300 MHz): 65.48 (a), 140.18 (b), 128.61 (c), 129.04 (d), 127.69 (e), 129.04 (f), 128.61 (g), 129.13 (h,l), 125.96 (q, 6, i,k), 139.95 (m), 160.21 (n). *Two signals not observed. Im9: ^1H NMR(C_6D_6 , 300 MHz): 4.61 (s, a), 7.32 (d, 8, c,g), 7.20 (t, 7, d,f), 7.11 (t, 8, e), 7.59 (s, h), 6.87 (d, 8, j), 7.08 (t, 7, k), 7.27 (d, 7, l), 8.01 (s, n), 3.27 (s, q). ^{13}C NMR (C_6D_6 , 300 MHz): 65.54 (a), 140.51 (b), 128.69 (c,g), 129.05 (d,f), 127.47 (e), 112.42 (h), 140.51 (i), 118.13 (j), 130.08 (k), 122.30 (l), 138.83 (m), 161.77 (n), 55.12 (q).

2. Synthesis of the imine complexes.

A 100 mL bomb reactor was charged with $\text{Fe}(\text{PMe}_3)_4\text{Me}_2$ (100-300 mg, 0.256-0.641 mmol) and imine (1 equiv). 15 mL benzene were transferred at -78°C , and the solution was allowed to warm 23°C and stir for 24 h. Upon removal of the solvent, the crude mixture was dissolved in Et_2O , filtered and washed (4 x 10 mL Et_2O). Crystallization from hexanes at -78°C afforded the product.

a. *trans*-{ $\kappa\text{-C,N,N'}$ -(Ph-2-yl) $\text{CH}_2\text{N}=\text{CH}$ -2-py} PMe_3 }_2 FeCH_3 (1). Dark green microcrystals (85 mg) were obtained in 79 % yield. Anal. Calcd. for $\text{C}_{20}\text{H}_{32}\text{N}_2\text{P}_2\text{Fe}$: C, 57.43; H, 7.71; N, 6.70. Found: C: 56.45; H: 7.36, N: 6.37.

b. *trans*-{ $\kappa\text{-C,N,N'}$ -(*p*-MeO-Ar-2-yl) $\text{CH}_2\text{N}=\text{CH}$ -2-py} PMe_3 }_2 FeCH_3 (2). Dark green microcrystals (102 mg from 0.383 mmol) were obtained in 59 % yield. Anal. Calcd. for $\text{C}_{21}\text{H}_{34}\text{N}_2\text{OP}_2\text{Fe}$: C, 56.26; H, 7.64; N, 6.25. Found: C: 55.98; H: 7.71, N: 5.96.

c. *trans*-{ $\kappa\text{-C,N,N'}$ -(*o*-Cl-Ar-2-yl) $\text{CH}_2\text{N}=\text{CH}$ -2-py} PMe_3 }_2 FeCH_3 (3). Dark green crystals (150 mg from 0.512 mmol) were obtained in 65 % yield. Anal. Calcd. for $\text{C}_{20}\text{H}_{31}\text{N}_2\text{P}_2\text{ClFe}$: C, 53.06; H, 6.90; N, 6.19. Found: C: 52.84; H: 6.62, N: 6.04.

d. *trans*-{ $\kappa\text{-C,N,N'}$ -(*p*-^tBu-Ar-2-yl) $\text{CH}=\text{NCH}_2$ -2-py} PMe_3 }_2 FeCH_3 (4). Midnight blue crystals (222 mg 0.641 mmol) were obtained in 73 % yield. Anal. Calcd. for $\text{C}_{24}\text{H}_{40}\text{N}_2\text{P}_2\text{Fe}$: C, 60.76; H, 8.50; N, 5.91. Found: C: 60.48; H: 8.23, N: 5.68. UV-vis: 266 nm ($12,100\text{ M}^{-1}\text{cm}^{-1}$), 417 (4,900), 506 (4,600), 613 (8,900).

e. {*mer*- $\kappa\text{-C,N,C'}$ -(Ph-2-yl) $\text{CH}_2\text{N}=\text{CH}$ (Ph-2-yl)} $\text{Fe}(\text{PMe}_3)_3$ (11). The brick-red microcrystalline solid (342 mg from 1.02 mmol) was obtained in 70 % yield. Anal. Calcd. for $\text{C}_{23}\text{H}_{38}\text{NP}_3\text{Fe}$: C, 57.87; H, 8.02; N, 2.93. Found: C: 57.82; H: 8.09, N: 2.81. UV-vis: 239 nm ($2,100\text{ M}^{-1}\text{cm}^{-1}$), 332 (3,900), 375 (1,700), 445 (2,400), 501 (1,000).

f. {*mer*- $\kappa\text{-C,N,C'}$ -(Ph-2-yl) $\text{CH}_2\text{N}=\text{CH}$ (Ar-2-yl-4-CF₃)} $\text{Fe}(\text{PMe}_3)_3$ (12). The dark pink microcrystalline solid (107 mg from 0.256 mmol) was obtained in 77 % yield. Anal. Calcd. for $\text{C}_{24}\text{H}_{37}\text{NP}_3\text{F}_3\text{Fe}$: C, 52.86; H, 6.84; N, 2.57. Found: C: 54.30; H: 7.03, N: 2.69.

3. Oxidation to give the iron(III) triflate complexes.

A 25 mL round bottom flask was charged with either *trans*-{ κ -C,N,N'-(*p*-^tBu-Ar-2-yl)CH=NCH₂-2-py}(PMe₃)₂FeCH₃ (**4**) or { κ -C,N,C'-(Ph-2-yl)CH₂N=CH(Ph-2-yl)}Fe(PMe₃)₃ (**11**) (typically ~100 mg) and AgOTf (1 equiv). 10 mL THF were vacuum transferred onto the solids at -78 °C. The solution was allowed to warm to 23 °C and stir for 12 h (**9**) or 48 h (**14**). The solvent was stripped and the resulting residue dissolved in 5 mL THF. After filtration through celite, the solution was layered with Et₂O and cooled to -30 °C to yield a crystalline solid. **a.** [*trans*-{ κ -C,N,N'-(*p*-^tBu-Ar-2-yl)CH=NCH₂-2-py}(PMe₃)₂FeCH₃]OTf (**9**). Red-orange crystals (116 mg from 0.291 mmol) were obtained in 64 % yield. Anal. Calcd. for C₂₅H₄₀N₂O₃P₂F₃SFe: C, 48.16; H, 6.47; N, 4.49. Found: C: 47.92; H: 6.27, N: 4.34. UV-vis: 270 nm (18,500 M⁻¹cm⁻¹), 396 (4,300), 419 (5,300), 490 (2,100), 565 (1,000), 607 (1,100), 646 (1,000). **b.** [*mer*- κ -C,N,C'-{(Ph-2-yl)CH₂N=CH(Ph-2-yl)}Fe(PMe₃)₃]OTf (**14**). Purple crystals (136 mg from 0.418 mmol) were obtained in 52 % yield. Anal. Calcd. for C₂₄H₃₈NO₃P₃F₃SFe: C, 46.02; H, 6.11; N, 2.24. Found: C: 45.94; H: 6.00, N: 2.11.

4. Synthesis of iron aza-allyl complexes.

Iron complex of [*mer*-{ κ -C,N,C'-(*p*-^tBu-Ar-2-yl)CH=NCH₂(2-py-NCH₃-3-yl)}(PMe₃)₃Fe]OTf (**7**) or [*trans*-{ κ -C,N,N'-(*p*-^tBu-Ar-2-yl)CH=NCH₂-2-py}(PMe₃)₂FeCH₃]OTf (**9**) (typically 0.160 mmol) and excess KH (26 mg, 0.642 mmol) were weighed into a 25 mL round bottom flask. THF (10 mL) was vacuum transferred at -78 °C. The emerald green solution was placed under argon and allowed to warm slowly to room temperature overnight. The solvent was removed and the mixture filtered and washed with Et₂O. Subsequent recrystallization from cold hexanes afforded clean product. **a.** *mer*-{ κ -C,N,C'-(*p*-^tBu-Ar-2-yl)CHNCH(2-py-NCH₃-3-yl)}(PMe₃)₃Fe (**8**). Dark green microcrystals (62 mg from 0.215 mmol)

were obtained in 61 % yield. Anal. Calcd. for $C_{27}H_{47}N_2P_3Fe$: C, 59.13; H, 8.64; N, 5.11. Found: C: 58.88; H: 8.38, N: 4.89. UV-vis: 358 nm ($13,400\text{ M}^{-1}\text{cm}^{-1}$), 417 (21,100), 570 (6,000), 613 (7,900). **b. *trans*-{ κ -C,N,N'-(*p*-^tBu-Ar-2-yl)CHNCH-2-py}(PMe₃)₂FeCH₃ (10).** Dark blue-green crystals (60 mg) were obtained in 75 % yield. Anal. Calcd. for $C_{24}H_{39}N_2P_2Fe$: C, 60.89; H, 8.30; N, 5.92. Found: C: 58.85; H: 8.27, N: 5.53. UV-vis: 338 nm ($5,800\text{ M}^{-1}\text{cm}^{-1}$), 377 (10,000), 417 (29,200), 485 (4,500), 566 (5,600), 606 (8,600), 646 (8,300).

5. Synthesis of *mer*-{ κ -C,N,C'-(*p*-^tBu-Ar-2-yl)CH=NCH₂(2-py-3-yl)}(PMe₃)₃Fe (6).

To a 200 mL bomb charged with *trans*-{ κ -C,N,N'-(*p*-MeO-Ar-2-yl)CH₂N=CH-2-py}(PMe₃)₂FeCH₃ (**2**, 600 mg, 1.26 mmol) were vacuum transferred 30 mL benzene. 1.5 equiv PMe₃ (0.20 mL, 1.90 mmol) were transferred via gas bulb. The reaction mixture was heated at 80 °C for 18 h. After cooling, the solvent was stripped and the remainder dissolved in Et₂O. The solution was filtered through a frit, washed three times with Et₂O, and concentrated. The crude solid was recrystallized from cold pentane/PMe₃ (5 mL/0.5 mL) to yield 453 mg golden brown solid (67 %). Anal. Calcd. for $C_{26}H_{45}N_2P_3Fe$: C, 58.43; H, 8.49; N, 5.24. Found: C: 58.17; H: 8.21, N: 5.13. UV-vis: 333 nm ($5,300\text{ M}^{-1}\text{cm}^{-1}$), 369 (3,400), 417 (3,800), 430 (3,500), 496 (1,100), 604 (500), 671 (300), 738 (100).

6. Synthesis of [*mer*-{ κ -C,N,C'-(*p*-^tBu-Ar-2-yl)CH=NCH₂(2-py-NCH₃-3-yl)}(PMe₃)₃Fe]OTf (7).

Into a solution of (**3**) (200 mg, 0.374 mmol) in benzene (20 mL) was syringed methyl triflate (42 μ L, 0.374 mmol) under argon. The solution was stirred for 4 h, then allowed to sit for 12 h. The resulting mixture was filtered to yield brown crystals, which were subsequently washed with hexanes (200 mg, 77 %). Anal. Calcd. for

C₂₈H₄₈N₂O₃P₃F₃SFe: C, 48.14; H, 6.93; N, 4.01. Found: C: 48.01; H: 7.08, N: 3.88.

UV-vis: 336 nm (6,900 M⁻¹cm⁻¹), 375 (5,300), 437 (4,000), 495 (2,300), 569 (1,000).

7. NMR tube reactions.

20 mg Fe(PMe₃)₄Me₂ (0.051 mmol) were placed into a flame-dried NMR tube which was sealed to a 14/20 joint and attached to a needle valve. A solution of imine (0.051 mmol) in benzene (0.7 mL) was added to the tube, at which point a color change was observed. The tube was degassed via freeze-pump-thaw and sealed under active vacuum. Loss of starting material was typically complete after 24 h. **a.**

trans,cis-(PMe₃)₂(CH₃)₂Fe{κ-N,N'-EtCH₂N=CH-2-py} (**5-Et**). Purple solution. **b.**

trans,cis-(PMe₃)₂(CH₃)₂Fe{κ-N,N'-^{neo}PeCH₂N=CH-2-py} (**5-^{neo}Pe**). Purple solution.

c. {mer-κ-C,N,C'-(Ph-2-yl)CH₂N=CH(Ar-2-yl-3-OMe)}Fe(PMe₃)₃ (**13**). Red solution.

C. Single crystal X-ray diffraction studies.

1. General.

Upon isolation, the crystals were covered in polyisobutenes and placed under a 173 K N₂ stream on the goniometer head of a Siemens P4 SMART CCD area detector (graphite-monochromated MoKα radiation, λ = 0.71073 Å). The structures were solved by direct methods (SHELXS). All non-hydrogen atoms were refined anisotropically unless stated, and hydrogen atoms were treated as idealized contributions (Riding model).

2. [*mer*-(κ-C,N,C'-(*p*-^tBu-Ar-2-yl)CH=NCH₂(2-py-NCH₃-3-yl))](PMe₃)₃Fe]OTf (**7**).

A red block (0.40 x 0.30 x 0.25 mm) was obtained from benzene. A total of 41,235 reflections were collected with 10,134 determined to be symmetry independent (*R*_{int} = 0.0346), and 7,579 were greater than 2σ(*I*). A semi-empirical absorption

correction from equivalents was applied, and the refinement utilized $w^{-1} = \sigma^2(F_o^2) + (0.0468p)^2 + 0.4618p$, where $p = ((F_o^2 + 2F_c^2)/3)$.

3. *mer*-{ κ -C,N,C'-(*p*-^tBu-Ar-2-yl)CHNCH(2-py-NCH₃-3-yl)}(PMe₃)₃Fe (8).

A dark green block (0.40 x 0.30 x 0.15 mm) was obtained from hexanes. A total of 23,971 reflections were collected with 8,674 determined to be symmetry independent ($R_{\text{int}} = 0.0413$), and 6,343 were greater than $2\sigma(I)$. A semi-empirical absorption correction from equivalents was applied, and the refinement utilized $w^{-1} = \sigma^2(F_o^2) + (0.0458p)^2 + 0.0000p$, where $p = ((F_o^2 + 2F_c^2)/3)$.

4. [*mer*- κ -C,N,C'-{(Ph-2-yl)CH₂N=CH(Ph-2-yl)}Fe(PMe₃)₃]OTf (14).

A dark purple block (0.50 x 0.25 x 0.10 mm) was obtained from THF/Et₂O. A total of 48,646 reflections were collected with 14,326 determined to be symmetry independent ($R_{\text{int}} = 0.0568$), and 9,881 were greater than $2\sigma(I)$. A semi-empirical absorption correction from equivalents was applied, and the refinement utilized $w^{-1} = \sigma^2(F_o^2) + (0.0426p)^2 + 0.3446p$, where $p = ((F_o^2 + 2F_c^2)/3)$.

REFERENCES

- 1) Kalyani, D.; Deprez, N. R.; Desai, L. V.; Sanford, M. S. *J. Am. Chem. Soc.* **2005**, *127*, 7330.
- 2) Daugulis, O.; Zaitsev, V. G. *Angew. Chem. Int. Ed.* **2005**, *44*, 4046.
- 3) Jun, C.-H.; Lee, H. *J. Am. Chem. Soc.* **1999**, *121*, 880-881.
- 4) Lafrance, M.; Gorelsky, S. I.; Fagnou, K. *J. Am. Chem. Soc.* **2007**, *129*, 14570.
- 5) Dong, C.-G.; Hu, Q.-S. *Angew. Chem. Int. Ed.* **2006**, *45*, 2289.
- 6) Ren, H.; Knochel, P. *Angew. Chem. Int. Ed.* **2006**, *45*, 3462.
- 7) Tsuchikama, K.; Kasagawa, M.; Endo, K.; Shibata, T. *Org. Lett.* **2009**, *11*, 1821.
- 8) Zaitsev, V. G.; Shabashov, D.; Daugulis, O. *J. Am. Chem. Soc.* **2005**, *127*, 13154.
- 9) Wang, D.-H.; Wasa, M.; Giri, R.; Yu, J.-Q. *J. Am. Chem. Soc.* **2008**, *130*, 7190.
- 10) Watanabe, T.; Oishi, S.; Fujii, N.; Ohno, H. *Org. Lett.* **2008**, *10*, 1759.
- 11) Wasa, M.; Engle, K. M.; Yu, J.-Q. *J. Am. Chem. Soc.* **2009**, *131*, 9886.
- 12) Canivet, J.; Yamaguchi, J.; Ban, I.; Itami, K. *Org. Lett.* **2009**, *11*, 1733-1736.
- 13) Hachiya, H.; Hirano, K.; Satoh, T.; Miura, M. *Org. Lett.* **2009**, *11*, 1737-1740.
- 14) Do, H.-Q.; Khan, R. M. K.; Daugulis, O. *J. Am. Chem. Soc.* **2008**, *130*, 15185-15192.
- 15) Yotphan, S.; Bergman, R. G.; Ellman, J. A. *Org. Lett.* **2009**, *11*, 1511-1514.
- 16) Chen, X.; Engle, K. M.; Wang, D.-H.; Yu, J.-Q. *Angew. Chem. Int. Ed.* **2009**, *48*, 5094-5115, and references therein.
- 17) Kakiuchi, F.; Kan, S.; Igi, K.; Chatani, N.; Murai, S. *J. Am. Chem. Soc.* **2003**, *125*, 1698.
- 18) Oi, S.; Fukita, S.; Inoue, Y. *Chem. Commun.* **1998**, 2439.
- 19) Park, Y. J.; Park, J.-W.; Jun, C.-H. *Acc. Chem. Res.* **2008**, *41*, 222-234, and references therein.

- 20) Frazier, B. A.; Wolczanski, P. T.; Lobkovsky, E. B. *Inorg. Chem.* **2009**, *131*, 11576-11585.
- 21) Frazier, B. A.; Wolczanski, P. T.; Lobkovsky, E. B.; Cundari, T. R. *J. Am. Chem. Soc.* **2009**, *131*, 3428-3429.
- 22) Klein, H.-F.; Camadanli, S.; Beck, R.; Flörke, U. *Chem. Comm.* **2005**, 381-382.
- 23) Klein, H.-F.; Camadanli, S.; Beck, R.; Leukel, D.; Flörke, U. *Angew. Chem. Int. Ed.* **2005**, *44*, 975-977.
- 24) Beck, R.; Zheng, T.; Sun, H.; Li, X.; Flörke, U.; Klein, H.-F. *J. Organomet. Chem.* **2008**, *693*, 3471-3478.
- 25) Shi, Y.; Li, M.; Hu, Q.; Li, X.; Sun, H. *Organometallics* **2009**, *28*, 2206-2210.
- 26) Camadanli, S.; Beck, R.; Flörke, U.; Klein, H.-F. *Organometallics* **2009**, *28*, 2300-2310.
- 27) Karsch, H. H. *Chem. Ber.* **1977**, *110*, 2699-2711.
- 28) The ^{31}P resonances manifest as an A_2B pattern.
- 29) Abraham, R. J.; Fisher, J.; Loftus, P. *Introduction to NMR Spectroscopy*; John Wiley & Sons, Ltd.: New York, 1988.
- 30) Balci, M. *Basic ^1H - and ^{13}C -NMR Spectroscopy*; Elsevier: New York, 2005.
- 31) Goedken, V. L.; Peng, S.-M.; Park, Y. *J. Am. Chem. Soc.* **1974**, *96*, 284-285.
- 32) Doppelt, P. *Inorg. Chem.* **1984**, *23*, 4009-4011.
- 33) Balch, A. L.; Olmstead, M. M.; Safari, N.; St. Claire, T. N. *Inorg. Chem.* **1994**, *33*, 2815-2822.
- 34) Kadish, K. M.; Tabard, A.; Van Caemelbecke, E.; Aukauloo, A. M.; Richard, P.; Guillard, R. *Inorg. Chem.* **1998**, *37*, 6168-6175.
- 35) Bill, E.; Schünemann, V.; Trautwein, A. X.; Weiss, R.; Fisher, J.; Tabard, D.; Guillard, R. *Inorg. Chim. Acta.* **2002**, *339*, 420-426.

- 36) Alonso, P. J.; Arauzo, A. B.; Forniés, J.; García-Monforte, M. A.; Martín, A.; Martínez, J. I.; Menjón, B.; Rillo, C.; Sáiz-Garitaonandia, J. J. *Angew. Chem. Int. Ed.* **2006**, *45*, 6707-6711.
- 37) Furstner, A.; Leitner, A.; Mendez, M.; Krause, H. *J. Am. Chem. Soc.* **2002**, *124*, 13856-13863.
- 38) Furstner, A.; Martin, R. *Chem. Lett.* **2005**, *34*, 624-629.
- 39) Sherry, B. D.; Furstner, A. *Acc. Chem. Res.* **2008**, *11*, 1500-1511.
- 40) O'Reilly, R. K.; Gibson, V. C.; White, A. J. P.; Williams, D. J. *Polyhedron* **2004**, *23*, 2921-2928.
- 41) Lau, W.; Huffman, J. C.; Kochi, J. K. *Organometallics* **1982**, *1*, 155-169.
- 42) **Im1**: Ceder, R. M.; Muller, G.; Ordinas, M.; Ordinas, J. I. *Dalt. Trans.* **2007**, *1*, 83-90. **Im2**, **Im5**: Grigg, R.; Donegan, G.; Gunaratne, H. Q. N.; Kennedy, D. A.; Malone, J. F.; Sridharan, V.; Thianpatanagul, S. *Tetrahedron*. **1989**, *45*, 1723-1746. **Im3**: Kouznetsov, V. V.; Castro, J. R.; Puentes, C. O.; Stashenko, E. E.; Martinez, J. R.; Ochoa, C.; Pereira, D. M.; Ruiz, J. J. N.; Portillo, C. F.; Serrano, S. M.; Barrio, A. G.; Bahsas, A.; Amaro-Luis, J. *Archiv der Pharmazie*. **2005**, *338*, 32-37. **Im7**: Bowman, R. K.; Johnson, J.S. *J. Org. Chem.* **2004**, *69*, 8537-8540. **Im8**: Kim, M.; Knettle, B. W.; Dahlén, A.; Hilmersson, G.; Flowers, R. A. *Tetrahedron*, **2003**, *59*, 10397-10402. **Im9**: Saha, M.; Chandrasekaran, S. *Bangladesh Journal of Scientific and Industrial Research*. **1999**, *34*, 120-123.
- 43) (a) Evans, D. F. *J. Chem. Soc.* **1959**, 2003-2005. (b) Schubert, E. M. *J. Chem. Educ.* **1992**, *69*, 62.
- 44) Carlin, R. L. *Magnetochemistry*; Springer-Verlag: Berlin, 1986.

CHAPTER 4

SYNTHESIS AND ELECTRONIC STRUCTURE OF BIS-(α -IMINOPYRIDINE) IRON COMPOUNDS, $(N,N'\text{-}\alpha\text{-IMINOPYRIDYL})_2\text{Fe}(\text{L}/\text{X})_n$ ($n = 1, 2$)

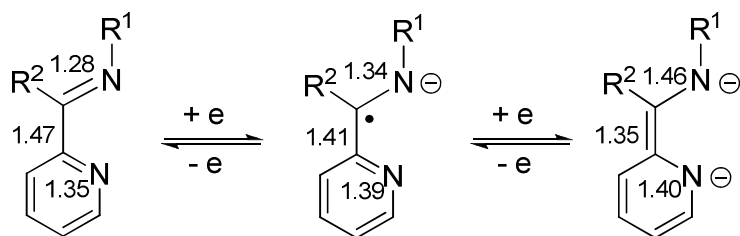
1. Introduction

Understanding the electronic structure of metal complexes is an ongoing goal in inorganic chemistry, as the arrangement of electrons in a complex is intimately related to its reactivity and properties. Valence bond theory is used quite successfully to think about electronic structure, especially for standard coordination compounds. Electronic structure determination becomes more complicated for many organometallic complexes, where metal-ligand interactions are especially covalent, and for complexes of redox non-innocent ligands, which may exist in multiple open- or closed-shell forms.

With regard to the latter, a host of classic chelating ligands such as *o*-phenylenediamine,^{1,2} benzene-1,2-dithiolate,^{3,4} α -diimine,⁵⁻⁷ α -iminopyridine,⁸ and bis(α -diimine)pyridine,⁹⁻¹¹ have been more recently reinvestigated in light of their redox-activity.¹² A variety of physical experimental means have been employed, often in combination, for this very purpose. X-ray crystallography, XAS, magnetic susceptibility, UV-visible, EPR and Mössbauer measurements are commonly used, along with help from an array of computational methods.

Despite a wealth of available physical and computational tools, electronic assignments are still often tentative, and a better understanding of these systems depends on comprehensive experimental data. Wieghardt has studied four-coordinate bis-(α -iminopyridine) complexes of the first-row metals, and his representation of the three redox states of the ligand are shown in Scheme 4.1, along with characteristic bond lengths.⁸ The ligands in the Wieghardt system originate from substituted

anilines, whereas the iminopyridine ligands discussed in the preceding chapter are alkyl-derived. This difference in substitution has been known to influence the electronic structure of complexes with redox-active ligands.^{13,14} Our previous studies offered us an opportunity to contribute to this field, and to further assess the strength of metal-carbon bonds, with a series of five- and six-coordinate bis-(α -iminopyridine) iron complexes as examined by X-ray crystallography and Mössbauer spectroscopy.

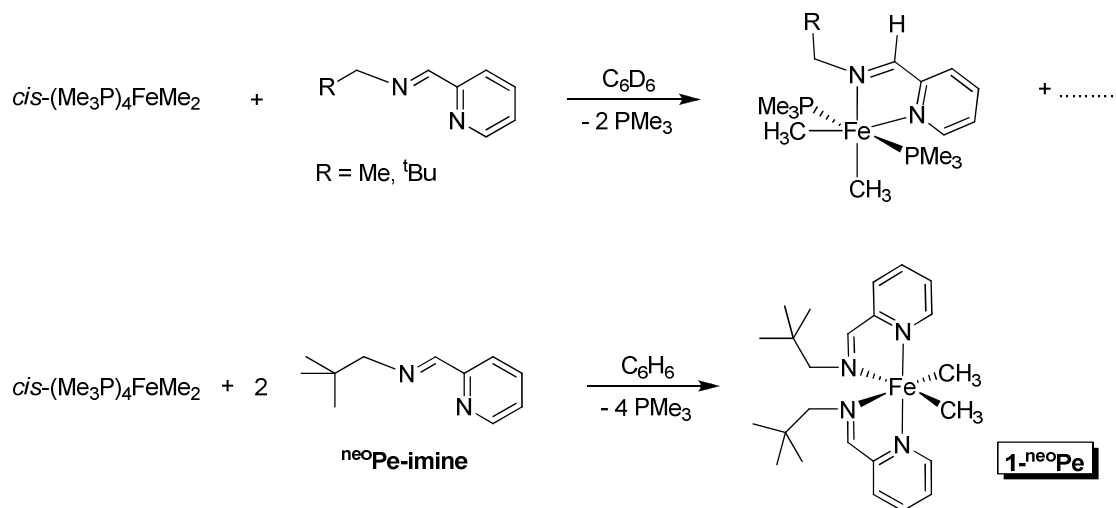


Scheme 4.1. Redox states of the α -iminopyridine ligand, with characteristic bond lengths (Å).⁸

II. Results and Discussion

A. Synthesis of *cis,cis*- $\{\kappa\text{-N,N'-(N-(2\text{-pyridinylmethylene})\text{neopentylamine})}\}_2\text{-Fe}(\text{CH}_3)_2$ (**1-neoPe**).

The previous chapter reported the reaction of *cis*-(Me_3P)₄FeMe₂ with alkylpyridine imines to give adducts *trans,cis*-(Me_3P)₂(CH₃)₂Fe{ $\kappa\text{-N,N'}$ -RCH₂N=CH-2-py} (R = Me, Et) (Scheme 4.2). A minor product was also observed in these reactions, and the amount of free PMe₃ exceeded the expected two equivalents. To test the possibility of additional PMe₃ being displaced by a second iminopyridine ligand, two equivalents of ^{neo}Pe-imine were added to *cis*-(Me_3P)₄FeMe₂. Diastereotopic methylene protons at δ 3.75 (d, J = 11, 1H) and 3.20 (d, J = 11, 1H) in the ¹H NMR spectrum, and the absence of a signal in the ³¹P spectrum indicated the proposed product, *cis,cis*- $\{\kappa\text{-N,N'-(N-(2\text{-pyridinylmethylene})\text{neopentylamine})}\}_2\text{Fe}(\text{CH}_3)_2$ (**1-neoPe**).¹⁵ **1-neoPe** was isolated as a crystalline purple solid in 80 % yield (Figure 4.1).



Scheme 4.2. Reactivity of $cis-(Me_3P)_4FeMe_2$ with alkyl pyridine imines.

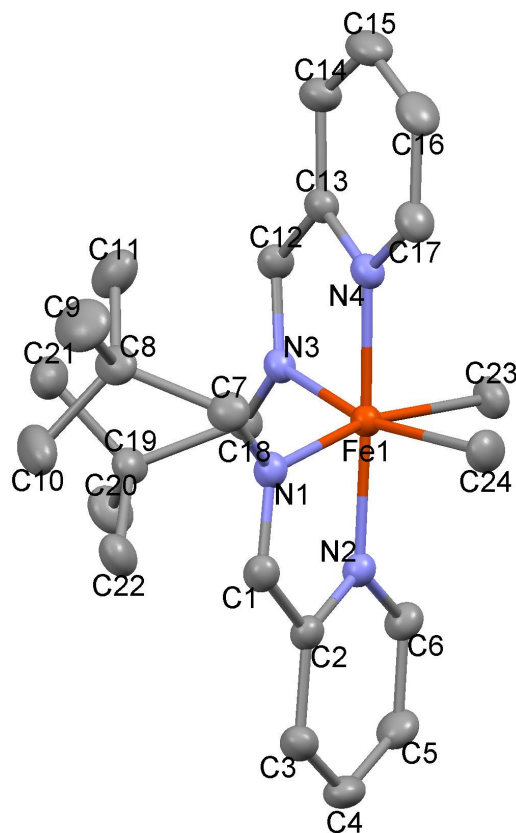


Figure 4.1. Molecular view of $cis,cis-\{\kappa-N,N'-(N-(2\text{-pyridinylmethylene})\text{neopentylamine})\}_2Fe(CH_3)_2$ ($1\text{-}^{neo}Pe$).

B. Bis-(iminopyridine) iron complexes via reduction.

1. Attempts to synthesize an olefin adduct.

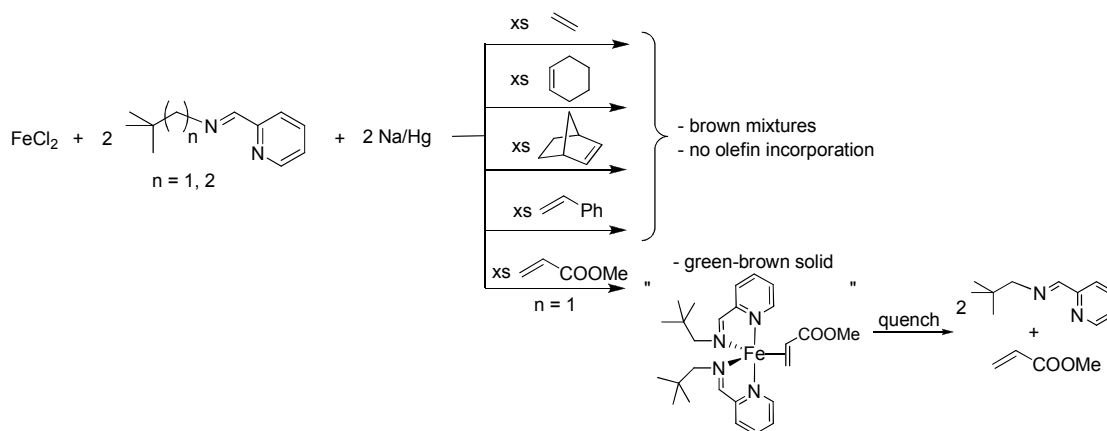
With **1-neoPe** in hand, we saw the opportunity investigate the redox behavior of the iminopyridine ligands in the context of a series of iron complexes of the form (iminopyridyl)₂Fe(L/X)_n, where L and X are ligands with varying donating abilities. Though similar systems have been studied extensively,^{8,16-18} to our knowledge only one series of six-coordinate iron complexes of two bidentate iminopyridine ligands (X = Cl, NCS) has been reported.¹⁹ Our use of ethyl-, neopentyl-, and neohexyl-substituted imines was predicated on attempts to affect sp³ C-H activation, but in the present context the latter two were chosen for their ability to improve solubility and to facilitate crystallization. No differences between the two were expected or observed unless otherwise noted.

Our synthetic approach to other (iminopyridyl)₂Fe(L/X)_n complexes involved *in situ* reduction of ferrous chloride with sodium/amalgam in the presence of a donor ligand. This method was attractive because it obviates the need to isolate a dichloride precursor and allows for introduction of donor ligands which have no corresponding Grignard or lithium reagent. Ethylene made a desirable target because of its potential to make either an olefin complex or a metallacyclopentane, the latter of which should be stable based on the existence of **1-neoPe**. The ambiguous bonding nature of the bound olefin, in combination with potentially redox-active pyridylimine ligands, means that an olefin complex of this type could possess a range of oxidation states from Fe(0) to Fe(IV).

Reaction of FeCl₂ with two equivalents of ^{neo}Pe-imine, two equivalents Na/Hg and excess ethylene produced a bright red solution which darkened to brown after several minutes. Unfortunately, ¹H NMR spectroscopy of the soluble portion of the

reaction showed a complex mixture of primarily diamagnetic products, which bore a striking resemblance to that obtained from the same reaction run without ethylene. Formally Fe(0) complexes of the type (pyridylimine)₂Fe have been isolated,^{5,8,20-22} but generally with fairly bulky aniline or amine-derived ligands. In this case, other deleterious reduction events appear to be operative [*vide infra*], perhaps because of the limited steric protection around the iron center.

The increased steric protection and electron-donating ability of a substituted alkene may be thought to provide the necessary stability to a putative olefin complex. Scheme 4.3 shows the spate of substituted olefins that were used in the reduction reaction; unfortunately, even in the presence of vast excess (≥ 20 equiv), no clean, tractable products were obtained. Only use of the electron-withdrawing olefin, methyl acrylate, provided evidence (by ¹H NMR) of the desired product; however, the small quantities of this species isolated from mixture precluded its further characterization.

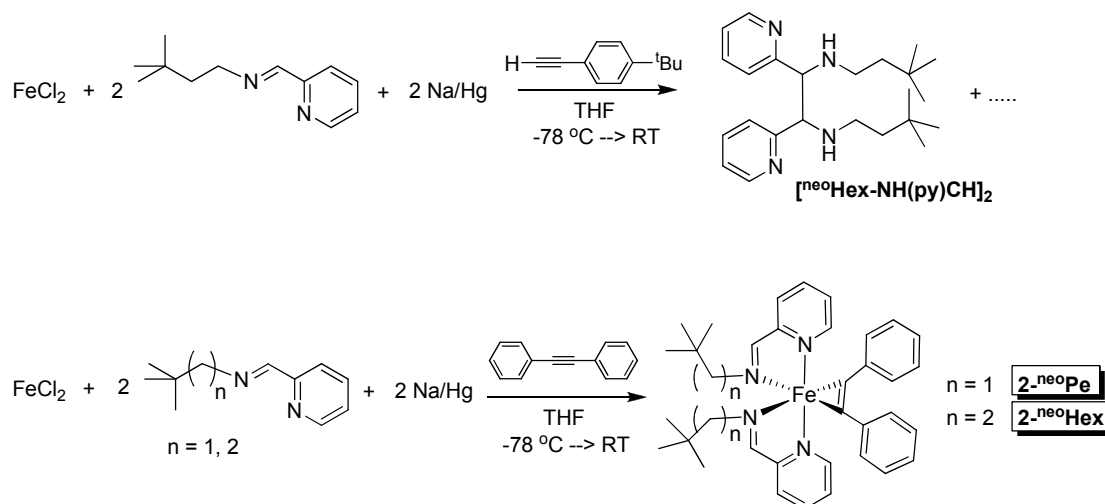


Scheme 4.3. Reduction attempts with ethylene and an array of substituted olefins.

2. The terminal alkyne case: evidence for ligand involvement.

Prompted by the limited success with olefin donors, and by the intriguing possibility of an alkyne to vinylidene rearrangement,^{23,24} attention was next focused on alkynes. Reduction of FeCl₂ and 2 equiv ^{neo}Hex-imine with (*p*-^tBu-phenyl)acetylene

led to a brown solution from which brown solid was obtained. Analysis of the solid by ^1H NMR (1D and COSY) revealed a modified pyridylimine framework, which was assigned as C-C coupling product [$^{\text{neo}}$ Hex-NH(py)CH] $_2$ (Scheme 4.4).



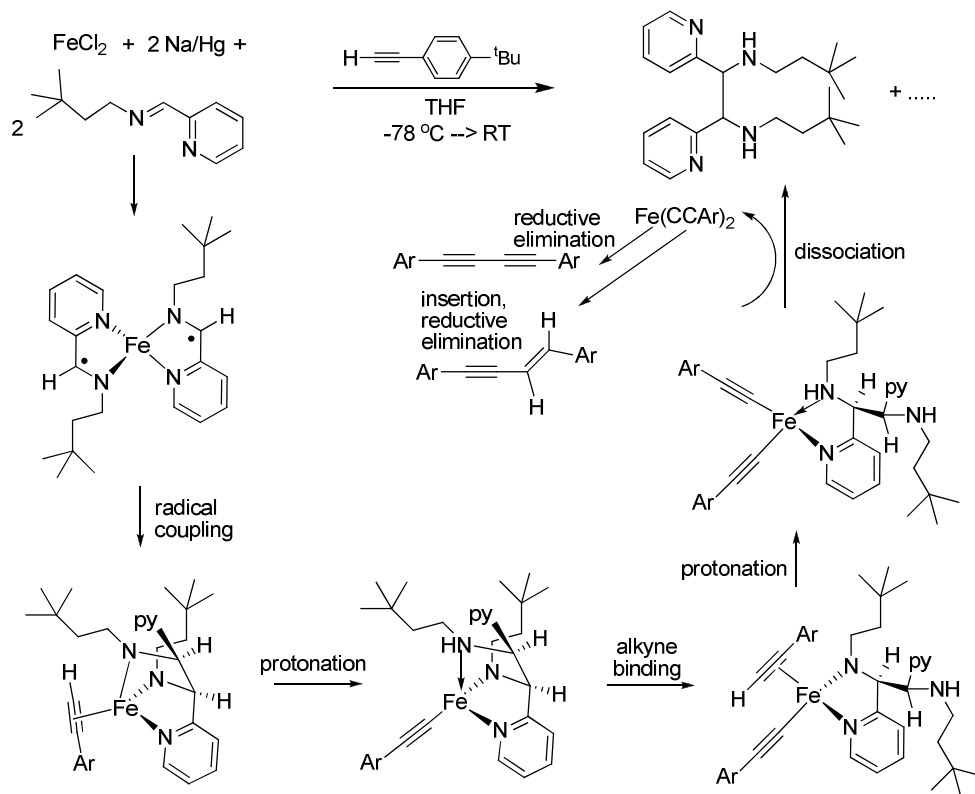
Scheme 4.4. Reductions with terminal or internal alkynes.

A possible mechanism for the formation of [$^{\text{neo}}$ Hex-NH(py)CH] $_2$ is shown in Scheme 4.5. Reduction to an intermediate *bis*-(iminopyridine)Fe complex may confer radical character to the imine carbons, which can then undergo radical coupling to form the new C-C bond. Protonation of one amide by a bound terminal acetylene would afford a secondary amine, and repetition of this process would afford the organic product. The fate of the alkyne itself may have ended in oligomeric polyphenylacetylene or alkenyl-phenylacetylene byproducts, which would likely have been removed by filtration during workup.

3. Successful reduction with an internal alkyne.

In the event that the terminal acetylenic proton contributed to detrimental behavior, an internal alkyne was employed. Performing the reduction with two equivalents of pyridylimine and diphenylacetylene led to a brown-black solution, from

which a black crystalline solid was isolated (Scheme 4.4). ^1H NMR spectroscopy clearly indicated a diamagnetic, C_2 -symmetric compound with incorporation of one diphenylacetylene, and X-ray crystallography confirmed the presence of *cis*- $\{\kappa\text{-N,N}'\text{-(N-(2-pyridinylmethylene)neoheptylamine))}_2\text{Fe(PhCCPh)}$ (**2-^{neo}Hex**, Figure 4.2).



Scheme 4.5. Proposed mechanism for the formation of $[\text{neoHex-NH(py)CH}]_2$.

C. Reduction with PMe_3 and related reactivity.

1. Synthesis of *cis*- $\{\kappa\text{-N,N}'\text{-(N-(2-pyridinylmethylene)alkylamine))}_2\text{Fe(PMe}_3\text{)}$ (alkyl = $\text{CH}_2\text{C}(\text{CH}_3)_3$, **3-^{neo}Pe**; $(\text{CH}_2)_2\text{C}(\text{CH}_3)_3$, **3-^{neo}Hex**).

We next sought a formally Fe(0) complex from an unambiguous neutral donor. In the presence of one or more equivalents of PMe_3 , reduction of FeCl_2 with two pyridylimine ligands afforded the PMe_3 complex as an iridescent green solid from an intense plum-colored solution (45-48 %, Scheme 4.6). Integration of ^1H NMR spectral signals indicated that one equivalent of PMe_3 was present in the diamagnetic, C_2 -

symmetric complex, which was revealed by X-ray crystallography as *cis*-{ κ -N,N'-(N-(2-pyridinylmethylene)alkylamine)}₂Fe(PMe₃) (**3-^{neo}Hex**, Figure 4.3).

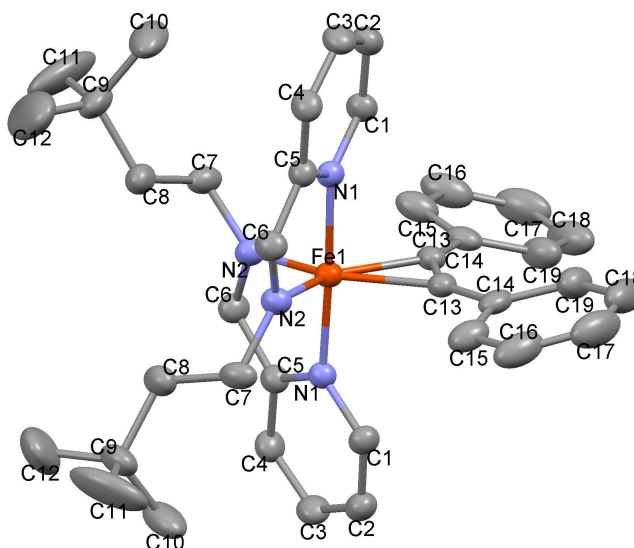
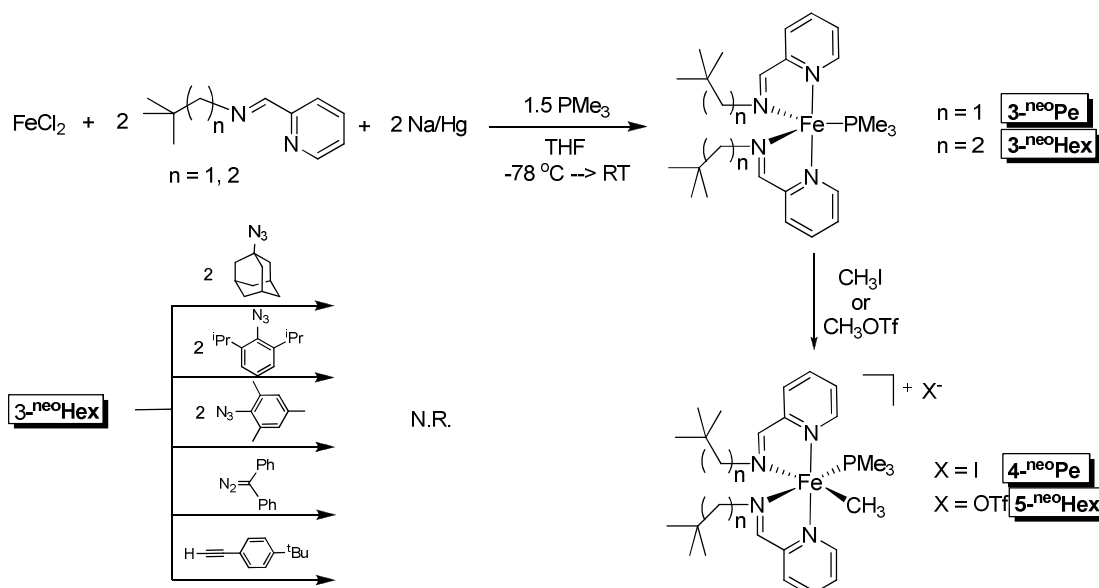


Figure 4.2. Molecular view of *cis*-{ κ -N,N'-(N-(2-pyridinylmethylene)neohexylamine)}₂Fe(PhCCPh) (**2-^{neo}Hex**).



Scheme 4.6. Synthesis and reactivity of *cis*-{ κ -N,N'-(N-(2-pyridinylmethylene)alkylamine)}₂Fe(PMe₃) (**3-^{neo}Hex**).

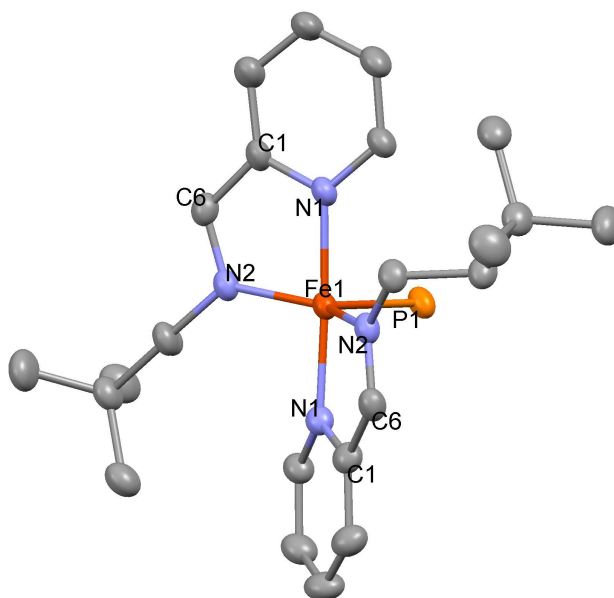


Figure 4.3. Molecular view of *cis*-{ κ -N,N'-(N-(2-pyridinylmethylene)alkylamine)}₂-Fe(PMe₃) (**3-^{neo}Hex**). Disordered methyl groups of the PMe₃ are removed for clarity.

Attempts to oxidize this formally Fe(0) phosphine complex with a variety of two-electron donors, such as azides, diazomethane derivatives, Wittig reagents and alkynes, were unsuccessful (Scheme 4.6). No reaction was obtained with H₂ or HSiPh₃, even with the application of heat. Apparently, the strongly-donating phosphine ligand is not easily removed.

2. Syntheses of [*cis*-{ κ -N,N'-(N-(2-pyridinylmethylene)alkylamine)}₂ - Fe(PMe₃)(CH₃)]X (X = I, **4-^{neo}Pe, **4-^{neo}Hex**; OTf, **5-^{neo}Hex**).**

In order to perform an oxidation that did not necessitate removal of the PMe₃, we employed the use of the alkylating agents CH₃I and CH₃OTf. Treatment of either **3-^{neo}Hex** or **3-^{neo}Pe** with one equivalent of CH₃I in THF resulted in the formation of a fairly insoluble green solid, formulated as [*cis*-{ κ -N,N'-(N-(2-pyridinylmethylene)alkylamine)}₂ Fe(PMe₃)(CH₃)]I (**4-^{neo}Pe**, **4-^{neo}Hex**, Scheme 4.6). ¹H NMR showed inequivalent pyridylimine ligands with diastereotopic methylene protons, and two doublets integrating 9:3 for the phosphine and methyl resonances,

respectively. Though the yields obtained were modest (56-76 %), diffraction-quality crystals of the proposed cation were elusive, and we could not rule out the possibility of unwanted reduction behavior from the non-innocent iodide anion. To provide the necessary assurance, **3-neoHex** was treated with one equivalent of CH₃OTf in THF at -78 °C, and the resulting green solid displayed very similar NMR spectra to those of **4-neoHex**. X-ray suitable crystals were obtained, confirming the assignment of **5-neoHex** as *[cis-{κ-N,N'-(N-(2-pyridinylmethylene)neohexylamine)}₂Fe(PMe₃)(CH₃)]OTf* (Figure 4.4).

The [M-CH₃]⁺ motif of **3** and **4** is reminiscent of many late metal polymerization catalysts based off of the Brookhart model, [(κ-N,N)M(L)(Me)]⁺ (κ-N,N = α-diimine; M = Ni, Pd),^{25,26} which are notable for their higher tolerance for heteroatom-containing functional groups compared to their early metal counterparts. For this reason, the iron complexes **4-neoPe**, **5-neoHex**, and **1-neoPe** were subjected to high pressures of ethylene under varying conditions.^{vi} Unfortunately, very little or no polymer was formed. It is possible that the PMe₃ ligand of **4-neoPe** and **5-neoHex** lacks the lability necessary for the metal to coordinate an olefin.

3. Oxidations with AgOTf

Attempted one-electron oxidation of either **2-neoHex** or **3-neoHex** led to intensely-colored purple solutions. ¹H NMR analysis of the crude reactions showed several species, but the major product that was isolated as a purple solid *from either starting material* appeared to possess three distinct ligand environments in a 1:1:1 ratio. The same spectral signature was observed in the reaction of **2-neoHex** with CH₃OTf, or when the reaction of **3-neoHex** with CH₃OTf was not performed under low-temperature conditions. Disproportionation to the tris-pyridylimine dication was suspected, and confirmation by independent synthesis was sought.

^{vi} Reactions were run for 2.5 h in toluene at 60 °C with 270 equiv PMAO, using up to 60 psi ethylene.

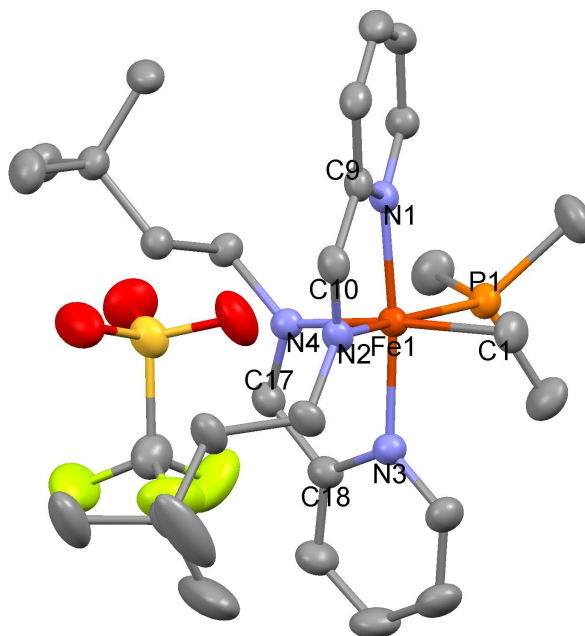
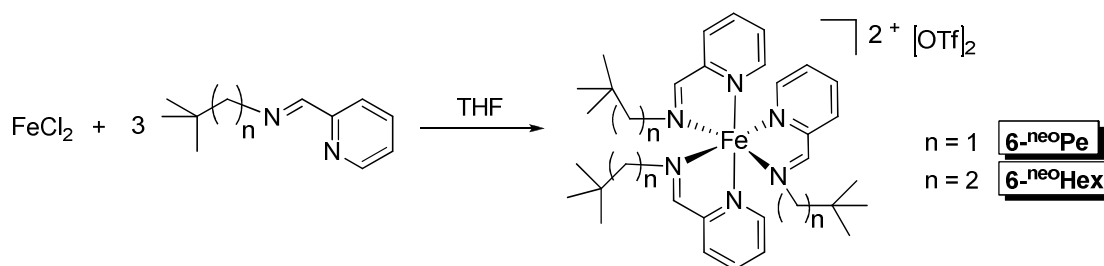


Figure 4.4. Molecular view of $[cis-\{\kappa-N,N'-(N-(2\text{-pyridinylmethylene})neoheptylamine)\}_2Fe(PMe_3)(CH_3)]OTf$ (**5-^{neo}Hex**).

D. Synthesis of $[\{\kappa-N,N'-(N-(2\text{-pyridinylmethylene})alkylamine)\}_3Fe][OTf]_2$ (alkyl = $CH_2C(CH_3)_3$, **6-^{neo}Pe; $(CH_2)_2C(CH_3)_3$, **6-^{neo}Hex**).**

$Fe(OTf)_2$ was added to three equivalents of vigorously stirred ^{neo}Pe-imine or ^{neo}Hex-imine in THF, resulting in a bright purple solution from which purple solid precipitated after about 30 min (Scheme 4.7). Extraction with CH_2Cl_2 and washing with Et_2O afforded very good yields of the dicationic complexes $[\{\kappa-N,N'-(N-(2\text{-pyridinylmethylene})alkylamine)\}_3Fe][OTf]_2$ (alkyl = $CH_2C(CH_3)_3$, **6-^{neo}Pe**; $(CH_2)_2C(CH_3)_3$, **6-^{neo}Hex**) (87-93 %). NMR spectra of these isolated materials matched those obtained in $AgOTf$ and CH_3OTf reactions mentioned previously. NMR spectra reveal **6-^{neo}Pe** to be a mixture of *fac* and *mer* isomers in a 1:2 ratio, similar to the statistical ratio of 1:3. Strangely, **6-^{neo}Hex** exhibits a spectrum of the *mer* isomer exclusively. Several authors have reported selectivity for a particular *fac* or *mer* isomer in tris-bidentate complexes, which they attribute either to pi-stacking of

pendant aromatic groups or to lengthening alkyl substituents.^{27,28} The latter is apparently operative in the case of **6-neoPe** versus **6-neoHex**, though the difference in selectivity based on one additional carbon in a chain is certainly surprising.



Scheme 4.7. Synthesis of [κ -N,N'-(N-(2-pyridinylmethylene)alkylamine)]₃Fe[OTf]₂ (alkyl = CH₂C(CH₃)₃, **6-neoPe**; (CH₂)₂C(CH₃)₃, **6-neoHex**).

E. Structural comparison of bis-(iminopyridine)iron complexes.

1. Structure of *cis,cis*-{ κ -N,N'-(N-(2-pyridinylmethylene)neopentylamine)}₂-Fe(CH₃)₂ (**1-neoPe**).

Figure 4.1 shows the structure of **1-neoPe**, while Table 4.1 contains crystallographic information and Table 4.2 lists pertinent bond distances and angles for all structurally characterized compounds. The pyridine moieties are positioned apically, while the imines are approximately trans to the methyl groups in the equatorial plane. The average Fe-N_{imine} bond lengths ($1.9800(12) \pm 0.0062$ Å) are significantly longer than the Fe-N_{py} ($1.9309(12) \pm 0.0013$ Å), as a result of the strongly-donating methyl groups trans to the imines. This is also manifested in the modest distortions of N_{im}-Fe-C ($164.94(6)$ and $164.64(6)$ °, respectively) away from 180°, and of N_{im}-Fe-N_{im} ($109.56(5)$ °) and C-Fe-C ($82.25(7)$ °) away from the ideal 90°. The Fe-C distances of $2.0455(15)$ and $2.0382(15)$ ° are normal. The chelate angles for the iminopyridine ligands ($80.88(5)$ and $81.10(5)$ °) are contracted, and the modest distortions in the remaining core angles are simply compensating.

Table 4.1. Selected crystallographic and refinement data for *cis,cis*-{ κ -N,N'-(N-(2-pyridinylmethylene)-neopentylamine) $_2$ Fe(CH $_3$) $_2$ (**1-neoPe**), *cis*-{ κ -N,N'-(N-(2-pyridinylmethylene)neohexylamine) $_2$ Fe(PhCCPh) (**2-neoHex**), *cis*-{ κ -N,N'-(N-(2-pyridinylmethylene)alkylamine) $_2$ Fe(PMe $_3$) (**3-neoHex**), and [*cis*-{ κ -N,N'-(N-(2-pyridinylmethylene)neohexylamine) $_2$ Fe(PMe $_3$)(CH $_3$)OTf (**5-neoHex**).

	1- neoPe	2- neoHex	3- neoHex	5- neoHex
Formula	C $_{24}$ H $_{38}$ N $_4$ Fe	C $_{38}$ H $_{46}$ N $_4$ Fe	C $_{27}$ H $_{45}$ N $_4$ PFe	C $_{29}$ H $_{48}$ N $_4$ PO $_3$ F $_3$ SFe
Formula weight	438.43	614.64	512.49	676.59
Crystal system	Monoclinic	Cubic	Monoclinic	Triclinic
Space group	P2 $_1$ /n	Ia-3d	C2/c	P-1
Z	4	48	4	2
<i>a</i> (Å)	11.5730(6)	35.4108(9)	18.3431(8)	10.0631(6)
<i>b</i> (Å)	15.2735(10)	35.4108(9)	7.3184(4)	11.1129(7)
<i>c</i> (Å)	13.3733(8)	35.4108(9)	21.4583(10)	16.4463(10)
α (°)	90	90	90	81.295(2)
β (°)	92.646(3)	90	102.803(2)	72.480(2)
γ (°)	90	90	90	73.226(2)
<i>V</i> (Å 3)	2361.3(2)	44402(2)	2809.0(2)	1675.06(18)
ρ_{calc} (gcm $^{-3}$)	1.233	1.103	1.212	1.341
μ (mm $^{-1}$)	0.655	0.436	0.615	0.612
T (K)	173(2)	173(2)	173(2)	173(2)
λ (Å)	0.71073	0.71073	0.71073	0.71073
Final R indices	R $_1$ = 0.0304 wR $_2$ = 0.0774	R $_1$ = 0.0403 wR $_2$ = 0.0996	R $_1$ = 0.0312 wR $_2$ = 0.0801	R $_1$ = 0.0399 wR $_2$ = 0.0992
R indices (all data) ^{a,b}	R $_1$ = 0.0424 wR $_2$ = 0.0849	R $_1$ = 0.0663 wR $_2$ = 0.1092	R $_1$ = 0.0385 wR $_2$ = 0.0848	R $_1$ = 0.0546 wR $_2$ = 0.1070
Goodness-of-fit ^c	1.004	1.002	1.060	1.063

^a $R_1 = \Sigma |F_o| - |F_c| / \Sigma |F_o|$. ^b $wR_2 = [\Sigma w(|F_o| - |F_c|)^2 / \Sigma wF_o^2]^{1/2}$. ^c GOF (all data) = $[\Sigma w(|F_o| - |F_c|)^2 / (n - p)]^{1/2}$, n = number of independent reflections, p = number of parameters.

Table 4.2. Selected distances (Å) and angles (°) for *cis,cis*-{κ-N,N'-(N-(2-pyridinylmethylene)neopentylamine)}₂-Fe(CH₃)₂ (**1-^{neo}Pe**), *cis*-{κ-N,N'-(N-(2-pyridinylmethylene)neohexylamine)}₂-Fe(PhCCPh) (**2-^{neo}Hex**), *cis*-{κ-N,N'-(N-(2-pyridinylmethylene)alkylamine)}₂-Fe(PMe₃) (**3-^{neo}Hex**), and [*cis*-{κ-N,N'-(N-(2-pyridinylmethylene)neohexylamine)}₂-Fe(PMe₃)(CH₃)]OTf (**5-^{neo}Hex**).

	3-^{neo}Hex	2-^{neo}Hex	1-^{neo}Pe	5-^{neo}Hex
Fe-N _{im}	1.9109(9)	1.9376(13)	1.9843(12)	1.9486(15)
Fe-N _{im'}	^a	^a	1.9756(12)	1.9670(15)
Fe-N _{py}	1.9493(9)	1.9294(13)	1.9300(12)	1.9503(16)
Fe-N _{py'}	^a	^a	1.9318(12)	1.9648(16)
Fe-C	-	1.9789(16)	2.0455(15)	2.060(2)
Fe-C'	-	^a	2.0382(15)	-
Fe-P	2.2351(5)	-	-	2.2552(5)
N _{im} -C _{im}	1.3372(14)	1.310(2)	1.3033(19)	1.284(2)
N _{im'} -C _{im'}	^a	^a	1.3059(19)	1.291(2)
C _{im} -C _{py}	1.3957(16)	1.423(2)	1.424(2)	1.429(3)
C _{im'} -C _{py'}	^a	^a	1.417(2)	1.435(3)
C≡C		1.289(3)		
<hr/>				
N _{py} -Fe-N _{py'}	176.11(6)	177.54(8)	178.08(5)	173.92(6)
N _{im} -Fe-N _{im'}	140.15(6)	108.09(8)	109.56(5)	100.13(6)
C-Fe-C'	-	38.02(9)	82.25(7)	-
C-Fe-P	-	-	-	82.80(6)
N _{im} -Fe-N _{py}	81.24(4)	80.71(5)	80.88(5)	80.57(6)
N _{im'} -Fe-N _{py'}	^a	^a	81.10(5)	80.16(6)
N _{im} -Fe-N _{py'}	97.42(4)	97.83(5)	97.94(5)	94.99(7)
N _{im'} -Fe-N _{py}	^a	^a	97.85(5)	96.46(6)
N _{im} -Fe-C	-	144.84(6)	164.94(6)	84.82(8)
N _{im'} -Fe-C'	-	^a	164.44(6)	-
N _{im} -Fe-C'	-	107.02(6)	84.82(6)	-
N _{im'} -Fe-C	-	^a	84.21(6)	172.27(7)
N _{im} -Fe-P	109.93(3)	-	-	167.30(5)
N _{im'} -Fe-P	^a	-	-	92.49(5)
N _{py} -Fe-C	-	89.50(6)	91.45(6)	90.19(8)
N _{py'} -Fe-C'	-	^a	90.13(6)	-
N _{py} -Fe-C	-	92.82(6)	90.04(6)	93.55(8)
N _{py'} -Fe-C'	-	^a	91.27(6)	-
N _{py} -Fe-P	91.94(3)	-	-	96.64(5)
N _{py'} -Fe-P		-	-	88.59(5)
Fe-C-C _{ipso}	-	139.94(13)	-	-
C _{ipso} -C-C'	-	148.33(10)	-	-

^aThe two imino-pyridine ligands of **neoHex-3** and **neoHex-2** are equivalent by symmetry, so relevant bond lengths and angles are identical.

Two parameters that are generally used to assess the amount of reduction of the iminopyridine ligand are the N_{im}-C_{im} and C_{im}-C_{py} distances. In **1-neoPe**, these are rather distinct (N_{im}-C_{im} = 1.3033(19), 1.3059(19) Å; C_{im}-C_{py} = 1.424(2), 1.417(2) Å), reflecting a significant amount of double bond character in the imine and single bond character in the carbon-carbon bond.

2. Structure of *cis*-{κ-N,N'-(N-(2-pyridinylmethylene)neohexylamine)}₂Fe(PhCCPh) (**2-neoHex**).

2-neoHex crystallizes in the highly symmetric cubic crystal system. The large unit cell volume of 44 402 Å³ accommodates 48 molecules! One of these molecules is represented in Figure 4.2. The C₂ symmetry of **2-neoHex** renders the two halves of the molecule crystallographically equivalent.

Like **1-neoPe**, the pyridine ligands in **2-neoHex** occupy the apical positions, and the imines lie in the same plane as the alkyne. The Fe-N_{im} distances of 1.9376(13) Å are much shorter than in **1-neoPe**, and closer to the Fe-N_{py} distances of 1.9294(13) Å. Since the acetylene carbons are constrained to be off-axis, the trans N_{im}-Fe-C angles are only 144.84(6) °. In this case, then, the slight widening of the N_{im}-Fe-Fe_{im} angle (108.09(8) °) must help relieve steric interaction between the neohexyl chains. The chelate angle is virtually identical (80.71 °) to that of **1-neoPe**, and the remaining core angles vary less than 8 ° from ideal.

The diphenylacetylene C-C bond length of 1.289(3) Å implies significant double bond character, and the angle α (which measures the deviance of the phenyl substituents from the C-C line) is 32.67 °, suggesting that the bound alkyne may be best described as a 2-electron donor. Slightly shorter Fe-C bonds (1.9789(16) Å) arise from being involved in the 3-membered metallacycle. With regard to the iminopyridine, the N-C_{im} and C_{im}-C_{py} bond lengths of 1.310(2) and 1.423(2) Å, respectively, show them to be the roughly same as in **1-neoPe**.

3. Structure of *cis*-{ κ -N,N'-(N-(2-pyridinylmethylene)alkylamine)}₂Fe(PMe₃) (alkyl = CH₂C(CH₃)₃, **3-^{neo}Pe; (CH₂)₂C(CH₃)₃, **3-^{neo}Hex**).**

The formally Fe(0) complex, **3-^{neo}Hex**, is shown in Figure 4.3. The *C*₂ symmetry of the molecule is observed crystallographically. Based on the nearly linear orientation of the pyridine ligands (*N*_{py}-Fe-*N*_{py} = 176.11(6) °) versus the bent *N*_{im}-Fe-*N*_{im} angle of 140.15(6) °, the complex has overall pseudo-trigonal bipyramidal geometry. Each P-Fe-*N*_{im} angle is 109.90(3) °, and the Fe-P bond is unremarkable at 2.2351(5) Å. Because of the lack of trans ligands, the Fe-*N*_{im} bond distances (1.9109(9) Å) are shorter than those in either **1-^{neo}Pe** or **2-^{neo}Hex**. The Fe-*N*_{py} bond lengths are correspondingly longer at 1.9493(9) Å.

While the bite angles of the chelates are virtually the same as **1-^{neo}Pe** and **2-^{neo}Hex** (81.24(4) °), the ligand distances are markedly different. The N-*C*_{im} bond has lengthened to 1.3372(14) Å and the *C*_{im}-*C*_{py} bond has contracted to 1.3957(16) Å. Though the ~0.3 Å changes seem subtle, the disparity is more evident in the difference between the N-*C*_{im} and *C*_{im}-*C*_{py} bonds, which roughly doubles going from **3-^{neo}Hex** to **1-^{neo}Pe**. The values for **3-^{neo}Hex** are also more consistent with Wieghardt's characteristic bond distances of an iminopyridine radical anion (Scheme 4.1).

An analogous compound using an *N*-phenyl-1,2-benzenediamine-derived ligand has been reported in the literature, which is also described as an iron with two radical monoanions (**7**, Figure 4.5).¹ In contrast to **3-^{neo}Hex**, this complex adopts a square pyramidal geometry with trans N-Fe-N angles of 164.26 and 164.00 °, and average P-Fe-N angles of 98 °. Since the chelate angle of this and **3-^{neo}Hex** are the same within a degree, and the difference in phosphine ligand cannot have much effect, the structural variation must be due to an inherent electronic difference in the two ligands (*vide infra*).

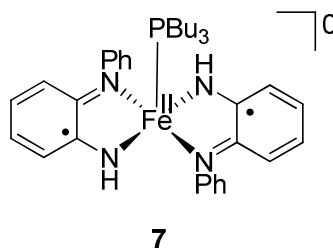


Figure 4.5. Wieghardt's five-coordinate bis-iminopyridine iron phosphine complex.¹

4. Structure of $[cis-\{\kappa\text{-N,N}'\text{-(N-(2-pyridinylmethylene)neohexylamine)}\}_2\text{Fe(PMe}_3\text{)(CH}_3\text{)}]\text{OTf}$.

Figure 4.4 shows **5-^{neo}Hex**, with trans pyridines and imines opposite the methyl and phosphine ligands. The trans $\text{N}_{\text{im}}\text{-Fe-P}$ at $167.30(5)^\circ$ is actually more bent than that of $\text{N}_{\text{im}}\text{-Fe-C}$ angle of $172.27(7)^\circ$, but the Fe-N_{im} bond trans to carbon ($1.9670(15) \text{ \AA}$) is modestly longer than the one trans to phosphorus ($1.9486(15) \text{ \AA}$), showing the influence of the strong trans methyl group. All Fe-N bonds are on the longer end of the spectrum, which might be expected for a cationic species. Excluding **3-^{neo}Hex**, the $\text{N}_{\text{im}}\text{-Fe-N}_{\text{im}}$ angle of **5-^{neo}Hex** is the smallest, probably to accommodate the bulky PMe_3 ligand. Ligand bond lengths ($\text{N}_{\text{im}}\text{-C}_{\text{im}} = 1.284(2), 1.291(2) \text{ \AA}$; $\text{C}_{\text{im}}\text{-C}_{\text{py}} = 1.429(3), 1.435(3) \text{ \AA}$) indicate that the imines of **5-^{neo}Hex** are the least reduced of all the compounds.

F. Mössbauer comparison of bis-(iminopyridine)iron complexes.

Zero-field Mössbauer data gathered for complexes **1-^{neo}Pe**, **2-^{neo}Hex**, **3-^{neo}Hex**, **5-^{neo}Hex**, and **6-^{neo}Hex** at 80 K are shown in Figure 4.6. Figure 4.7 shows the isomer shifts plotted on a scale including those of relevant compounds from the literature. The isomer shift (δ) range is fairly narrow ($0.19 - 0.37 \text{ mm/s}$), and the quadrupole splitting (ΔE_Q) range is more significant ($0.47 - 1.63 \text{ mm/s}$). In general, isomer shift values decrease with increasing oxidation state and are larger for high-spin complexes than

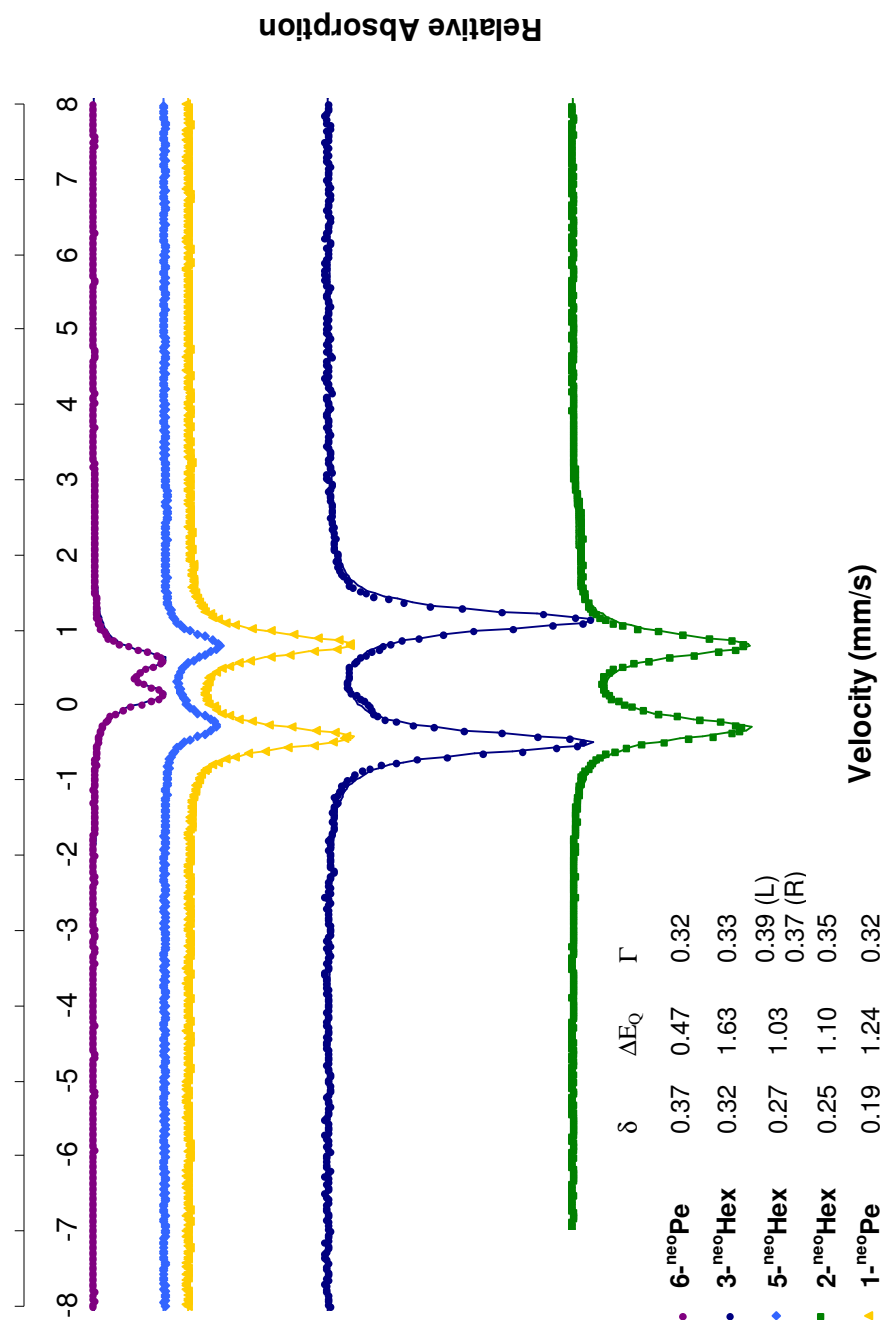


Figure 4.6. Mössbauer spectra (overlaid) of six-coordinate $[\{\kappa\text{-N,N'-(N-(2\text{-pyridinylmethylene})\text{neopentyl-amine})}_3\text{Fe}][\text{OTf}]_2$ (**6-^{neo}Pe**), $[\text{cis-}\{\kappa\text{-N,N'-(N-(2\text{-pyridinylmethylene})\text{-neohexylamine})}_2\text{Fe(PMe}_3\text{)(CH}_3\text{)}]\text{OTf}$ (**5-^{neo}Hex**) and $\text{cis,cis-}\{\kappa\text{-N,N'-(N-(2\text{-pyridinylmethylene})\text{neopentylamine})}_2\text{Fe(CH}_3\text{)}_2$ (**1-^{neo}Pe**), and five-coordinate $\text{cis-}\{\kappa\text{-N,N'-(N-(2\text{-pyridinylmethylene})\text{alkylamine})}_2\text{Fe(PMe}_3\text{)}$ (**3-^{neo}Hex**) and $\text{cis-}\{\kappa\text{-N,N'-(N-(2\text{-pyridinylmethylene})\text{neohexyl-amine})}_2\text{Fe(PhCCPh)}$ (**2-^{neo}Hex**).

for low-spin complexes.^{vii} The quadrupole splitting values are fairly intuitive, as the most symmetric **6-neoPe** exhibits the lowest value, i.e., the smallest electric field gradient. **3-neoHex**, being five-coordinate, exhibits the highest. The fact that **1-neoPe** has a larger quadrupole splitting than **2-neoHex** and **5-neoHex** remains an oddity. All values fall within the range of a low-spin Fe(II) center, with the variation reflective of the oxidizing ability of the X_n ligand(s). At the lower end of the spectrum, **1-neoPe** exhibits an isomer shift of 0.19 mm/s, followed by **2-neoHex** at 0.25 mm/s, **5-neoHex** at 0.27 mm/s, and **3-neoHex** at 0.32 mm/s. This trend supports the strong-field nature of carbon-based ligands, as the addition of an alkyl or alkenyl group makes the complex appear more oxidized.

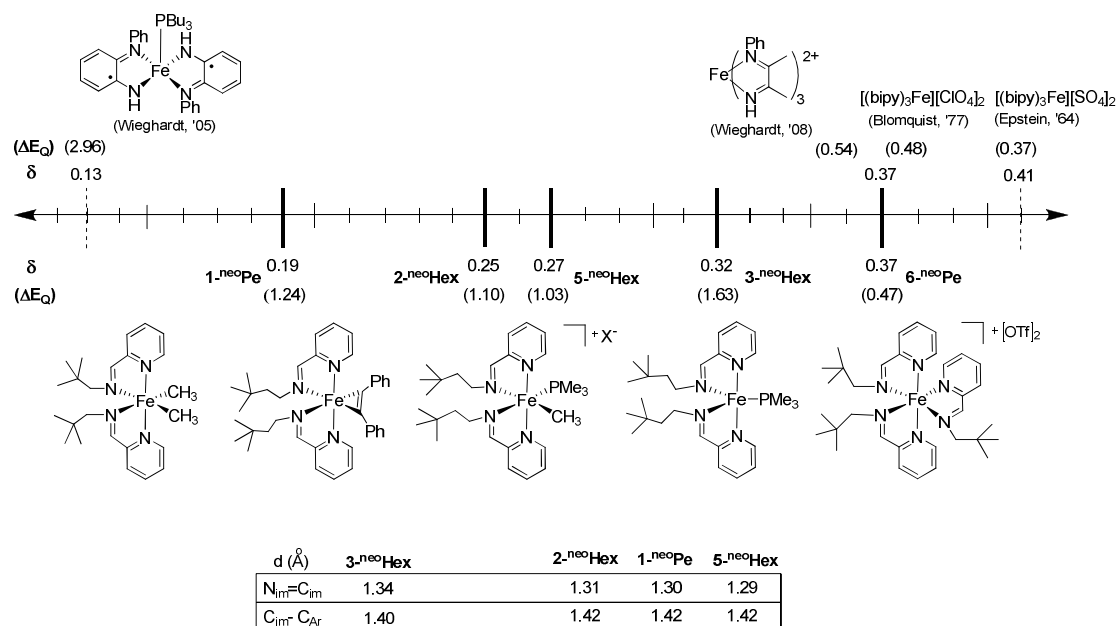


Figure 4.7. Mössbauer comparison including related complexes from the literature.^{1,30-32}

^{vii} Accepted ranges for high-spin (HS) and low-spin (LS) iron complexes are as follows, in mm/s: HS Fe(II), +0.6 to +1.7; LS Fe(II), -0.2 to +0.4; HS Fe(III), +0.1 to +0.5; LS Fe(III), -0.1 to +0.5. Fe(0) complexes fall within the range of -0.2 to -0.1.²⁹

The parameters for **3-^{neo}Hex** do not unequivocally support either an $(L^0)_2Fe^0(PMe_3)$ or an $(L^\bullet)_2Fe^{II}(PMe_3)$ configuration. Mössbauer data would seem to support the latter; the isomer shift of **3-^{neo}Hex** lies amid those of other low-spin Fe(II) centers, whereas Fe(0) centers exhibit much lower values (e.g., $Fe(CO)_5$ ³³ and $Fe(CO)_4(PPh_3)$ ³⁴ have isomer shifts of -0.10 mm/s). Structural data also shows evidence of reduced iminopyridine ligands in comparison to complexes with the same ligand. The similar Wieghardt phosphine complex, **7**, is described as having two reduced ligands. However, ¹H NMR supports an Fe(0) assignment, as the imine C-H resonance ranges from 8.27 (for **2-^{neo}Hex**) to 10.30 ppm (for the *mer* isomer of **6-^{neo}Pe**), with **3-^{neo}Hex** falling nearly in the center at 8.90 ppm. Structural differences in **3-^{neo}Hex** are very subtle, particularly C_{im}-C_{Ar}, and could alternatively be attributed to the variation in coordination number. This discrepancy may also influence the isomer shift of **3-^{neo}Hex**. Notably, the Mössbauer parameters of Wieghardt's square pyramidal phosphine complex, **7**, are strikingly different. The divergent geometry, a much larger quadrupole splitting parameter ($\Delta E_Q = 2.96$ mm/s), and a much lower isomer shift ($\delta = 0.13$ mm/s) imply a significant electronic difference, presumably originating from increased π back-bonding in the aryl-substituted *N*-phenyl-*o*-diiminobenzosemiquinone versus the alkyl-substituted iminopyridine radical. Assignment of the same $(L^\bullet)_2Fe^{II}(PMe_3)$ configuration to **3-^{neo}Hex** would seem to disregard these obvious electronic disparities.

It should be mentioned that another possible description of **1-^{neo}Pe**, **5-^{neo}Hex**, and **2-^{neo}Hex** is of an Fe(III) center with one reduced iminopyridine, $(L^\bullet)(L^0)Fe^{III}X_2$, where the lone electrons on the iron and ligand couple antiferromagnetically to give an overall $S = 0$ spin state. The isomer shift of 0.25 does lie within the range for LS Fe(III). This description has previously been used to rationalize intermediate bond lengths in a series of cationic bis-iminopyridine complexes.⁸ In this case, however, the

ligand distances conform to the neutral iminopyridine description, ^1H NMR data lacks evidence of a reduced ligand, and there are no other parameters to suggest that an alternative to the standard $(\text{L}^0)_2\text{Fe}^{\text{II}}(\text{X})_2$ model is necessary; therefore, the latter description is proposed for **1-neoPe**, **5-neoHex**, and **2-neoHex**.

The Mössbauer spectrum of **6-neoPe** was obtained as a calibration for the remaining complexes. Similar low-spin tris-diimine or -bipyridyl dications have been known for decades in the inorganic literature, and several are shown in Figure 4.7.^{1,30-32} The isomer shift of 0.37 mm/s for **6-neoPe** is very close or identical to that of $[(\text{bipy})_3\text{Fe}][\text{X}]_2$ (bipy = 2,2'-bipyridyl; $\text{X} = \text{ClO}_4, \text{SO}_4$)^{viii} and the tris-diimine shown, and the quadrupole splitting parameters are very similar (0.47, 0.48, 0.54 mm/s, respectively). The minor discrepancy in the tris-bipyridine measurements is likely due to the accompanying counterions, since this effect is seen even within an individual set of experimental results.³²

III. Conclusions

A series of bis-iminopyridine iron complexes have been synthesized and their structural and Mössbauer data compared. At this point, the data is insufficient to assign **3-neoHex** as a formally Fe(0) complex or as Fe(II) with two monoreduced iminopyridine ligands. The remaining bis-ligand complexes are low-spin Fe(II) with neutral iminopyridines. The variation in isomer shifts reinforces the strong-field nature of both sp^2 and sp^3 carbon-based ligands, with the most covalent **1-neoPe** exhibiting the lowest value. In the series, the tris-chelated **6-neoPe** remains a modest outlier, though it agrees with data for similar compounds in the literature. The lack of an obvious overall trend highlights the sensitivity of Mössbauer spectroscopy to subtle variations

^{viii} In these and other, older references, isomer shifts are referenced to different standards. A convenient isomer shift reference table for common standards has been published.³⁵

in coordination geometry, ligand field, ligand substitution, and overall charge, thereby cautioning that comparisons are best within a particular structural framework.

IV. Experimental

A. General Considerations.

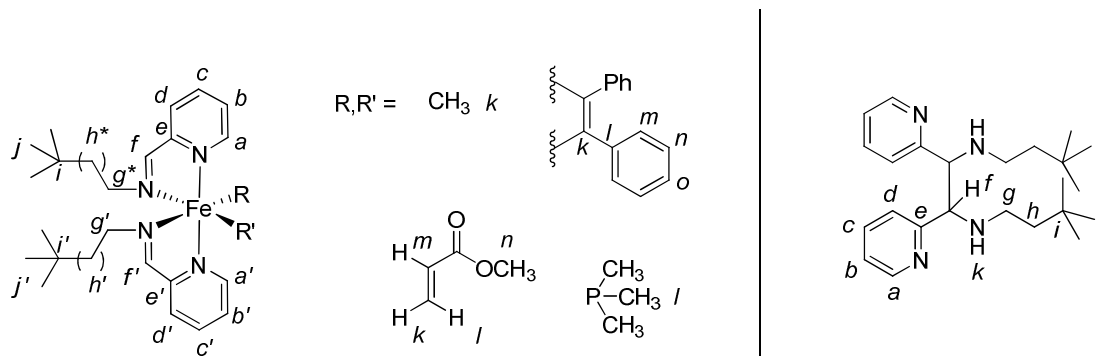
All manipulations were performed using either glovebox or high vacuum line techniques. Hydrocarbon solvents containing 1-2 mL of added tetraglyme, and ethereal solvents were distilled under nitrogen from purple sodium benzophenone ketyl and vacuum transferred from same prior to use. Benzene- d_6 and toluene- d_8 were dried over sodium, vacuum transferred and stored under N_2 . THF- d_8 was dried over sodium benzophenone ketyl. Methylene chloride- d_2 was dried over CaH_2 , vacuum transferred and stored over activated 4 Å molecular sieves. Trimethylphosphine was dried and stored over activated 4 Å molecular sieves. *cis*-(Me_3P) $_4$ FeMe $_2$ was prepared according to literature procedure.³⁶ All other chemicals were commercially available and used as received. All glassware was oven dried.

NMR spectra were obtained using Varian XL-400, INOVA 400, and Unity-500 spectrometers. Chemical shifts are reported relative to benzene- d_6 (1H δ 7.16; $^{13}C\{^1H\}$ δ 128.39), THF- d_8 (1H δ 3.58; $^{13}C\{^1H\}$ δ 67.57), and CD_2Cl_2 (1H δ 5.32; $^{13}C\{^1H\}$ δ 54.00). Assignments are given according to Figure 4.8. Infrared spectra were recorded on a Nicolet Avatar 370 DTGX spectrophotometer interfaced to an IBM PC (OMNIC software). UV-Vis spectra were obtained on a Shimadzu UV-2102 interfaced to an IBM PC (UV Probe software). Elemental analyses were performed by Robertson Microlit Laboratories, Madison, New Jersey.

B. General procedure for synthesis of imines.

To a suspension of $MgSO_4$ (5-8 equiv.) in CH_2Cl_2 were added 1.5 mmol of 2-pyridinecarboxaldehyde and 1.5 mmol of amine. After stirring for 2 h, the mixture was

filtered and concentrated to yield a pale yellow oil in >98 % purity (by ^1H NMR). A spectrum and synthesis for $^{\text{neo}}\text{Pe-imine}$ has been reported.³⁷



*Diastereotopic protons are designated as a or b .

Figure 4.8. Labeling scheme for ^1H and ^{13}C NMR assignments.

C. Synthesis of bis-(iminopyridine) complexes.

1. *cis,cis*- $\{\kappa\text{-N,N}'\text{-(N-(2-pyridinylmethylene)neopentylamine)}\}_2\text{Fe}(\text{CH}_3)_2$ (1- $^{\text{neo}}\text{Pe}$).

To a solution of $\text{Fe}(\text{PMe}_3)\text{Me}_2$ (140mg, 0.359mmol) in benzene was added a solution of $^{\text{neo}}\text{Pe-im}$ (127 mg, 0.718 mmol) in benzene. The bright purple solution was allowed to stir at room temperature for 18 h. After removal of solvent, the mixture was filtered and washed with Et_2O (3 x 8 mL). Concentration under vacuum revealed black crystalline solid (125 mg, 80 %). ^1H NMR (400MHz, benzene- d_6): 8.28 (d, 3, a), 6.62 (t, 7, b), 6.90 (t, 8, c), 7.03 (d, 8, d), 9.09 (br s, f), 3.75 (d, 11, g_a), 3.20 (d, 11, g_b), 0.45 (s, j), 0.97 (s, k). ^{13}C NMR (400MHz, benzene- d_6): 152.71 (a), 124.83 (b), 126.24 (c), 117.26 (d), 157.83 (e), 158.00 (f), 68.76 (g), 32.47 (i), 28.19 (j), 21.14 (k). Anal. Calcd for $\text{C}_{24}\text{H}_{38}\text{N}_4\text{Fe}$: C, 65.75; H, 8.74; N, 12.78. Found: C, 65.54; H, 8.60; N, 12.60.

2. Proposed methyl acrylate adduct ($^{\text{neo}}\text{Pe-COOMe}$).

10 mL THF were vacuum transferred to a flask containing FeCl_2 (35 mg, 0.276 mmol) and 2.2 equivalents sodium amalgam (1.770 g, 0.79%) in a -78°C bath. Under argon purge, methyl acrylate (0.50 mL, 5.5 mmol) and a solution of $^{\text{neo}}\text{Pe-im}$ (97 mg,

0.552 mmol) in THF were added via syringe. The mixture was allowed to warm slowly to room temperature overnight. The reaction was stripped, redissolved in Et₂O and filtered through Celite. Concentration of the green-brown solution followed by concentration in cold hexane solution yielded ~15 mg olive green solid. ¹H NMR (400MHz, benzene-*d*₆): 8.52 (br s, *a*, *a'*), 6.47 (t, 6, *b*), 6.41 (t, 6, *b'*), 6.69-6.75 (m, *c*, *c'*), 6.83 (d, 7, *d*), 6.78 (d, 7, *d'*), 8.05 (s, *f*), 8.02 (s, *f'*), 4.29-4.18 (m, *g_a*, *g_{a'}*, *l*), 3.53 (d, 11, *g_b*), 3.41 (d, 12, *g_{b'}*), 0.56 (*j*), 0.54 (*j'*), 1.88 (d, 7, *k*), 4.96 (t, 10, *m*), 2.84 (s, *n*).

3. Reduction with HC≡C(4-^tBuPh) to make coupled organic.

10 mL THF were vacuum transferred to a flask containing FeCl₂ (48 mg, 0.381 mmol) and 2.2 equivalents sodium amalgam (2.676 g, 0.72%) in a -78 °C bath. Under argon purge, a solution of ^{neo}Hex-im (145 mg, 0.762 mmol) and *p*-(*tert*-butyl)phenylacetylene (60 mg, 0.381 mmol) were added via syringe. The mixture was allowed to warm slowly to room temperature overnight. The reaction was stripped, redissolved in THF and filtered through Celite. Concentration of the solution, triturating with pentane, and further concentration revealed a brown, foamy solid (125 mg). Brown solid was obtained from cold hexane solution. ¹H NMR (500MHz, C₆D₆): 8.41 (d, 4, *a*), 6.56 (t, 6, *b*), 7.02 (t, 8, *c*), 7.17 (*d*), 4.28 (t, 4, *f*), 2.54 (m, *g*), 1.47 (m, *h*), 0.77 (s, *j*), 2.88 (d, 6, *k*). ¹³C NMR (500MHz, C₆D₆): 149.55 (*a*), 122.02 (*b*), 135.69 (*c*), 123.53 (*d*), 163.32 (*e*), 70.64 (*f*), 45.16 (*g*), 45.18 (*h*), 30.23 (*i*), 30.10 (*j*).

4. *cis*-{κ-N,N'-(N-(2-pyridinylmethylene)alkylamine)}₂Fe(PhCCPh) (alkyl = CH₂C(CH₃)₃, 2-^{neo}Pe; (CH₂)₂C(CH₃)₃, 2-^{neo}Hex).

A 50 mL round bottom flask was charged with 75 mg FeCl₂ (0.592 mmol), diphenylacetylene (116 mg, 0.651 mmol) and 2.2 equivalents sodium amalgam (3.79 g, 0.79 %). 20 mL THF were vacuum distilled at -78 °C, and a solution of imine (1.18 mmol) in 5 mL THF were added via syringe under argon purge. The reaction mixture was allowed to stir and slowly warm to room temperature overnight. The crude

reaction was stripped and filtered through Celite in Et₂O and THF. The brown solution was concentrated and subsequently filtered and washed with Et₂O (3 x 15 mL).

Concentration followed by cooling to -78 °C yielded dark brown crystalline solid that was collected by filtration. a. **2-^{neo}Hex**: 220 mg, 60%. ¹H NMR (500MHz, benzene-*d*₆): 8.67 (d, 5, *a*), 6.27 (t, 6, *b*), 6.63 (t, 7, *c*), 6.83 (d, 8, *d*), 8.27 (s, *f*), 4.25 (td, 12, 4, *g_a*), 4.09 (td, 11, 4, *g_b*), 1.20 (td, 12, 5, *h_a*), 0.56 (td, 13, 3, *h_b*), 0.64 (s, *j*), 7.61 (d, 8, *m*), 7.22 (t, 7, *n*), 7.02 (t, 7, *o*). ¹³C NMR (500MHz, C₆D₆): 150.88 (*a*), 122.78 (*b*), 125.24 (*c*), 117.83 (*d*), 155.12 (*e*), 155.88 (*f*), 58.79 (*g*), 46.80 (*h*), 29.73 (*i*, *j*), 138.66 (*k*), 120.86 (*l*), 128.73 (*m*), 129.79 (*n*), 125.41 (*o*). Anal. Calcd for C₄₀H₄₆N₄Fe: C, 74.26; H, 7.54; N, 9.12. Found: C, 72.03; H, 7.41; N, 8.43. b. **2-^{neo}Pe**: 165 mg, 45%. ¹H NMR (400MHz, benzene-*d*₆): 8.63 (*a*), 6.25 (*b*), 6.62 (*c*), 6.81 (*d*), 8.16 (*f*), 4.45 (*g_a*), 3.72 (*g_b*), 0.53 (*j*), 7.49 (*m*), 7.18 (*n*), 7.04 (*o*). Anal. Calcd for C₃₈H₄₂N₄Fe: C, 73.71; H, 7.22; N, 9.55. Found: C, 73.48; H, 7.50; N, 9.27.

5. *cis*-{κ-N,N'-(N-(2-pyridinylmethylene)alkylamine)}₂Fe(PMe₃) (alkyl = CH₂C(CH₃)₃, 3-^{neo}Pe; (CH₂)₂C(CH₃)₃, 3-^{neo}Hex).

A round bottom flask was charged with FeCl₂ (100-166 mg) and sodium amalgam (2.2 equiv). A 15 mL amount of THF and 1.5 equiv PMe₃ were vacuum distilled at -78 °C, and a solution of imine (1 equiv) in 10 mL THF were added via syringe under argon purge. The reaction mixture was allowed to stir and slowly warm to room temperature overnight. The crude reaction was stripped and filtered through Celite in Et₂O and THF. The purple solution was concentrated and subsequently filtered and washed with Et₂O (3 x 15 mL). Green crystals were grown out of concentrated Et₂O and isolated by filtration. a. **3-^{neo}Hex**: Bright green microcrystals (300 mg) were obtained in 45% yield. ¹H NMR (300MHz, benzene-*d*₆): 8.40 (*a*), 6.95 (*b*), 6.95 (*c*), 7.25 (*d*), 8.90 (*f*), 4.25 (*g_a*), 3.95 (*g_b*), 1.66 (*h_a*), 1.25 (*h_b*), 0.89 (*j*), 0.62 (*d*, 7, *l*). ¹³C NMR (500MHz, C₆D₆): 146.24 (*a*), 123.21 (*b*), 120.62 (*c*), 111.44 (*d*),

153.76 (e), 157.40 (f), 58.15 (g), 48.56 (h), 30.62 (i), 30.15 (j), 14.45 (l). ^{31}P NMR (400MHz, C_6D_6): 3.65 (s). Anal. Calcd for $\text{C}_{27}\text{H}_{45}\text{N}_4\text{PFe}$: C, 63.28; H, 8.85; N, 10.93. Found: C, 61.31; H, 7.80; N, 10.94. b. **3- $^{\text{neo}}$ Pe**: Bright green crystals (193 mg) were obtained in 48% yield.

6. [*cis*-{ κ -N,N'-(N-(2-pyridinylmethylene)neohexylamine)} $_2\text{Fe}(\text{PMe}_3)(\text{CH}_3)$]OTf (5- $^{\text{neo}}$ Hex).

To a cold solution of $^{\text{neo}}$ Hex-3 (70 mg, 0.136 mmol) in 10 mL THF under an argon blanket was syringed CH_3OTf (15 μL , 0.136 mmol). The mixture was allowed to stir at -78°C for 6 h, then slowly warmed to room temperature overnight. The dark green solution was triturated several times with THF to remove any excess CH_3OTf , then stripped to yield 75 mg dark green solid (82 %). Green-black crystals were grown from slow diffusion of Et_2O into a THF solution. ^1H NMR (400MHz, $\text{THF}-d_8$): 8.85 (d, 4, *a*), 7.45 (t, 6, *b*), 7.81 (t, 7, *c*), 8.07 (d, 8, *d*), 9.54 (s, *f*), 3.89 (m, *g_a*), 3.38 (m, *g_b*), 1.19 (m, *h_a*), 0.41 (m, *h_b*), 0.52 (s, *j*), 0.14 (d, 10, *k*), 0.83 (d, 9, *l*), 8.90 (d, 5, *a'*), 7.38 (t, 6, *b'*), 7.68 (t, 7, *c'*), 7.88 (d, 8, *d'*), 8.68 (br s, *f'*), 4.33 (m, *g_a'*), 3.70 (m, *g_b'*), 0.99 (m, *h_a'*), 0.85 (m, *h_b'*), 0.45 (s, *j'*). ^{13}C NMR (500MHz, $\text{THF}-d_8$): 154.47 (*a*), 125.03 (*b*), 127.76 (*c*), 134.27 (*d*), 161.27 (*e*), 167.26 (*f*), 57.14 (*g*), 46.01 (*h*), 30.21 (*i*), 29.49 (*j*), 6.88 (*d*, 30, *k*), 12.17 (*d*, 23, *l*), 161.52 (*a'*), 124.04 (*b'*), 127.59 (*c'*), 132.35 (*d'*), 159.98 (*e'*), 157.76 (*f'*), 59.25 (*g'*), 46.83 (*h'*), 30.37 (*i'*), 29.59 (*j'*). ^{31}P NMR (400MHz, $\text{THF}-d_8$): 13.36 (s). Anal. Calcd for $\text{C}_{29}\text{H}_{48}\text{N}_4\text{F}_3\text{O}_3\text{PSFe}$: C, 51.48; H, 7.15; N, 8.28. Found: C, 50.05; H, 6.18; N, 8.22.

7. [*cis*-{ κ -N,N'-(N-(2-pyridinylmethylene)alkylamine)} $_2\text{Fe}(\text{PMe}_3)(\text{CH}_3)$]I (alkyl = $\text{CH}_2\text{C}(\text{CH}_3)_3$, 4- $^{\text{neo}}$ Pe; $(\text{CH}_2)_2\text{C}(\text{CH}_3)_3$, 4- $^{\text{neo}}$ Hex).

Same as above, using $^{\text{neo}}$ Hex-3 or $^{\text{neo}}$ Pe-3 and CH_3I . a. **4- $^{\text{neo}}$ Hex**: Green solid (76 %). ^1H NMR (400MHz, CD_2Cl_2): 8.63 (d, 6, *a*), 7.42 (t, 7, *b*), 7.79 (m, *c*), 7.92 (d, 8, *d*), 9.35 (s, *f*), 3.79 (t, 11, *g_a*), 3.27 (t, 11, *g_b*), 1.12 (td, 11,5, *h_a*), 0.41 (td, 13,4, *h_b*),

0.54 (s, *j*), 0.09 (d, 9, *k*), 0.85 (d, 8, *l*), 8.68 (d, 5, *a'*), 7.28 (t, 7, *b'*), 7.68 (t, 8, *c'*), 7.79 (m, *d'*), 8.58 (d, 6, *f'*), 4.21 (t, 11, *g_a'*), 3.60 (t, 11, *g_b'*), 1.01 (td, 13, 6, *h_a'*), 0.36 (td, 14, 5, *h_b'*), 0.51 (s, *j'*). ³¹P NMR (400MHz, CD₂Cl₂): 13.10 (s). b. **4-^{neo}Pe**: Green solid (56 %). ¹H NMR (400MHz, CD₂Cl₂): 8.60-8.63 (m, *a*), 7.48 (t, 7, *b*), 7.80-7.82 (m, *c*), 7.94 (d, 8, *d*), 9.26 (s, *f*), 4.02 (d, 11, *g_a*), 3.92 (d, 12, *g_b*), 0.52 (s, *j*), 0.14 (d, 10, *k*), 0.83 (d, 9, *l*), 8.71 (d, 7, *a'*), 7.35 (t, 6, *b'*), 7.71 (t, 8, *c'*), 7.80-7.82 (m, *d'*), 8.60-8.63 (m, *f'*), 3.48 (m, *g_a'*), 3.42 (m, *g_b'*), 0.45 (s, *j'*). ³¹P NMR (400MHz, CD₂Cl₂): 11.70 (s).

8. [{κ-N,N'-(N-(2-pyridinylmethylene)alkylamine)}₃Fe][OTf]₂ (alkyl = CH₂C(CH₃)₃, **6-^{neo}Pe; (CH₂)₂C(CH₃)₃, **6-^{neo}Hex**).**

To a solution of imine (0.263-0.848 mmol) in THF was added Fe(OTf)₂ (31-100 mg, 0.088-0.283 mmol). The bright purple solution was allowed to stir for 4 h, then stripped. The purple material was filtered and washed several times with CH₂Cl₂, concentrated, triturated vigorously with Et₂O and filtered to yield a purple solid. a. **6-^{neo}Hex**: 75 mg pink-purple solid (93 %). The product contained only the *mer* isomer. ¹H NMR (400MHz, CD₃CN): 8.27 (d, 7, *a¹*), 8.17-8.19 (m, *a²*, *a³*), 7.58 (t, 6, *b¹*), 7.52 (t, 6, *b²*), 7.44 (t, 6, *b³*), 8.03-8.12 (m, *c¹*, *c²*, *c³*, *d¹*, *d²*), 7.21 (d, 6, *d³*), 9.23 (s, *f¹*), 9.19 (s, *f²*), 9.04 (s, *f³*), 3.85 (td, 5, 13, *g¹*), 3.48 (td, 5, 13, *g²*, *g³*), 3.27 (td, 4, 13, *g⁴*), 3.08 (td, 4, 13, *g⁵*, *g⁶*), 1.27-1.43 (m, *h¹*, *h²*, *h³*), 1.15 (td, 5, 13, *h⁴*), 1.04 (td, 4, 13, *h⁵*), 0.66 (td, 5, 13, *h⁶*), 0.83 (s, *j¹*), 0.61 (s, *j²*, *j³*). ¹³C NMR (400MHz, CD₃CN): 156.89 (*a¹*), 156.42 (*a²*), 155.88 (*a³*), 130.13 (*b¹*), 129.93 (*b²*), 129.42 (*b³*), 139.65 (*c¹*, *c²*), 139.54 (*c³*), 128.93 (*d¹*), 128.86 (*d²*), 128.73 (*d³*), 160.18 (*e¹*), 159.49 (*e²*), 159.06 (*e³*), 174.09 (*f¹*), 173.80 (*f²*), 173.49 (*f³*), 57.38 (*g¹*), 57.07 (*g²*), 56.80 (*g³*), 45.24 (*h¹*), 44.82 (*h²*, *h³*), 30.77 (*i¹*), 30.30 (*i²*, *i³*), 29.34 (*j¹*), 29.05 (*j²*, *j³*). b. **6-^{neo}Pe**: 218 mg bright purple solid (87 %). The product contained a mixture of *fac* and *mer* isomers in a 1:2 ratio. ¹H NMR (400MHz, CD₃CN): (*fac*) 8.36 (d, 8, *a*), 7.54 (t, 6, *b*), 8.15 (t, 8, *c*), 7.04 (d, 6,

d), 9.12 (s, *f*), 3.85 (d, 15, *g*), 3.25 (s, 15, *g'*), 0.77 (s, *j*); (*mer*) 8.87 (br s, *a*¹, *a*²), 8.76 (d, 8, *a*³), 7.96 (t, 6, *b*¹), 7.77 (t, 7, *b*²), 7.85-7.88 (m, *b*³, *c*¹), 8.01-8.10 (m, *c*², *c*³, *d*¹), 8.53 (d, 8, *d*²), 8.50 (d, 8, *d*³), 10.30 (br s, *f*¹, *f*²), 10.15 (s, *f*³), 4.73 (d, 14, *g*¹), 4.39 (d, 16, *g*²), 4.29 (d, 14, *g*³), 3.69 (d, 14, *g*⁴), 3.10 (d, 16, *g*⁵), 2.94 (d, 16, *g*⁶), 0.88 (s, *j*¹), 0.82 (s, *j*²), 0.69 (s, *j*³). Anal. Calcd for C₃₅H₄₈N₆F₆O₆S₂Fe: C, 47.62; H, 5.48; N, 9.52. Found: C, 47.51; H, 5.54; N, 9.48.

D. Polymerization screening procedure.

In a typical screening, a reaction vessel was charged with olefin and a suspension of the iron complex in 25 mL toluene. A solution of PMAO (270 equiv) in toluene was added via syringe. After the appropriate reaction time, the reactor was vented, and the mixture quenched with methanol/HCl to precipitate any polymer present. If no precipitation occurred, no further characterization was attempted. Conditions for each run are listed in Table 4.3.

Table 4.3. Reaction conditions for each attempted polymerization run.

Entry	Complex	P _{olefin} / V _{olefin} ^a (psi)/[mL]	PMAO ^b (equiv)	Additive (equiv)	T _{rxn} (°)	t _{rxn} (h)	Yield (g)
1	4^{neo}Hex	15	PMAO (270)	-	0	0.5	0
2	4^{neo}Hex	40	PMAO (270)	-	25	1.0	0
3	4^{neo}Hex	60	PMAO (270)	-	60	1.0	0
4	4^{neo}Hex	60	PMAO (270)	-	25	2.0	0
5	4^{neo}Hex	60	PMAO (270)	Ni(COD) ₂ ^c (2)	25	3.0	0
6	5^{neo}Hex	60	PMAO (270)	-	25	2.5	0
7	5^{neo}Hex	60	PMAO (270)	-	40	2.5	0
8	1^{neo}Pe	60	-	[Ph ₃ C][B(C ₆ F ₅) ₄] (1)	25	3.0	0
9	1^{neo}Pe	[2]	-	[Ph ₃ C][B(C ₆ F ₅) ₄] (1)	25	3.0	0
10	1^{neo}Pe	60	-	(TIBA ^d /BHT ^e) (2)	25	3.0	trace
11	1^{neo}Pe	60	PMAO (270)	-	25	3.0	trace

^aReactions with ethylene are reported in psi; reaction with 1-hexene is reported in mL. ^bPMAO = polymethylalumoxane. Used as a solution in toluene. ^cAdded as a phosphine scavenger. ^dTIBA = triisobutylaluminum. ^eBHT = butylated hydroxytoluene, a radical stabilizer.

When the borate additive was employed, a reaction vessel was charged with olefin and a suspension of $[\text{Ph}_3\text{C}][\text{B}(\text{C}_6\text{F}_5)_4]$ in toluene. A suspension of the iron complex in toluene was added via syringe. Workup was as described above.

E. Single Crystal X-Ray Diffraction Studies.

Upon isolation, the crystals were covered in polyisobutenes and placed under a 173 K N_2 stream on the goniometer head of a Siemens P4 SMART CCD area detector (graphite-monochromated $\text{MoK}\alpha$ radiation, $\lambda = 0.71073 \text{ \AA}$). The structures were solved by direct methods (SHELXS). All non-hydrogen atoms were refined anisotropically unless stated, and hydrogen atoms were treated as idealized contributions (Riding model).

1. *cis,cis*- $\{\kappa\text{-N,N}'\text{-(N-(2-pyridinylmethylene)neopentylamine)}\}_2\text{Fe}(\text{CH}_3)_2$ (1-^{neo}Pe).

A black block (0.40 x 0.25 x 0.15 mm) was obtained from Et_2O . A total of 17,741 reflections were collected with 5,842 determined to be symmetry independent ($R_{\text{int}} = 0.0311$), and 4,779 were greater than $2\sigma(I)$. A semi-empirical absorption correction from equivalents was applied, and the refinement utilized $w^{-1} = \sigma^2(F_o^2) + (0.0418p)^2 + 0.7577p$, where $p = ((F_o^2 + 2F_c^2)/3)$.

2. *cis*- $\{\kappa\text{-N,N}'\text{-(N-(2-pyridinylmethylene)neohexylamine)}\}_2\text{Fe}(\text{PhCCPh})$ (2-^{neo}Hex).

A red block (0.40 x 0.30 x 0.25 mm) was obtained from $\text{Et}_2\text{O}/\text{THF}$. A total of 29,730 reflections were collected with 3,799 determined to be symmetry independent ($R_{\text{int}} = 0.0661$), and 2,599 were greater than $2\sigma(I)$. A semi-empirical absorption correction from equivalents was applied, and the refinement utilized $w^{-1} = \sigma^2(F_o^2) + (0.0621p)^2 + 0.0000p$, where $p = ((F_o^2 + 2F_c^2)/3)$.

3. *cis*- $\{\kappa\text{-N,N}'\text{-(N-(2-pyridinylmethylene)neohexylamine)}\}_2\text{Fe}(\text{PMe}_3)$ (3-^{neo}Hex).

A green block (0.40 x 0.20 x 0.10 mm) was obtained from Et_2O . A total of 12,529 reflections were collected with 3,761 determined to be symmetry independent

($R_{\text{int}} = 0.0293$), and 3,272 were greater than $2\sigma(I)$. A semi-empirical absorption correction from equivalents was applied, and the refinement utilized $w^{-1} = \sigma^2(F_o^2) + (0.0398p)^2 + 1.8440p$, where $p = ((F_o^2 + 2F_c^2)/3)$.

4. [*cis*-{ κ -N,N'-(N-(2-pyridinylmethylene)neohexylamine)}₂Fe(PMe₃)(CH₃)]OTf (5-^{neo}Hex).

A red block (0.30 x 0.20 x 0.15 mm) was obtained from THF/hexanes. A total of 25,651 reflections were collected with 8,102 determined to be symmetry independent ($R_{\text{int}} = 0.0315$), and 6,436 were greater than $2\sigma(I)$. A semi-empirical absorption correction from equivalents was applied, and the refinement utilized $w^{-1} = \sigma^2(F_o^2) + (0.0498p)^2 + 0.6586p$, where $p = ((F_o^2 + 2F_c^2)/3)$.

REFERENCES

- 1) Chlopek, K.; Bill, E.; Weyhermüller, T.; Wieghardt, K. *Inorg. Chem.* **2005**, *44*, 7087-7098.
- 2) Chlopek, K.; Bothe, E.; Neese, F.; Weyhermüller, T.; Wieghardt, K. *Inorg. Chem.* **2006**, *45*, 6298-6307.
- 3) Kapre, R.; Ray, K.; Sylvestre, I.; Weyhermüller, T.; George, S. D.; Neese, F.; Wieghardt, K. *Inorg. Chem.* **2006**, *45*, 3499-3509.
- 4) Kapre, R.; Bothe, E.; Weyhermüller, T.; George, S. D.; Neese, F.; Wieghardt, K. *Inorg. Chem.* **2007**, *46*, 5642-5650.
- 5) Muresan, N.; Lu, C. C.; Ghosh, M.; Peters, J. C.; Abe, M.; Henling, L. M.; Weyhermüller, T.; Bill, E.; Wieghardt, K. *Inorg. Chem.* **2008**, *47*, 4579-4590.
- 6) Muresan, N.; Chlopek, K.; Weyhermüller, T.; Neese, F.; Wieghardt, K. *Inorg. Chem.* **2007**, *46*, 5327-5337.
- 7) Muresan, N.; Weyhermüller, T.; Wieghardt, K. *Dalt. Trans.* **2007**, 4390-4398.
- 8) Lu, C. C.; Bill, E.; Weyhermüller, T.; Bothe, E.; Wieghardt, K. *J. Am. Chem. Soc.* **2008**, *130*, 3181-3197.
- 9) de Bruin, B.; Bill, E.; Bothe, E.; Weyhermüller, T.; Wieghardt, K. *Inorg. Chem.* **2000**, *39*, 2936-2947.
- 10) Bart, S. C.; Chlopek, K.; Bill, E.; Bouwkamp, M. W.; Lobkovsky, E.; Neese, F.; Wieghardt, K.; Chirik, P. J. *J. Am. Chem. Soc.* **2006**, *128*, 13901-13912.
- 11) Bart, S. C.; Lobkovsky, E.; Bill, E.; Wieghardt, K.; Chirik, P. J. *Inorg. Chem.* **2007**, *46*, 7055-7063.
- 12) Chirik, P. J.; Wieghardt, K. *Science*. **2010**, *327*, 794-795, and references therein.
- 13) Wile, B. M.; Trovitch, R. J.; Bart, S. C.; Tondreau, A. M.; Lobkovsky, E. B.; Milsmann, C.; Bill, E.; Wieghardt, K.; Chirik, P. J. *Inorg. Chem.* **2009**, *48*, 4190-4200.

- 14) Tondreau, A. M.; Darmon, J. D.; Wile, B. M.; Floyd, S. K.; Lobkovsky, E. B.; Chirik, P. J. *Organometallics* **2009**, 28, 3928-3940.
- 15) For a report of a related complex, see: Vedder, C.; Schaper, F.; Brintzinger, H.-H.; Kettunen, M.; Babik, S.; Fink, G. *Eur. J. Inorg. Chem.* **2005**, 1071-1080.
- 16) Trifonov, A. A.; Gudilenkov, I. D.; Larionova, J.; Luna, C.; Fukin, G. K.; Cherkasov, A. V.; Poddel'sky, A. I.; Druzhkov, N. O. *Organometallics* **2009**, 28, 6707-6713.
- 17) Mondal, A.; Weyhermüller, T.; Wieghardt, K. *Chem. Commun.* **2009**, 6098-6100.
- 18) Lu, C. C.; Weyhermüller, T.; Wieghardt, K. *Inorg. Chem.* **2009**, 48, 6055-6064.
- 19) Maeda, Y.; Takashima, T.; Nishida, Y. *Bull. Chem. Soc. Jpn.* **1976**, 49, 2427-2432.
- 20) tom Dieck, H.; Bruder, H. *J. Chem. Soc., Chem. Comm.* **1974**, 24-25.
- 21) tom Dieck, H.; Diercks, R.; Stamp, L.; Bruder, H.; Schuld, T. *Chem. Ber.* **1987**, 120, 1943-1950.
- 22) Bart, S. C.; Hawrelak, E. J.; Lobkovsky, E.; Chirik, P. J. *Organometallics* **2005**, 24, 5518-5527.
- 23) Bruce, M. I.; Swincer, A. G. *Adv. Organomet. Chem.* **1983**, 22, 59-128.
- 24) Bruce, M. I. *Chem. Rev.* **1998**, 98, 2797-2858.
- 25) Johnson, L. K.; Killian, C. M.; Brookhart, M. *J. Am. Chem. Soc.* **1995**, 117, 6414-6415.
- 26) Ittel, S. D.; Johnson, L. K.; Brookhart, M. *Chem. Rev.* **2000**, 100, 1169-1203.
- 27) Fletcher, N. C.; Nieuwenhuyzen, M.; Rainey, S. *J. Chem. Soc. Dalt. Trans.* **2001**, 2641-2648.
- 28) Howson, S. E.; Allan, L. E. N.; Chmel, N. P.; Clarkson, G. J.; van Gorkum, R.; Scott, P. *Chem. Commun.* **2009**, 1727-1729.

- 29) Parish, R. V. *NMR, NQR, EPR, and Mössbauer Spectroscopy in Inorganic Chemistry*; Ellis Horwood: West Sussex, England, 1990.
- 30) a) Khusniyarov, M. M.; Weyhermüller, T.; Bill, E.; Wieghardt, K. *Angew. Chem. Int. Ed.* **2008**, *47*, 1228-1231. b) Khusniyarov, M. M.; Bill, E.; Weyhermüller, T.; Bothe, E.; Harms, K.; Sundermeyer, J.; Wieghardt, K. *Chem. Eur. J.* **2008**, *14*, 7608-7622.
- 31) Blomquist, J.; Helgeson, U.; Moberg, L. C.; Larsson, R.; Miezi, A. *J. Inorg. Nucl. Chem.* **1977**, *39*, 1539-1542.
- 32) Epstein, L. M. *J. Chem. Phys.* **1964**, *40*, 435.
- 33) Vasudev, P.; Jones, C. H. W. *Can. J. Chem.* **1973**, *51*, 405-410.
- 34) Collins, R. L.; Pettit, R. *J. Chem. Phys.* **1963**, *39*, 3433-3466.
- 35) Stevens, J. G. *Hyperfine Interactions* **1983**, *13*, 221-236.
- 36) Karsch, H. H. *Chem. Ber.* **1977**, *110*, 2699-2711.
- 37) Zoet, R.; van Koten, G.; Vrieze, K. *Inorg. Chim. Acta.* **1988**, *148*, 71-84.

CHAPTER 5

A HIGHLY-FLUORINATED DIARYLIMINE: TOWARDS A STABLE Fe(III) DIARYL AZAALLYL

I. Introduction

Chapter 3 related the synthesis of a stable, Fe(III) azaallyl with a chelating arylpyridylimine ligand. The failure to achieve an analogous diarylimine azaallyl species was rationalized on the basis of the orbital positioning, as shown in Figure 5.1. If the azaallyl non-bonding orbitals lie above the metal “ t_{2g} ,” then removal of an electron yields an unstable organic radical. However, if the CNC^{nb} orbital lies below one of the d orbitals, oxidation occurs at the metal to give a stable Fe(III).

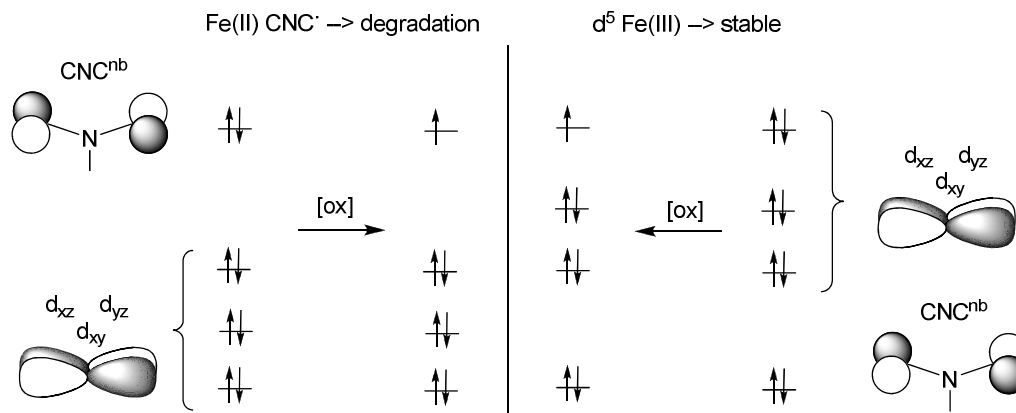


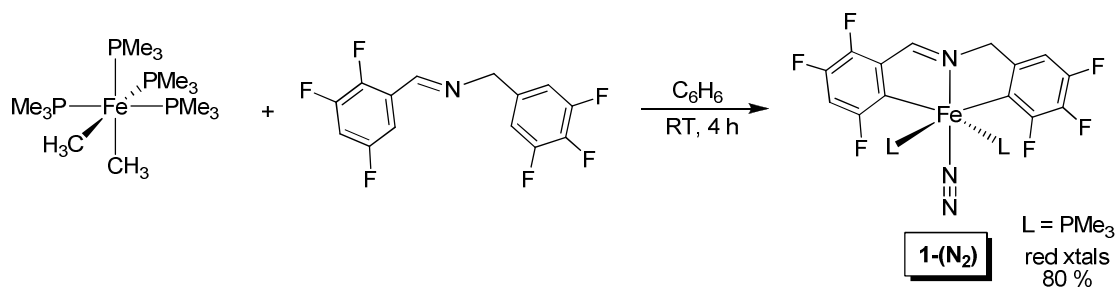
Figure 5.1. Proposed molecular orbital description for the formation of both stable and unstable Fe(III) azaallyl species.

If this premise is correct, then it is the inductively-withdrawing pyridine group that lowers the CNC^{nb} orbital of the stable Fe(III) complexes. The diarylimine ligand requires a different source of stabilization, which could be provided by electronegative substituents on the aryls. The aim of this work is to achieve an Fe(III) azaallyl using a highly-fluorinated diarylimine ligand, thereby lending greater credence to the orbital picture previously described.

II. Results and Discussion

A. Synthesis and structure of *trans*-{ κ -C,N,C'-(2,4,5-trifluorophen-2-yl)CH=N-CH₂(3,4,5-trifluorophen-2-yl)}Fe(PMe₃)₂(N₂) (**1**-(N₂)).

A fluorinated diarylimine was simply prepared by condensation of 2,4,5-trifluorobenzaldehyde with 3,4,5-trifluorobenzylamine. The particular substitution patterns were chosen simply based on the superior affordability of the starting materials, in addition to one requisite *o*-CH. Treatment of Karsch's *cis*-(PMe₃)₄FeMe₂ with one equivalent of the imine immediately afforded a dark red solution accompanied by gas evolution (Scheme 5.1). Workup using high-vacuum techniques gave a red solid which appeared to be a mixture by ³¹P NMR; the characteristic pattern for meridional phosphine ligands (δ 14.20 (d, 2P); 9.74 (t, 1P)) was accompanied by a singlet at 19.96. After one week under a nitrogen atmosphere, the spectrum displayed only the singlet and free PMe₃. An IR spectrum of the product displayed a band at 2107 cm⁻¹, indicating that the dissociated phosphine was likely replaced by a coordinated dinitrogen molecule. X-ray crystallography confirmed this structure as the N₂ adduct, **1**-(N₂) (Figure 5.2). Workup of the reaction after removal of PMe₃ and reintroduction to a nitrogen atmosphere enabled the clean, reproducible isolation of **1**-(N₂) in 70 % yield.



Scheme 5.1. Synthesis of *trans*-{ κ -C,N,C'-(2,4,5-trifluorophen-2-yl)CH=N-CH₂(3,4,5-trifluorophen-2-yl)}Fe(PMe₃)₂(N₂) (**1**-(N₂)).

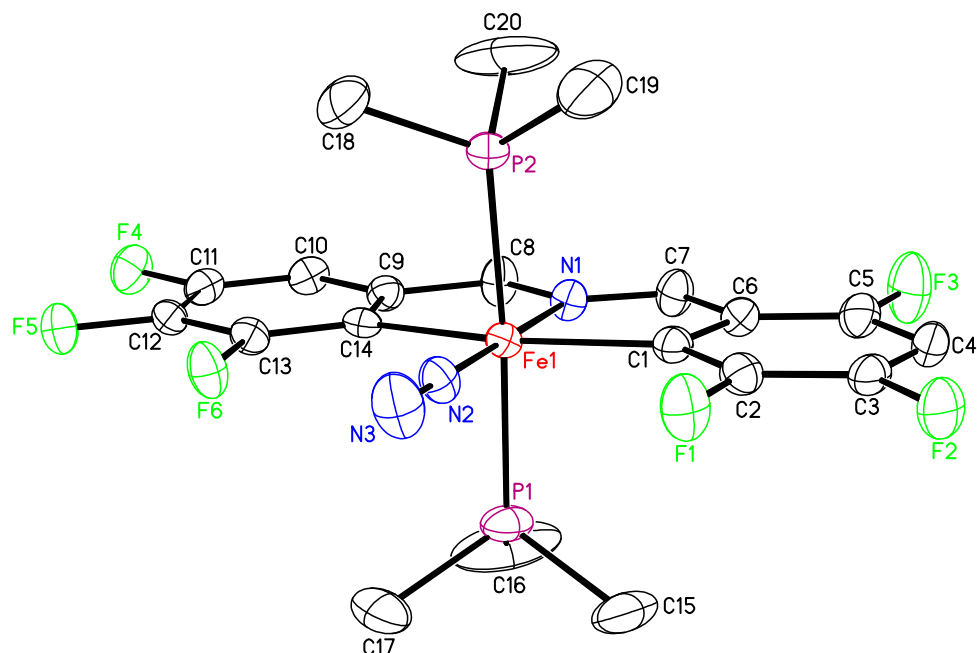


Figure 5.2. Molecular view of *trans*-{ κ -C,N,C'-(2,4,5-trifluorophen-2-yl)CH=N-CH₂(3,4,5-trifluorophen-2-yl)}Fe(PMe₃)₂(N₂) (**1**-(N₂)). Selected bond distances (Å) and angles (°) are as follows: Fe-C1, 1.996(2); Fe-C14, 2.014(2); Fe-N1, 1.9347(19); Fe-N2, 1.811(2); Fe-P1, 2.2202(7); Fe-P2, 2.2389(7); N2-N3, 1.104(3); N1-C7, 1.308(3); N1-C8, 1.459(3); C6-C7, 1.443(3); C8-C9, 1.501(4); N1-Fe-N2, 178.17(10); C1-Fe-C14, 163.06(9); N1-Fe-C1, 81.25(9); N1-Fe-C14, 81.82(9); N-Fe-Pav, 90.11(7)±1.8; Fe-N2-N3, 178.9(2); Fe-C1-C2, 134.17(19); Fe-C1-C6, 111.81(15); Fe-C14-C13, 131.84(16); Fe-C14-C9, 113.79(18).

Crystallographic details for **1**-(N₂) are listed in Table 5.1, and pertinent bond distances and angles are contained in the caption of Figure 5.2. The core bond lengths are remarkably similar to those of the arylpyridylimine and diarylimine complexes in Chapter 3, namely the iron-imine distance of 1.9347(19) Å, the iron-carbon distances of 1.996(2) and 2.014(2) Å, and the average iron-phosphorus distance of 2.2341(7) Å. The iron-carbon and iron-phosphorus lengths are slightly longer for the Fe(III) cation, as previously discussed. An attenuated iron-dinitrogen distance of 1.811(2) Å results from modest π -backbonding, but the short N-N bond length of 1.104(3) Å corroborates the IR stretching frequency of 2107 cm⁻¹ as that of an unreduced dinitrogen ligand. A clear distinction between the imine N=C and N-C bonds is

evident in their bond lengths (1.308(3) and 1.459(3) Å, respectively), as well as by the substitution pattern on their adjacent aryl rings.

Table 5.1. Crystallographic data for *trans*-{ κ -C,N,C'-(2,4,5-trifluorophen-2-yl)CH=N-CH₂(3,4,5-trifluorophen-2-yl)}Fe(PMe₃)₂(N₂) (**1**-(N₂)).

Formula	C ₂₀ H ₂₃ F ₆ FeN ₃ P ₂
Formula weight	537.20
Crystal system	Monoclinic
Space group	Cc
<i>Z</i>	4
<i>a</i> (Å)	19.0597(7)
<i>b</i> (Å)	9.1733(4)
<i>c</i> (Å)	15.7972(10)
α (°)	90
β (°)	121.8450(10)
γ (°)	90
<i>V</i> (Å ³)	2346.2(2)
<i>r</i> _{calc} (g cm ⁻³)	1.521
μ (mm ⁻¹)	0.839
Temperature (K)	173(2)
λ (Å)	0.71073
Final R indices [<i>I</i> > 2 σ (<i>I</i>)] ^{a,b}	R ₁ = 0.0364, wR ₂ = 0.0815
R indices (all data) ^{a,b}	R ₁ = 0.0434, wR ₂ = 0.0858
Goodness-of-fit ^c	1.024

^a $R_1 = \sum ||F_o| - |F_c|| / \sum |F_o|$. ^b $wR_2 = [\sum w(|F_o| - |F_c|)^2 / \sum wF_o^2]^{1/2}$. ^c GOF (all data) = $[\sum w(|F_o| - |F_c|)^2 / (n - p)]^{1/2}$, *n* = number of independent reflections, *p* = number of parameters.

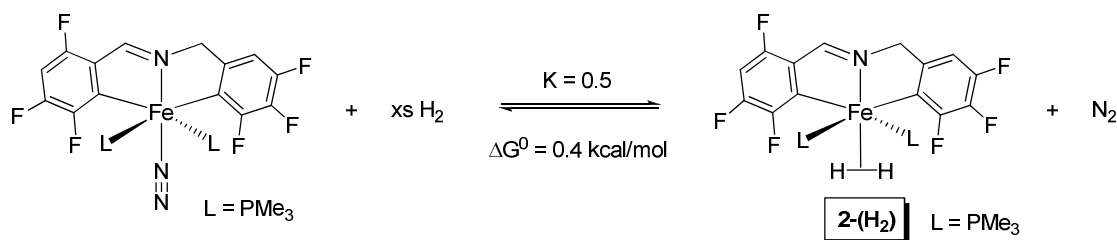
Core angles of **1**-(N₂) reveal a slightly distorted octahedron, with an imine-iron-dinitrogen angle of 178.17(10) °, a phosphorus-iron-phosphorus angle of 176.04(3) °, an aryl-iron-aryl angle of 163.06(9) °, imine-iron-aryl chelates of 81.82(9) and 81.25(9) °, and an average nitrogen-iron-phosphorus angle of 90.11(7)±1.8 °. Asymmetry in the chelation of the aryl rings is seen by the difference in the “outer” and “inner” Fe-C-C angles, which is mildly greater for the imine-containing chelate (Fe-C1-C2 = 134.17(19) °; Fe-C1-C6 = 111.81(15) °) than for the other (Fe-C14-C13

= 131.84(16) °; Fe-C14-C9 = 113.79(18) °). Unsurprisingly, the Fe-N2-N3 angle of 178.9(2) ° indicates a very linear dinitrogen.

B. Dinitrogen displacement.

Isolation of **1-(N₂)** revealed significant lability of the ligand trans to the imine nitrogen, and pointed towards possible isolation of a five-coordinate, square pyramidal complex. Attempts were made to synthesize and isolate this species in the absence of nitrogen, or by cycles of evacuation and redissolution, but uptake of N₂ was evident even in the short time necessary to prepare an IR (Nujol) or NMR sample. Efforts to isolate and crystallize this compound using an argon glovebox are underway.

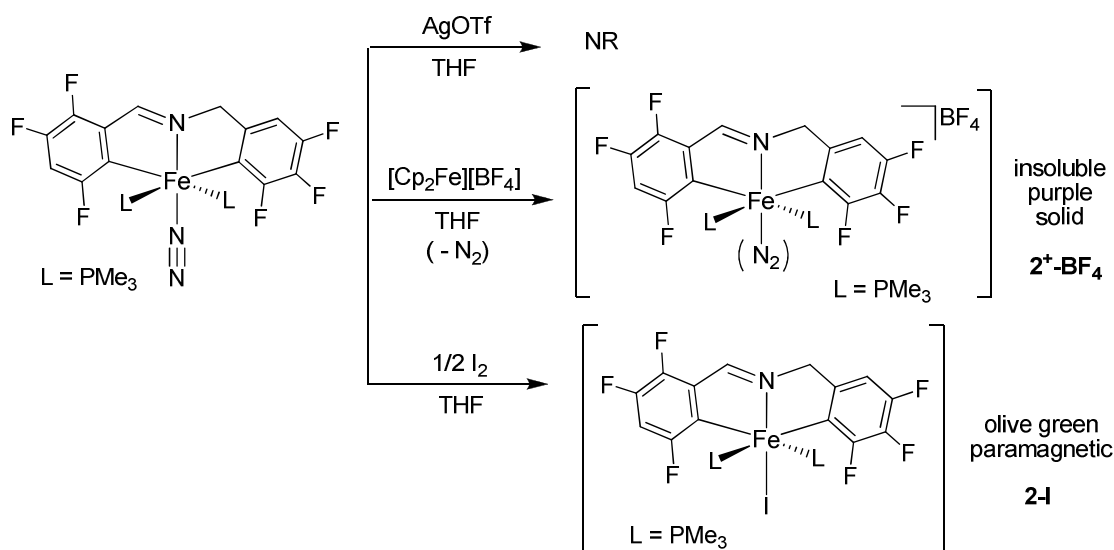
Displacement of dinitrogen by H₂ appeared to be a reasonable goal, and one that also bore the possibility of oxidative addition to an Fe(IV) dihydride. Addition of 1 atm H₂ to **1-(N₂)** in C₆D₆ led to the observation of a new product by ¹H NMR which exhibited a broad singlet at -13.88 ppm. This peak could be further resolved to an apparent triplet (J_{PH} = 12 Hz). The broadened signal and small coupling constant suggested an η²-dihydrogen complex, **1-(H₂)**, which was verified by a measured T₁(min) of 11 ms and estimated H-H distance of 0.77 Å.^{1,2} Product formation ceased after two days, and the ratio of remaining **1-(N₂)** to **1-(H₂)** (2:1) established an equilibrium between the two species (Scheme 5.2). At 25 °C, K_{eq} = 0.5 for this reaction, and ΔG⁰ = 0.4 kcal/mol. An attempt was made to drive the reaction towards **1-(H₂)** by successive evacuation and re-addition of hydrogen, but the appearance of metallic iron hampered further monitoring by NMR methods.



Scheme 5.2. Equilibrium between **1-(N₂)** and **1-(H₂)**.

C. Oxidation attempts.

Formation of a stable azaallyl was envisioned by oxidation and subsequent deprotonation of **1-(N₂)**. While oxidation of the non-fluorinated analog, [*mer*-κ-C,N,C'-{(Ph-2-yl)CH₂N=CH(Ph-2-yl)}Fe(PMe₃)₃]OTf, was accomplished with AgOTf in THF, no reaction was observed when **1-(N₂)** was treated with this oxidant (Scheme 5.3). Treatment of **1-(N₂)** with one equivalent of [Cp₂Fe][BF₄] in THF resulted in an insoluble red-orange solid. Bubbling was observed during the reaction, indicating possible loss of the N₂ ligand. These observations are consistent with the intended product, **2⁺-BF₄**; unfortunately, insolubility in common solvents, including THF and CH₂Cl₂ prevented characterization by NMR spectroscopy.



Scheme 5.3. Oxidation attempts with *trans*-{κ-C,N,C'-(2,4,5-trifluorophen-2-yl)CH=N-CH₂(3,4,5-trifluorophen-2-yl)}Fe(PMe₃)₂(N₂) (**1-(N₂)**).

The increased solubility which would likely accompany a *neutral* oxidized species prompted the use of I₂ as an oxidant. Low-temperature treatment of **1-(N₂)** with I₂ (1/2 equiv) led to the isolation of a small amount of olive-green material which was soluble in benzene. Its ¹H NMR spectrum exhibited five paramagnetic peaks at

19.95, 12.35, -10.25, -13.49, and -16.62, which along with the increased solubility lead to a tentative assignment as the six-coordinate Fe(III) complex, **2-I**.

Unfortunately, attempts to isolate **2-I** on a larger scale were consistently hampered by the presence of remaining starting material. The possibility of intrusion by I_3^- may necessitate further change of oxidant, and oxidation reactions with Br_2 are currently underway.

III. Conclusions

The goal of achieving a stable Fe(III) diaryl azaallyl has not yet been accomplished, but preliminary results are promising. Use of the fluorinated diarylimine has led to divergent reactivity from that of the parent ligand. The increased lability of one coordination site allowed the isolation of an N_2 adduct, and permitted the observation of a novel dihydrogen complex. Efforts to cleanly oxidize the Fe(II) compound and generate an azaallyl are currently in progress.

IV. Experimental

A. General considerations.

All manipulations were performed using either glovebox or high vacuum line techniques. Hydrocarbon solvents containing 1-2 mL of added tetraglyme, and ethereal solvents were distilled under nitrogen from purple sodium benzophenone ketyl and vacuum transferred from same prior to use. Benzene- d_6 and toluene- d_8 were dried over sodium, vacuum transferred and stored under N_2 . THF- d_8 was dried over sodium benzophenone ketyl. Methylene chloride- d_2 was dried over CaH_2 , vacuum transferred and stored over activated 4 Å molecular sieves. H_2 gas was dried by passing through a trap at 78 K. Trimethylphosphine was dried and stored over activated 4 Å molecular sieves. *cis*-(Me_3P) $_4$ FeMe $_2$ was prepared according to literature

procedure.³ All other chemicals were commercially available and used as received. All glassware was oven dried.

NMR spectra were obtained using Varian XL-400, INOVA 400, and Unity-500 spectrometers. Chemical shifts are reported relative to benzene-*d*₆ (¹H δ 7.16; ¹³C{¹H} δ 128.39), THF-*d*₈ (¹H δ 3.58; ¹³C{¹H} δ 67.57), and CD₂Cl₂ (¹H δ 5.32; ¹³C{¹H} δ 54.00). Infrared spectra were recorded on a Nicolet Avatar 370 DTGX spectrophotometer interfaced to an IBM PC (OMNIC software). Elemental analyses were performed by Robertson Microlit Laboratories, Madison, New Jersey.

B. Synthesis of compounds.

1. (^FAr)ImCH₂(^FAr)

100 mg each of 2,4,5-trifluorobenzaldehyde (0.625 mmol) and 3,4,5-trifluorobenzylamine (0.625 mmol) were dissolved in 15 mL CH₂Cl₂ and stirred with MgSO₄ (8-10 equiv) for 10 h. After filtration and concentration of the solvent, the clear oil was triturated with Et₂O and stripped to reveal a white solid (166 mg, 88 %). ¹H NMR (benzene-*d*₆): δ 7.98 (s, *g*), 7.70 (m, *d*), 6.52 (t, 8, *j*, *n*), 6.23 (td, 6, 10, *a*), 3.92 (s, *h*). ¹⁹F NMR (benzene-*d*₆): δ -123.87 (m, *b*), -128.47 (m, *c*), -134.76 (dd, *k*, *m*), -141.26 (m, *e*), -168.18 (tt, *l*).

2. *trans*-{κ-C,N,C'-(2,4,5-trifluorophen-2-yl)CH=N-CH₂(3,4,5-trifluorophen-2-yl)}Fe(PMe₃)₂(N₂) (1-(N₂)).

A solution of (^FAr)ImCH₂(^FAr) (156 mg, 0.513 mmol) in 5 mL benzene were added to 200 mg *cis*-(Me₃P)₄FeMe₂ (0.513 mmol) in 15 mL benzene and allowed to stir under 1 atm N₂ for 4 h. The red solution was stripped, redissolved in Et₂O under N₂, filtered, and recrystallized from concentrated Et₂O to yield dark red crystalline solid (186 mg, 67 %). ¹H NMR (benzene-*d*₆): δ 7.79 (s, *g*), 6.36 (m, *d*, *j*), 3.95 (s, *h*), 0.44 (s, *o*). ¹⁹F NMR (benzene-*d*₆): δ -118.92 (“ddd,” 3,9,23, *c*), -119.36 (d, 31, *b*), -128.81 (“t,” 29, *m*), -132.18 (“ddd,” 3,10,30, *n*), -145.94 (m, *e*), -166.13 (“dd,” 20,30,

l). ^{31}P NMR (benzene- d_6): δ 19.95. $\nu_{\text{NN}} = 2107 \text{ cm}^{-1}$. Anal. Calcd for $\text{C}_{20}\text{H}_{23}\text{N}_3\text{F}_6\text{FeP}_2$: C, 44.72; H, 4.32; N, 7.82. Found: C, 44.85; H, 4.22; N, 7.88.

3. Observation of 1-(H₂).

Into a J-Young tube (2.1 mL volume) was added **1**-(N₂) (20 mg, 0.037 mmol) in C₆D₆ (356 mL) or toluene- d_8 and degassed by multiple freeze-pump thaw cycles. Dihydrogen (660 torr) was then added at 25 °C and the reaction monitored by ^1H and ^{19}F NMR. ^1H NMR (benzene- d_6): δ 8.08 (s, g), 6.48 (m, d, j), 4.24 (s, h), 0.22 (t, 3, o), -13.88 (t, 12, p). ^{19}F NMR (benzene- d_6): δ -107.83 (d, 35, b), -118.85 (m, c, m), -133.23 (dd, 8, 30, k), -146.57 (br s, e), -166.00 (m, l). ^{31}P NMR (benzene- d_6): δ 20.54.

4. Synthesis of proposed Fe(III) compound, 2-I.

To a solution of **1**-(N₂) (35 mg, 0.065 mmol) in 3 mL THF at -78 °C were syringed 0.35 mL of a 0.1 M solution of I₂ in THF. This mixture was allowed to slowly warm to room temperature overnight. The green-brown mixture was stripped, redissolved in THF and filtered through celite to give an olive green solution. Removal of solvent gave a green oil. ^1H NMR (benzene- d_6): δ 19.95 (2H), 12.35 (1H), -10.25 (1H), -13.49 (1H), -16.62 (18H).

C. T₁(min) measurement.

1-(H₂) was prepared as described in toluene- d_8 and allowed to equilibrate for 48 h. ^1H NMR spectra were recorded on the Varian 500 MHz spectrometer. Temperature calibration was performed for each measurement. The T₁(min) was obtained by plotting $\ln T_1$ (ms) vs. $1/T$ and fitting the data with a linear regression curve (Figure 5.3).¹ The H-H distance of 0.77 Å was obtained using the following equations, and by assuming rapid rotation of H₂.^{2,4} Dipolar relaxation equation: $1/T_1 = 0.3\gamma_{\text{H}}^4(\hbar/2\pi)^2(J(\omega) + 4J(2\omega))/r_{\text{HH}}^6$. Spectral density function $J(\omega) = A\tau / (1 + \omega^2\tau^2)$ where $A = 0.25$ for rapid rotation. The temperature dependence of the correlation time is $\tau = \tau_0 e^{E_a/RT}$. At T₁, $\tau = 0.62/(2\pi\nu)$. Simplifying, $r_{\text{HH}} = 4.611(T_1(\text{min})/\nu)^{1/6}$.

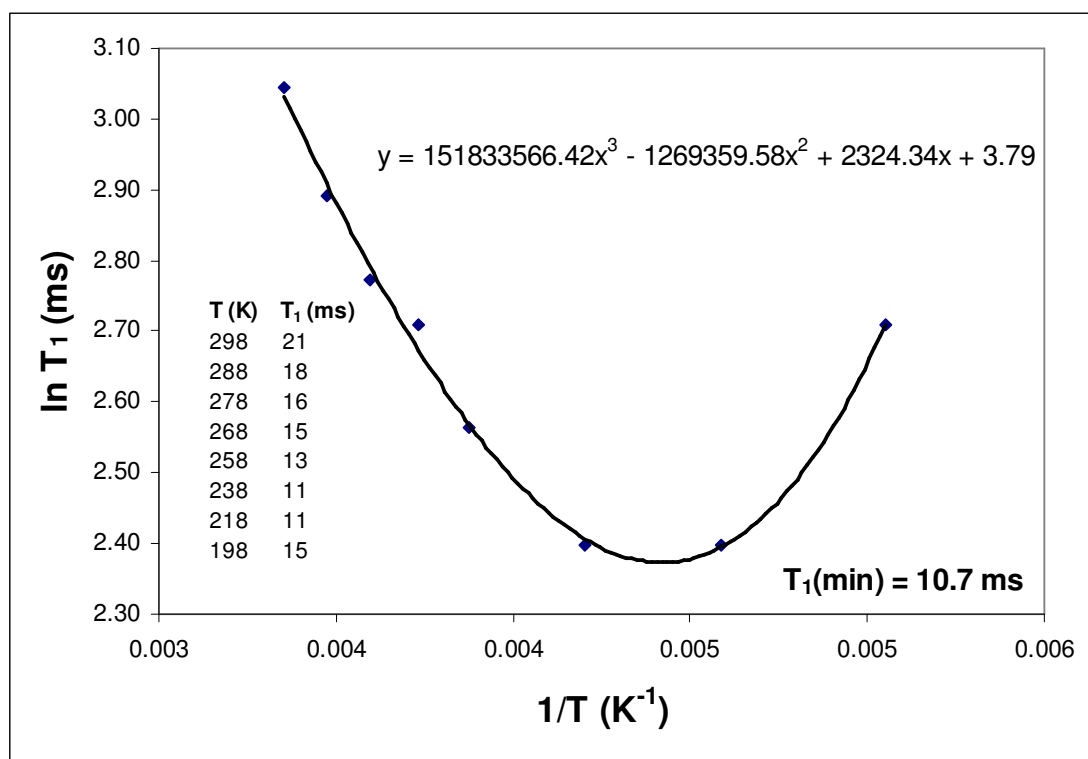


Figure 5.3. Plot of $\ln T_1$ (ms) versus $1/T$ (K^{-1}) for **1-(H₂)**.

D. K_{eq} measurement.

1-(H₂) was prepared as described in C₆D₆ and allowed to equilibrate for 48 h. The ¹H spectrum was recorded at 25 °C, and the K_{eq} measured using integrations of **1-(N₂)**, **1-(H₂)**, and H₂ in solution, and by calculating the amount of N₂ in solution using the known Henry's Law constant for N₂ in benzene.⁵

E. Single crystal X-ray diffraction studies.

1. General.

Upon isolation, the crystals were covered in polyisobutenes and placed under a 173 K N₂ stream on the goniometer head of a Siemens P4 SMART CCD area detector (graphite-monochromated MoK α radiation, $\lambda = 0.71073$ Å). The structures were solved by direct methods (SHELXS). All non-hydrogen atoms were refined

anisotropically unless stated, and hydrogen atoms were treated as idealized contributions (Riding model).

2. *trans*-{ κ -C,N,C'-(2,4,5-trifluorophen-2-yl)CH=N-CH₂(3,4,5-trifluorophen-2-yl)}Fe(PMe₃)₂(N₂) (1-(N₂)).

A red block (0.25 x 0.20 x 0.15 mm) was obtained from benzene. A total of 9,138 reflections were collected with 5,119 determined to be symmetry independent ($R_{\text{int}} = 0.0298$), and 4,493 were greater than $2\sigma(I)$. A semi-empirical absorption correction from equivalents was applied, and the refinement utilized $w^{-1} = \sigma^2(F_o^2) + (0.0437p)^2 + 0.1193p$, where $p = ((F_o^2 + 2F_c^2)/3)$.

REFERENCES

- 1) Hamilton, D. G.; Crabtree, R. H. *J. Am. Chem. Soc.* **1988**, *110*, 4126-4133.
- 2) Bautista, M. T.; Earl, K. A.; Maltby, P. A.; Morris, R. H.; Schweitzer, C. T.; Sella, A. *J. Am. Chem. Soc.* **1988**, *110*, 7031-7036.
- 3) Karsch, H. H. *Chem. Ber.* **1977**, *110*, 2699-2711.
- 4) Bautista, M. T.; Cappellani, E. P.; Drouin, S. D.; Morris, R. H.; Schweitzer, C. T.; Sella, A.; Zubkowski, J. *J. Am. Chem. Soc.* **1991**, *113*, 4876-4887.
- 5) Pierotti, R. A. *J. Phys. Chem.* **1963**, *67*, 1840-1845.